

Loop flows in the Kuramoto model

DELABAYS, Robin

Abstract

Le modèle de Kuramoto s'est imposé comme un outil de première importance pour décrire un grand nombre de phénomènes de synchronisation. Il décrit la dynamique d'un groupe d'oscillateurs couplés de manière non-linéaire. Nous abordons ici la question du nombre d'états synchrones du modèle de Kuramoto en fonction de la topologie du graphe des interaction entre oscillateurs. Nous observons que le nombre d'états synchrones est directement relié au nombre de cycles dans le réseau d'interaction et à leurs longueurs. Nous donnons d'abord une borne supérieure sur le nombre d'états synchrones dans les réseaux cycliques et planaires. Le nombre d'états synchrones est linéaire en la longueur des cycles du réseau. Nous décrivons ensuite des transformations du réseau pouvant amener à un changement d'état synchronie. Nous donnons finalement une estimation de la taille des bassins d'attractions des états synchrones.

Reference

DELABAYS, Robin. *Loop flows in the Kuramoto model*. Thèse de doctorat : Univ. Genève, 2018, no. Sc. 5227

DOI : [10.13097/archive-ouverte/unige:106921](https://doi.org/10.13097/archive-ouverte/unige:106921)

URN : [urn:nbn:ch:unige-1069216](https://urn.unige.ch/urn:nbn:ch:unige-1069216)

Available at:

<http://archive-ouverte.unige.ch/unige:106921>

Disclaimer: layout of this document may differ from the published version.



UNIVERSITÉ
DE GENÈVE

UNIVERSITÉ DE GENÈVE
Section de Mathématiques

FACULTÉ DES SCIENCES
Professeur Y. Velenik

LOOP FLOWS IN THE KURAMOTO MODEL

THÈSE

Présentée à la Faculté des Sciences de l'Université de Genève
Pour obtenir le grade de Docteur ès sciences, mention Mathématiques

Par
Robin DELABAYS
de
Le Châtelard (FR)

Thèse N° 5227

GENÈVE
Atelier d'impression ReproMail
2018



DOCTORAT ÈS SCIENCES, MENTION MATHEMATIQUES

Thèse de Monsieur Robin DELABAYS

intitulée :

«Loop Flows in the Kuramoto Model»

La Faculté des sciences, sur le préavis de Monsieur Y. VELENIK, professeur ordinaire et directeur de thèse (Section de mathématiques), Monsieur J.-P. ECKMANN, professeur honoraire et codirecteur de thèse (Département de physique théorique), Monsieur D. CIMASONI, docteur et codirecteur de thèse (Section de mathématiques), Monsieur P. JACQUOD, professeur et codirecteur de thèse (HES-SO Valais-Wallis, Sion, Suisse), et Monsieur F. DÖRFLER, docteur (Eidgenössische Technische Hochschule (ETHZ), Zürich, Switzerland), autorise l'impression de la présente thèse, sans exprimer d'opinion sur les propositions qui y sont énoncées.

Genève, le 25 juin 2018

Thèse - 5227 -

Le Décanat

Contents

Acknowledgments	5
Foreword	7
1 Introduction	9
1.1 From the swing equations to the Kuramoto model	9
1.2 Synchronization and the Kuramoto model	10
1.3 Overview of the results	13
2 Preliminaries	15
2.1 Loop flows	17
2.2 The winding number	19
2.3 Linear and nonlinear stability	20
2.4 Toolbox of linear algebra	22
3 The number of stable equilibria in locally coupled Kuramoto models on single-cycle networks	23
3.1 Angle differences and sum of angle differences	23
3.2 Infinite coupling	24
3.3 Finite coupling	26
4 The number of stable equilibria in equal-frequency Kuramoto models on planar graphs	37
4.1 Bound on the number of stable fixed points	40
4.2 Angle differences exceeding $\pi/2$	42
5 Protected loop flows	45
5.1 Process 1: Creating Loop Flows via Change of Natural Frequencies	45
5.2 Process 2: Creating Loop Flows via Edge Removing	48
5.3 Process 3: Creating Loop Flows via Edge Addition	49
6 The size of the sync basin revisited	53
6.1 Identical frequencies: Analytical approach	54
6.2 Identical frequencies: Numerical approach	56
6.3 The size of the sync basin revisited	57
6.4 Non-identical frequencies	59
6.5 Meshed networks	60
6.5.1 Identifying stable fixed points	61
6.5.2 Estimating the volume of basins of attraction	62
7 Bridging the gap between Kuramoto and electrical networks	65
7.1 Non-identical coupling	65
7.2 Second-order dynamics	66
7.3 Dissipative lines	67
8 Conclusion	73

Acknowledgments

First of all, I deeply thank Philippe Jacquod for his supervision along these three and a half years. He committed himself to give me a space of freedom for my research. He managed to keep a healthy balance between supervision to keep me focused and freedom in my work to let me be creative. He taught me most of what I know about research and academia to this day and his influence will follow me in my future researches.

I am very grateful to my supervisors in Geneva as well, Yvan Velenik, David Cimasoni and Jean-Pierre Eckmann. Since the first moment of my PhD they trusted me without hesitation and kept their doors open to talk with me at each of my drops in Geneva.

I thank Florian Dörfler, who did not hesitate to host me at the IfA in ETHZ for three months. He has been and still is very available for discussions, that sometimes took significant parts of our days, and he is never short on new creative ideas. This time in Zürich was an opportunity to meet many interesting people. I thank Marcello, Jeremy, Enrique, Ilnura and Ashish for the time shared during my intense stay in Zürich.

Many thanks go to my colleagues in Sion. To Tommaso for his constant and subtle supervision, and for all the tips and tricks to be a good PhD student. To Laurent and Melvyn for all the constructive and deconstructive, funny and serious discussions that took place between the office A301b, Serge's cafeteria and building G. To the ones who make the School of Engineering a great place to work, ordered by increasing walking distance from my desk: David T., Didier, Pablo, Lucas, Frédéric, David M., Vincent, Sébastien. Last but not least, to the two most reliable people in this school, Véronique and Aline.

I also thank my friends in the Valais how welcomed me in this beautiful region. My (very) old friends Sylvain and Justine, my co-gardeners and my basketball team, who created a pleasant social network in the Valais. I especially thank my flatmate Yao, with whom I met (a part of) Chinese culture.

I kept a home at the 2-4 Rue du Lièvre in Geneva, thank to my thirsty friends of the Section de Math, Elise, Mounir, Anthony, Jérémie, Sébastien, Joakim and Anders. At each of my surprise appearances in their offices, I always found one of them available for a coffee, a beer or more. Thank you all for the (too rare) awesome moments shared in Calvin's city.

When tired of working with my brain, I knew I could always count on my mountain friends, Raph, Sarah, Ophélie, Olivier, Yannick and Kevin, to wake me up early on week-ends and to go climb one of the many summits of the Alps. Exhausting for the body, but relaxing for the brain, all the outdoor activities played a crucial role in the achievement of my thesis.

A very special thank goes to Elodie, with whom I walk, cycle, fly, paddle, ski, telemark, dance, sail. In short, everything that prevents me to get bored. Along these last years she managed to keep me as far as possible from my work, keeping my mind healthy and boosting my creativity when coming back to it.

Finally, I thank my family. My grandmother who shares with me her world of yesterday. My parents, who paved my path to this day. My brother and sister who show me the possible worlds for tomorrow.

To Granny and Grampy.

Foreword

The aim of the project I joined at the begining of my PhD in 2014 is to investigate how the Energy Transition will impact the electrical network in Switzerland, in particular at the high voltage level. The ongoing Energy Transition aims at getting rid of fossil and/or nuclear energy sources, which we call *conventional*, for various reasons such as environmental, security or financial issues. Despite the increasing energy efficiency of most of our devices and processes, their increasing number results in an non-decreasing energy consumption [1]. To achieve the Energy Transition, we then have to rely on new energy sources. In Switzerland, as in most of the developed countries, the more promising energy sources are photovoltaic solar panels and wind turbines [2], referred to as *new renewables*.

The intrinsic natures of conventional and new renewable energy sources imply some fundamental changes in the way electricity is produced, transmitted and distributed as the penetration of photovoltaic and wind turbines increases, replacing fossil sources of energy and nuclear power plants. Switching from conventional sources of energy to renewable ones implies a transition from a few large centralized power plants providing a large amount of power to many small energy sources, scattered over large regions, modifying the size and location of electricity producers. The direction of power flows changes as well with the increasing amount of power produced, by individual solar panels for instance. And finally, renewable resources are known to fluctuate on time scales ranging from a minute to a year.

These changes of location of resources, direction of power flows and fluctuation of production raise the concern about stability of the electrical network. In order to better understand stability properties of electrical networks, I focused on the equations used by electrical engineers to describe the dynamics of voltages in electrical networks, namely the *swing equations* [3]. Having a background in mathematics, I prioritized an analytical approach. Simplifying the swing equations under several assumptions detailed in Section 1.1, emphasizes that the question of the stability of high voltage electrical networks is related to the question of synchronization in networks of coupled oscillators.

For this reason, most of the work during my PhD is related to the Kuramoto model, which is the canonical model to describe synchronization phenomena. It combines a simple and explicit definition with some rather rich and complex behaviors, and it is a first step toward a better understanding of the swing equations and the dynamics of electrical networks.

1 Introduction

For the sake of readability, technical and detailed definitions are postponed to further sections. Some terms in this introductory part are then used before being properly defined. We refer the reader to Section 2 for most of the formal definitions.

Most power grids are alternating current (AC) electric networks. Power grids span different voltage levels, separated by transformers which, to a good approximation, conserve power but neither current nor voltage. Electrical networks can be modeled as graphs with n vertices (called *buses* in this context), corresponding to transformers, where each vertex $i = 1, \dots, n$ injects (resp. consumes) a certain amount of active power $P_i \geq 0$ (resp. $P_i < 0$). The edges of the graph represent electrical lines characterized by a conductance G and a susceptance B , which determine the amount of power that can be transported through the line, and the amount of power that is dissipated by ohmic losses along the line. The control variables are the injected and consumed powers at the buses of the network, therefore the equations governing the behavior of the system are expressed in terms of electric powers and not currents. In AC electric networks, current and voltage are alternating quantities which we model as sinusoidal oscillators

$$i_j(t) = |I_j| \cos(\omega t + \varphi_j), \quad v_j(t) = |V_j| \cos(\omega t + \theta_j), \quad (1.1)$$

where φ_j and θ_j are phase shifts with respect to a reference frame, and ω is the network's angular frequency (ω being $2\pi \cdot 50$ [Hz] in Europe and $2\pi \cdot 60$ [Hz] in Northern America). In normal operation of the network, these quantities rotate with the same frequency everywhere in the network, ω is then the same at all buses and the system is said to be synchronized, meaning that all angles rotate at the same velocity. Considering a generating power plant, the change of kinetic energy of the rotating machines is given by the **swing equations** [3], which take into account a damping term, which is proportional to the velocity of the machine, and the balance between the mechanical power generated and the electrical power transmitted

$$I_i \ddot{\theta}_i + D_i \dot{\theta}_i = P_i - \sum_{j=1}^n |V_i| |V_j| [G_{ij} \cos(\theta_i - \theta_j) + B_{ij} \sin(\theta_i - \theta_j)], \quad i = 1, \dots, n, \quad (1.2)$$

where G_{ij} and B_{ij} are the elements of the conductance and susceptance matrices respectively [4], with $G_{ii} = -\sum_j G_{ij}$ and $B_{ii} = -\sum_j B_{ij}$, θ_i is the angle of the voltage at bus i , and I_i and D_i are inertia and damping coefficient at bus i . Assessing the stability of a network requires then to understand Eq. (1.2). Let allow ourselves some simplifying assumptions to tackle analytically these dynamics.

1.1 From the swing equations to the Kuramoto model

We are interested in the stability properties of synchronous states of Eq. (1.2). To begin with, we can then neglect the second-order term, which does not influence stability of synchronous states (note that the inertia term influences stability time scales [3, 5]), and we will consider homogeneous dampings D_i , such that we can factor them out. In most of our discussion we make a second approximation and consider networks of purely susceptive, i.e. lossless, lines with $G_{ij} = 0$. This is a leading order approximation in the small parameter $G_{ij}/B_{ij} < 0.1$ valid for very high voltage networks. With this approximation, lines have no ohmic losses and all buses are at the same voltage. In Section 7.3, we relax this assumption and investigate how some of our results remain valid with such dynamics. For the sake of readability, we will gather the voltage amplitudes and the susceptance in a unique parameter $K_{ij} := |V_i| |V_j| B_{ij}$. With these approximations, Eq. (1.2) yields

$$\dot{\theta}_i = P_i - \sum_{j=1}^n K_{ij} \sin(\theta_i - \theta_j), \quad i = 1, \dots, n, \quad (1.3)$$

where K_{ij} is non-zero if and only if buses i and j are connected in the electrical network under consideration.

Under the assumption that angle differences are small (which is true in electrical networks), Eq. (1.3) can be further simplified, by linearizing the sine function, which yields

$$\dot{\theta}_i = P_i - \sum_{j=1}^n K_{ij}(\theta_i - \theta_j), \quad i = 1, \dots, n, \quad (1.4)$$

which gives, in matricial form,

$$\dot{\vec{\theta}} = \vec{P} - \mathbb{L}_{\mathcal{G}} \vec{\theta}, \quad (1.5)$$

where $\mathbb{L}_{\mathcal{G}} \in \mathbb{R}^{n \times n}$ is the Laplacian matrix of graph \mathcal{G} with edge weights K_{ij} , $\vec{\theta} = (\theta_1, \dots, \theta_n)^T \in \mathbb{R}^n$ and $\vec{P} = (P_1, \dots, P_n)^T \in \mathbb{R}^n$. Such Laplacian dynamics are well understood, and it is clear that Eq. (1.5) has at most one fixed point (up to a constant shift of all angles), and the stability of this fixed point is determined by the signs of the eigenvalues of $\mathbb{L}_{\mathcal{G}}$.

The fixed points of Eq. (1.3) are the solutions of a set of transcendental equations

$$P_i = \sum_{j=1}^n K_{ij} \sin(\theta_i - \theta_j), \quad i = 1, \dots, n, \quad (1.6)$$

which can admit multiple solutions. After the linearization giving Eq. (1.5), the richness of solutions of Eq. (1.6) is lost. The linearized Eq. (1.5) then oversimplifies the dynamics. To preserve the multiplicity of fixed points, this work will focus on Eq. (1.3), which is a generalized version of the *Kuramoto model*. It might still seem oversimplified to accurately describe the voltage dynamics in electrical networks, but we believe that understanding the dynamics of Eq. (1.3) will give some insight to better understand and describe the dynamics of the more accurate Eq. (1.2).

1.2 Synchronization and the Kuramoto model

Synchronization occurs when a group of heterogeneous time-varying objects follow the same dynamics, due to some interactions between them. Synchronization phenomena appear in a wide variety of natural and artificial systems. The scale of these synchronizing systems ranges from the size of human cells, with the synchronization of neurons in Parkinson's disease, to the size of continents, with synchronous AC power grids.

Scientific interest in such phenomena can be traced back to the end of the XVIIth century with the work of Christiaan Huygens [6], who observed that two connected pendulum clocks, initially out of phase, ended up synchronizing. Along the XXth century, various models were developed to describe synchronizing behaviors such as Van der Pol oscillators [7] or Stuart-Landau oscillators [8]. In 1967, Arthur T. Winfree defined and investigated a mathematical model of coupled dynamical agents [9]. He managed to prove the existence of a phase transition between incoherence of the individuals' trajectories and synchrony when the coupling strength is increased. However, his model was too general to be analytically tractable and to obtain more precise results.

Refining Winfree's model, in 1975, Yoshiki Kuramoto [10] considered a system of n coupled oscillators, each described by an angle θ_i , whose dynamics is

$$\dot{\theta}_i = P_i - \frac{K}{n} \sum_{j=1}^n \sin(\theta_i - \theta_j), \quad i = 1, \dots, n, \quad (1.7)$$

where $P_i \in \mathbb{R}$ is the i^{th} oscillator's natural frequency and $K \geq 0$ is the coupling strength.

In [10, 11], based on a mean-field approach, Kuramoto proved that there exists a coupling strength K_s such that if $K > K_s$, then a finite fraction of the oscillators synchronize. Furthermore, if the support of the distribution of natural frequencies is included in a bounded interval, then there exists a critical coupling strength K_c such that full synchronization, $\dot{\theta}_i = \dot{\theta}_j$ for all i, j , is achieved if $K > K_c$ [12, 13].

Kuramoto's mean-field approach relies on the definition of an order parameter

$$re^{i\psi} := \frac{1}{n} \sum_{j=1}^n e^{i\theta_j}, \quad (1.8)$$

which can be splitted in real and imaginary parts

$$r \cos(\psi) = \frac{1}{n} \sum_{j=1}^n \cos(\theta_j), \quad r \sin(\psi) = \frac{1}{n} \sum_{j=1}^n \sin(\theta_j). \quad (1.9)$$

By definition, $r \in [0, 1]$ and $\psi \in (-\pi, \pi]$. Replacing this order parameter in Eq. (1.7) yields

$$\dot{\theta}_i = P_i - Kr \sin(\theta_i - \psi). \quad (1.10)$$

Assuming constant r as $t \rightarrow \infty$, and bounded natural frequencies, Kuramoto [11] proved the existence of synchronous state for large enough K . The assumption of constant r was validated later by a time scale separation argument [14].

The simple expression of Eq. (1.7) makes the Kuramoto model very tractable. Nonetheless, the nonlinearity of the interactions allows it to capture non-trivial synchronization behaviors. The trade-off between simple formulation and complex behavior makes it a powerful tool to better understand synchronization phenomena, and the interest for the Kuramoto model increased significantly during the last decades.

It turned out that many real-world synchronizing systems can be approximated by the Kuramoto model, at least in a first order approximation. Among others, biological synchronizing systems encompass groups of fireflies flashing in unison [15, 16], firing neurons in the brain, where synchronization is related to the occurrence of Parkinson's disease [17] or epilepsy [18], or cells of the brain governing the circadian rhythm in mammals [19]. The Kuramoto model also describes some synchronizing systems observed in chemistry and physics, such as arrays of coupled Josephson junctions [20, 21] or chemical reactions oscillations [8]. Some human-made system also exhibit synchronizing behavior that can be modeled by the Kuramoto model, such as clocks in decentralized computing networks [22, 23, 24] and droop-controlled inverters in microgrids [25]. The largest human-made synchronous systems to this day are undoubtedly continental-scale high voltage AC power grids [26]. In this manuscript, we consider the Kuramoto model as first order approximation of the swing equations [3], describing the voltage dynamics at the buses in AC power grids.

Eq. (1.7) assumes all-to-all identical coupling, meaning that each oscillator interacts with the same strength with all other oscillators. This approximation is quite accurate for densely connected systems, but many synchronizing systems, and AC power grids in particular, often display sparse or even planar interconnections, with heterogeneous couplings. The interest drawn by the Kuramoto model in many applications generated some variations of its initial formulation Eq. (1.7). A more general version of it considers a weighted coupling graph, where the weight of an edge $\langle ij \rangle$ is the coupling strength K_{ij} between oscillators i and j . The oscillators' dynamics are then given by Eq. (1.3). For the sake of simplicity, from now on, we will consider identical couplings, $K_{ij} \equiv K$ for all connected vertices i and j , and $K_{ij} = 0$ otherwise. Eq. (1.3) then yields

$$\dot{\theta}_i = P_i - K \sum_{j=1}^n a_{ij} \sin(\theta_i - \theta_j), \quad i = 1, \dots, n, \quad (1.11)$$

where a_{ij} is the element in the i^{th} row and j^{th} column of the adjacency matrix. We argue in Section 7.1 that assuming identical couplings does not jeopardize our results. Other generalizations and refinements of the Kuramoto model have been investigated to this day, such as time-varying natural frequencies or couplings [27], interactions with delay [28] or second-order Kuramoto models [26]. See [29, 30, 31] for extensive surveys.

In the general case of sparse coupling, the mean-field approach breaks down and the existence of a synchronous state does not depend only on the distribution of natural frequencies, but on the interaction graph as well. Some sufficient conditions for the existence of a synchronous state on general interaction graphs were given in [26, 31, 32, 33]. More recently, Jafarpour and Bullo derived a new sufficient condition improving all previous ones [34]. Theorem 13 in [34] gives an explicit inequality, involving the distribution frequencies and the interaction graph, which, if satisfied, guarantees the existence of a stable synchronous state.

The relevance of synchronous states in applications of the Kuramoto model depends on their dynamical stability properties. A state in any physical system remains synchronous only if it is

Reference	Stability of fixed points considered	Number of fixed points bounded by	Conditions on the graph
[41]	Stable & unstable	$\propto 2^{n-1}$	Any network
[42]	Stable & unstable	$\binom{2n-2}{n-1}$	Any network
[44]	Stable	$2 \cdot \text{Int}(n/4) + 1$	Cycles, directed coupling
[45]	Stable	$2 \cdot \text{Int}(n/4) + 1$	Cycles, $\Delta_{ij} < \pi/2, \forall \langle ij \rangle$
[46, 47]	Stable & unstable	$\propto 2^n$	Any network
	Stable	$\ll 2^n$	Any network
[48] & Sec. 3	Stable	$2 \cdot \text{Int}((n-1)/4) + 1$	Cycles
[49] & Sec. 4	Stable	$\prod_{k=1}^c [2 \cdot \text{Int}(n_k/4) + 1]$	Planar, $\Delta_{ij} < \pi/2, \forall \langle ij \rangle$

Table 1: Existing bounds on the number of stable fixed points of the Kuramoto model.

robust against perturbations imposed by the environment. We are then interested to characterize *linearly stable* synchronous states. It has been shown that there is a unique stable synchronous state for all-to-all coupling, Eq. (1.7), with $K > K_c$ [35, 36], as well as for identical natural frequencies if the network is sufficiently connected [37]. In this case “sufficiently connected” means that the degree of each vertex of the network is larger than $0.9395 \cdot (n - 1)$.

When the interaction graph is sparser, more stable synchronous states may appear. The question of the number of stable synchronous states can be traced back at least to 1972 with the work of Korsak [38], and of Tavora and Smith [39]. Both articles give examples of networks where Eq. (1.2) admits multiple stable fixed points, i.e. synchronous states, and show that, when seen as power flows on electrical lines, they correspond to different current circulating around the cycles of the network. In [40], the authors numerically explore the number of synchronous states for a cycle of coupled oscillators. Following Korsak’s work, some bounds on the number of such fixed points were given, which we summarize in Table 1. In [41], the authors discuss the existence of, a priori, 2^{n-1} fixed points for Eq. (1.3). Baillieul and Byrnes [42], used Morse theory [43] to show that the number of synchronous states of Eq. (1.3) for general interaction graphs, and consequently the number of such stable synchronous states, is upper bounded by $\binom{2n-2}{n-1}$. More recently, Rogge and Aeyels [44] gave an upper bound to the number of stable synchronous states in cycles of coupled oscillators with directed interactions. They showed that such networks have at most $2 \cdot \text{Int}[(n-1)/4] + 1$ stable synchronous states. Ochab and Góra [45] obtained the same bound for undirected couplings, provided that we consider only states where the angles differences are lower than $\pi/2$. Based on algebraic geometrization methods, Mehta et al. [46, 47] obtained an upper bound proportional to 2^n for the number of fixed points of Eq. (1.3), for any interaction graph. They numerically showed as well that the number of stable fixed points is much smaller than this bound.

Algebraic geometrization consists in rewriting Eq. (1.3) as polynomials in trigonometric functions of angles. The method provides a list of candidate fixed points of Eq. (1.3) whose stability needs to be confirmed or discarded numerically. This method guarantees that all fixed points are found but leads to a bound on the number of stable fixed points which is exponential in the number n of oscillators.

Exponential bounds are easy to understand qualitatively since new fixed point solutions to Eq. (1.3) can be obtained in principle from any known fixed point solution by replacing $\theta_i - \theta_j$ by $\pi - (\theta_i - \theta_j)$ for any edge $\langle ij \rangle$. The latter substitution leads to an exponential number $\propto 2^n$ of fixed point solutions. It is expectable that much better bounds exist.

The bound by Rogge and Aeyels [44], and the one by Ochab and Góra [45] both directly rely on the concept of *winding numbers*. The winding number on a cycle of a network of Kuramoto oscillators is the integer that, once multiplied by 2π , is equal to the sum of the consecutive angle differences along the edges of the cycle. Different synchronous states are characterized by different winding numbers on the cycles of the network under consideration. This concept in the scope of Kuramoto oscillators was initially mentioned by Lüders in a referee discussion at the end of [38] as well as by Ermentrout in [12]. But as far as we know, Janssens and Kamagata [50] were the first

to formally characterize the different stable synchronous states of a cycle of Kuramoto oscillators by winding numbers. Roy and Lahiri [51] classified the synchronous states of Eq. (1.3) on a cycle, based on the winding number q and the number ℓ of angle differences larger than $\pi/2$.

The winding numbers of fixed points are directly related to *loop flows* (defined in Section 2.1), which, according to Theorem 2.3 and [26, Supporting Information, Theorem 1], relate the different fixed points of Eq. (1.11)

Winding numbers and loop flows are a key ingredient in investigating the multiplicity of stable fixed points of Eq. (1.3) as they are invariants of fixed points. Namely, if two states $\vec{\theta}^*$ and $\vec{\theta}^{**}$ represent the same fixed point, then their winding numbers on each cycle are the same. Two stable fixed points can then be distinguished by their winding numbers, if the latter are not the same. However, it still unclear if the winding numbers are perfect invariants, in the sense that we do not know if two different fixed points necessarily have different winding numbers. In Section 4 we give some condition under which the winding numbers are perfect invariants.

1.3 Overview of the results

The results presented in this manuscript are twofolds. Sections 3 and 4 focus on the number of stable fixed points of Eq. (1.3). The approach therein is static, and the dynamics only determine the linear stability of the fixed points. Sections 5 and 6 are concerned about the dynamical properties of Eq. (1.3). Investigating the trajectories of the system is complicated to tackle in general, these two Sections then largely rely on numerical simulations.

In Section 3, we extend the bound $2 \cdot \text{Int}[(n - 1)/4] + 1$ on the number of stable synchronous states for the Kuramoto model on a cycle with arbitrary natural frequencies, obtained in [45] to any stable fixed point (not limited to angle differences lower than $\pi/2$). To prove this, based on a lemma by Taylor [37, Lemma 2.1], we show that a stable synchronous state has at most one angle difference larger than $\pi/2$. We prove as well that for a cycle network with identical frequencies, a fixed point with one angle difference larger than $\pi/2$ is necessarily unstable, but that cycle networks with non-identical frequencies may have some stable fixed points with one angle difference larger than $\pi/2$.

In Section 4, we generalize this bound to planar networks with identical frequencies, with the caveat that it applies only to stable synchronous states with all angle differences less than $\pi/2$. We also characterize classes of planar graphs where stable synchronous states necessarily have all angle differences below $\pi/2$. For such networks, our bound is then the upper bound on the number of stable fixed point, regardless of the angle differences. Finally we give some examples of planar graphs where there exists stable synchronous states with some angle differences larger than $\pi/2$ and show that for some of them, the number of stable fixed points is larger than our bound.

As soon as we know that a dynamical system may possess multiple stable fixed points, some natural questions are raised. First, we are interested in describing some mechanisms bringing the system from a stable fixed point to another. According to simulations, time-varying natural frequencies can do this [27]. In Section 5, we perform numerical simulations describing three mechanisms bringing some oscillators systems from a stable fixed point to another. It turns out that these changes of fixed points need some strong modifications of the network to occur, such as saturation of the coupling strength between two oscillators, or the deletion or addition of an edge. We show as well that after such a drastic modification of the network, bringing the system back to its initial state is not an easy task, and in particular it cannot be done by a smooth change of the parameters.

Second, a natural question that is raised is to assess the relative stability of the different fixed points. A measure of the stability of a fixed point in a dynamical system is the volume of its basin of attraction. The basin of attraction of a fixed point is the set of initial conditions that converge to this fixed point. If a fixed point is stable, it means that there is a subdomain of the state space with finite measure where all initial conditions dynamically converge to the fixed point. It is a fair assumption to say that the larger the basin of attraction, the more likely it is to reach the corresponding fixed point dynamically. This gives a global measure of the stability of a fixed point.

Considering a cycle of Kuramoto oscillators, Wiley et al. [52] numerically estimated the volume of the basins of attraction of the various stable fixed points. Taking random initial conditions, and dynamically evolving them, they find a Gaussian relation between the winding number and the

volume of the basin of attraction. In Section 6, building on our knowledge of the fixed points of Eq. (1.3) on a cycle, we propose a new method to estimate these volume and find a exponential relation between the winding number and the volume of the basin of attraction.

Finally, in Section 7 we review the assumptions made in the preliminary Section 2 and try to show how our results extend (or not) if these assumptions are relaxed.

2 Preliminaries

After briefly recalling basic definitions of graph theory, we define the fundamental concepts needed for the remainder of the manuscript, such as loop flows and winding numbers.

Definition 2.1. A **graph** $\mathcal{G} = (\mathcal{V}_\mathcal{G}, \mathcal{E}_\mathcal{G})$ is a set of vertices $\mathcal{V}_\mathcal{G} = \{1, \dots, n\}$, denoted as indices, with a set of edges $\mathcal{E}_\mathcal{G} \subset \mathcal{V}_\mathcal{G} \times \mathcal{V}_\mathcal{G}$, each of which is an unordered pair of connected vertices. The number of vertices is $n = |\mathcal{V}_\mathcal{G}|$ and the number of edges is $m = |\mathcal{E}_\mathcal{G}|$. For $i, j \in \mathcal{V}_\mathcal{G}$, the edge connecting i to j is $\langle ij \rangle \in \mathcal{E}_\mathcal{G}$. A **path** from vertex i to vertex j in a graph \mathcal{G} is a sequence \mathcal{P} of edges in $\mathcal{E}_\mathcal{G}$,

$$\mathcal{P} = (\langle ii_1 \rangle, \langle i_1 i_2 \rangle, \dots, \langle i_{\ell-1} j \rangle) . \quad (2.1)$$

A path can as well be defined as a sequence of vertices

$$\tilde{\mathcal{P}} = (i, i_1, \dots, i_{\ell-1}, j) , \quad (2.2)$$

such that $\langle i_k i_{k+1} \rangle \in \mathcal{E}_\mathcal{G}$, for all k . A graph is **connected** if for any two vertices $i, j \in \mathcal{V}_\mathcal{G}$ there exists a path from i to j . A **cycle** in a graph is a path from a vertex to itself going at most once through any edge. A **tree** is a connected graph with no cycle. Given a graph $\mathcal{G} = (\mathcal{V}_\mathcal{G}, \mathcal{E}_\mathcal{G})$, a **spanning tree** \mathcal{T} of \mathcal{G} is a tree such that $\mathcal{V}_\mathcal{T} = \mathcal{V}_\mathcal{G}$ and $\mathcal{E}_\mathcal{T} \subset \mathcal{E}_\mathcal{G}$. The **adjacency matrix** $A \in \mathbb{R}^{n \times n}$ of a graph \mathcal{G} has elements

$$a_{ij} := \begin{cases} 1, & \text{if } \langle ij \rangle \in \mathcal{E}_\mathcal{G} , \\ 0, & \text{otherwise.} \end{cases} \quad (2.3)$$

As edges of \mathcal{G} are unordered pairs of vertices, the adjacency matrix is symmetric. An **orientation** $O_\mathcal{G}$ of a graph is the choice, for each edge, of a **source** vertex and of a **target** vertex. Given any orientation of the graph \mathcal{G} , its **incidence matrix** $B \in \mathbb{R}^{n \times m}$ is defined by

$$b_{i\ell} := \begin{cases} 1, & \text{if vertex } i \text{ is the source of edge } \ell , \\ -1, & \text{if vertex } i \text{ is the target of edge } \ell , \\ 0, & \text{otherwise.} \end{cases} \quad (2.4)$$

Remark. A tree with n vertices has exactly $n - 1$ edges.

In what follows, we use the term **network** to denote physical objects. When referring to networks, we mean the whole system composed of oscillators whose interactions are given by a graph, coupling strengths are K_{ij} 's and natural frequencies are P_i 's.

Each vertex i of the graph \mathcal{G} represents an oscillator, which is a point on the circle \mathbb{S}^1 , whose position is given by an angle $\theta_i \in \mathbb{R}$. We define it as a real number, but any shift of 2π gives an equivalent position of the oscillator on the circle as shown in Figure 1. The **Kuramoto model** on \mathcal{G} is the dynamical system defined by the differential equations

$$\dot{\theta}_i = P_i - K \sum_{j=1}^n a_{ij} \sin(\theta_i - \theta_j) , \quad i = 1, \dots, n , \quad (2.5)$$

where $P_i \in \mathbb{R}$ is the **natural frequency** of oscillator θ_i , and $K \in \mathbb{R}$ is the **coupling** between oscillators which is the same between any pair of coupled oscillators. A **state** of the dynamical system described by Eq. (2.5) is a vector $\vec{\theta} \in \mathbb{R}^n$, which can naturally be mapped to a point of the n -torus \mathbb{T}^n . Hence it can be seen as a compact variable. Furthermore, the dynamics depends only on angle differences, thus any constant shift of all angles $\vec{\theta} + (\phi, \dots, \phi)^\top$ gives an equivalent state according to the dynamics of Eq. (2.5). From now on we then consider any state $\vec{\theta}$ where

$$\theta_i = \theta_i^* + 2\pi k_i + \phi , \quad i = 1, \dots, n , \quad (2.6)$$

where $k_i \in \mathbb{Z}$ and $\phi \in \mathbb{R}$, as equivalent to the state $\vec{\theta}^*$.

When dissipation is neglected in an electrical network [i.e. the conductance $G_{ij} = 0$ in Eq. (1.2)], power injections and consumptions are balanced,

$$\sum_i P_i = 0 , \quad (2.7)$$

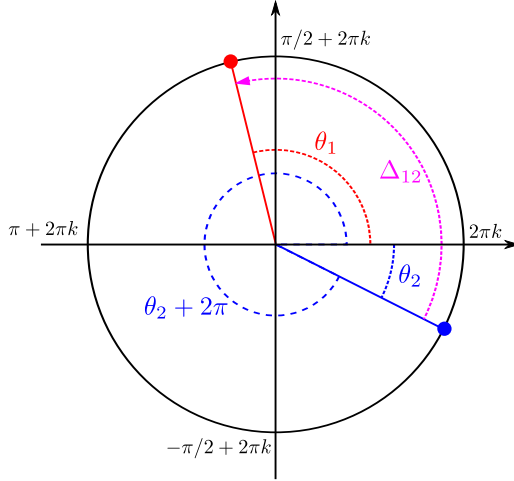


Figure 1: *Oscillators represented on the circle (black line). The two blue dashed lines are two equivalent values for oscillator θ_2 . The purple dashed line is the angle difference Δ_{12} between oscillators θ_1 and θ_2 , by definition it is contained in the interval $(-\pi, \pi]$. Coordinates are defined up to a shift of $2\pi k$, $k \in \mathbb{Z}$.*

and this can be assumed without loss of generality for the natural frequencies of any system of Kuramoto oscillators. The mean frequency P_0 of oscillators is preserved by the dynamics Eq. (2.5),

$$\sum_{i=1}^n \dot{\theta}_i = \sum_{i=1}^n P_i - K \sum_{i,j=1}^n a_{ij} \sin(\theta_i - \theta_j) = \sum_{i=1}^n P_i = nP_0. \quad (2.8)$$

We can then consider all oscillators in a frame rotating at the mean natural frequency, changing the variable θ_i to $\theta_i + P_0 t$. The individual natural frequencies are then considered as deviations from the mean natural frequency. The sum of natural frequencies vanishes, and the mean frequency of the system is then zero.

Definition 2.2. *Two oscillators i and j are said to be **synchronized** if they rotate at the same velocity, i.e. $\dot{\theta}_i(t) = \dot{\theta}_j(t)$ for all $t \geq 0$. The dynamical system described by Eq. (2.5) is said to be **synchronized** if all its oscillators are synchronized. In this case, the system is at a **synchronous state**.*

As the number of oscillators is finite, the natural frequencies are distributed on the interval $[P_{\min}, P_{\max}]$. The support of the distribution of frequencies is then compact, which is a necessary condition to achieve full synchrony [12, 13]. The mean frequency being zero at all time, it implies that at a synchronous state, all oscillators have zero frequency. A synchronous state is then an equilibrium of Eq. (2.5) and solves

$$P_i = K \sum_{j=1}^n a_{ij} \sin(\theta_i - \theta_j), \quad i = 1, \dots, n, \quad (2.9)$$

which are the **power flow equations** of [4] after our simplifying assumptions of Section 1.1.

In the context of electrical networks, natural frequencies correspond to power injections ($P_i \geq 0$) or power consumptions ($P_i < 0$) at the vertices of the graph. From this point of view, the strength of the interaction between oscillators i and j ,

$$P_{ij} = K a_{ij} \sin(\theta_i - \theta_j), \quad (2.10)$$

is the magnitude of a power flow from i to j , which we will often call the **flow** from i to j . With this notation, Eq. (2.9) reads

$$P_i = \sum_{j=1}^n P_{ij}, \quad i = 1, \dots, n, \quad (2.11)$$

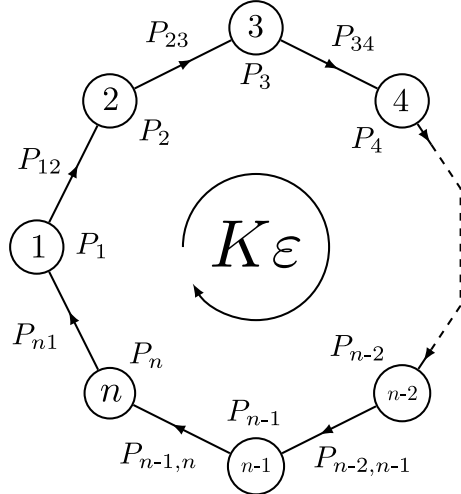


Figure 2: (Figure taken from [48]) Cycle network of length n . Oscillator i has natural frequency P_i , while a flow of magnitude P_{ij} runs along edge $\langle ij \rangle$. Edges correspond to couplings of strength K . A loop flow of intensity $K\varepsilon$ is circulating around the cycle, where $\varepsilon \in \mathbb{R}$.

which is a version of Kirchhoff's current law. We remark that the value of the flow on an edge $\langle ij \rangle$ is bounded, in absolute value, by $K a_{ij}$.

2.1 Loop flows

Indexing the vertices along a cycle of the network, we write $P_{i,i+1}$ the flow from vertex i to vertex $i + 1$, with indices taken modulo n . We define **loop flows** as constant flows circulating around a cycle in the network.

For identical natural frequencies, $P_i \equiv 0$, a loop flow is given by a constant value of $P_{i,i+1} = K\varepsilon$ for all i , where $\varepsilon \in \mathbb{R}$ is called the **loop flow parameter**. More generally, for finite natural frequencies, any flow $\{P_{i,i+1}\}$ on a cycle can be written as the sum of a reference flow, characterized by a reference flow $\{P_{i,i+1}^*\}$, and a loop flow of intensity $K\varepsilon$, circulating around the cycle (see Figure 2),

$$P_{i,i+1} = P_{i,i+1}^* + K\varepsilon. \quad (2.12)$$

It is only defined with respect to the reference flow, which can be conveniently constructed on cyclic networks from the P_i 's as

$$P_{i,i+1}^* := \sum_{j=1}^i P_j, \quad i = 1, \dots, n. \quad (2.13)$$

Similarly, on any network, such a reference flow can be constructed recursively on any spanning tree. Note that this reference flow depends on vertex numbering and any other flow distribution satisfying Kirchhoff's currents law, Eq. (2.11), can be taken as reference flow.

We show now that different solutions of Eq. (2.9) for any network differ only by circulating loop flows. This rigorous result, which appeared in slightly different form in [26], sheds light on the common wisdom that Eq. (2.5) may have multiple stable fixed points for meshed networks [38, 44, 45, 50, 52].

Let \mathcal{G} be a graph and $O_{\mathcal{G}}$ an arbitrary orientation of this graph. The positive direction of an edge is the one going from the source to the target, the other direction being negative. Consider the m -dimensional real vector space $C_1(\mathcal{G}; \mathbb{R})$ of flows, y_{ij} , on the m edges of a graph \mathcal{G} . It is the

vector space of formal sums of edges

$$C_1(\mathcal{G}; \mathbb{R}) := \left\{ \sum_{\langle ij \rangle \in \mathcal{E}_{\mathcal{G}}} y_{ij} \langle ij \rangle \mid y_{ij} \in \mathbb{R} \right\} \simeq \mathbb{R}^m, \quad (2.14)$$

where the flow from i to j is minus the flow from j to i , $y_{ij} \langle ij \rangle = -y_{ji} \langle ji \rangle$. We equivalently define the n -dimensional vector space of natural frequencies which is the vector space of formal sums of vertices

$$C_0(\mathcal{G}; \mathbb{R}) := \left\{ \sum_{i \in \mathcal{V}_{\mathcal{G}}} x_i i \mid x_i \in \mathbb{R} \right\} \simeq \mathbb{R}^n. \quad (2.15)$$

The component v_{ℓ} of a flow vector $\vec{v} \in C_1$ describes the intensity of the flow on the ℓ^{th} edge of \mathcal{G} , with $v_{\ell} > 0$ if the direction of the flow agrees with the orientation of this edge given by $O_{\mathcal{G}}$, and $v_{\ell} < 0$ otherwise. The canonical basis of C_1 is the set of flow vectors $\vec{v}^{(\ell)}$, $\ell = 1, \dots, m$, with unit flow on edge ℓ and zero flow on all other edges. Given a vector of natural frequencies at every vertex,

$$\vec{P} = (P_1, \dots, P_n) \in C_0(\mathcal{G}; \mathbb{R}), \quad (2.16)$$

a flow vector $\vec{v} \in C_1$ satisfies Kirchhoff's current law Eq. (2.11) if

$$P_i = \sum_{\ell \in \mathcal{E}_{\mathcal{G}}} b_{i\ell} v_{\ell}, \quad i = 1, \dots, n, \quad (2.17)$$

where $b_{i\ell}$ are the elements of the incidence matrix defined in Eq. (2.4). We are now ready to formulate and prove our theorem.

Theorem 2.3. *Let $\mathcal{G} = (\mathcal{V}_{\mathcal{G}}, \mathcal{E}_{\mathcal{G}})$ be a connected graph with $|\mathcal{V}_{\mathcal{G}}| = n$ vertices and $|\mathcal{E}_{\mathcal{G}}| = m$ edges. Let $\vec{P} \in C_0$ be a vector of natural frequencies at each vertex whose components sum to zero. Then two distributions of flows on \mathcal{G} , represented by flow vectors \vec{v} and $\vec{w} \in C_1(\mathcal{G}; \mathbb{R})$ satisfying Kirchhoff's currents law, Eq. (2.17), differ by a combination of loop flows on the different cycles of \mathcal{G} .*

Connection with Algebraic Topology. From an topological point of view, the graph \mathcal{G} is a CW complex where the vertices are 0-cells and edges are 1-cells [53]. Elements of C_1 and C_0 are then 1-chains and 0-chains respectively. The linear map defined by the incidence matrix defines the boundary map $\partial: C_1 \rightarrow C_0$. We then obtain the chain complex

$$0 \xleftarrow{0} C_0(\mathcal{G}) \xleftarrow{\partial} C_1(\mathcal{G}) \xleftarrow{0} 0. \quad (2.18)$$

As both \vec{v} and \vec{w} satisfy Eq. (2.17) for \vec{P} , it means that $\partial(\vec{v}) = \partial(\vec{w})$. Thus the difference $\vec{v} - \vec{w}$ belongs to the kernel of ∂ which is exactly the first homology group of the graph \mathcal{G} .

Remark. *In particular, Theorem 2.3 implies that the flow distributions of two different solutions of Eq. (2.9) differ by a collection of loop flows. This result already appeared in slightly different form in the Supporting Information of [26].*

Proof. If $m = n - 1$, then \mathcal{G} is a tree and the flows on the edges are uniquely determined, which agrees with the statement because \mathcal{G} has no cycle. Therefore, from now on we assume $m \geq n$.

Let \mathcal{T} be a spanning tree of \mathcal{G} and let us number the edges of \mathcal{T} from 1 to $n - 1$ and the edges of $\mathcal{G} \setminus \mathcal{T}$ from n to m . Let $\vec{u} := \vec{v} - \vec{w}$ be the difference between the two flow vectors. Then, for any i we have

$$\sum_{\ell \in \mathcal{E}_{\mathcal{G}}} b_{i\ell} u_{\ell} = \sum_{\ell \in \mathcal{E}_{\mathcal{G}}} b_{i\ell} (v_{\ell} - w_{\ell}) = P_i - P_i = 0, \quad (2.19)$$

from which we conclude that \vec{u} is a solution of Eq. (2.17) with $\vec{P} = 0$.

Therefore, we need to show that any solution \vec{v} of the system of equations

$$\sum_{\ell \in \mathcal{E}_G} b_{i\ell} v_\ell = 0, \quad i = 1, \dots, n, \quad (2.20)$$

is a combination of loop flows. To do this we write Eq. (2.20) in matricial form,

$$\mathcal{B}\vec{v} = 0. \quad (2.21)$$

By definition, the set of solutions of Eq. (2.21) is the kernel of \mathcal{B} , which is a subspace of C_1 .

In algebraic graph theory, $\ker(\mathcal{B})$ is referred to as the **cycle space** and it is a standard result [54] that any element in $\ker(\mathcal{B})$ is a linear combination of unitary flows along the cycles of the network considered. This completes the proof. \square

Theorem 2.3 states in particular that multiple solutions to Eq. (2.9) can appear only when there are closed cycles in the network.

2.2 The winding number

Let $\vec{\theta} \in \mathbb{R}^n$ be a state of the system under consideration, and assume that the oscillators are numbered such that the sequence of vertices $\mathcal{C} = (1, 2, \dots, n_c, 1)$ is a cycle. Summing directly the angle differences around the cycle, we necessarily obtain zero,

$$(\theta_{n_c} - \theta_1) + \sum_{i=1}^{n_c-1} (\theta_i - \theta_{i+1}) = \sum_{i=1}^{n_c} (\theta_i - \theta_i) = 0. \quad (2.22)$$

In Eq. (1.3), only the sine of the angle differences are considered and angle differences can then be considered modulo 2π . For any pair of connected vertices i and j , we define then the angle difference

$$\Delta_{ij} := \theta_i - \theta_j + 2\pi k_{ij}, \quad (2.23)$$

where $k_{ij} \in \mathbb{Z}$ is the unique integer such that $\Delta_{ij} \in (-\pi, \pi]$. Summing the angle differences gives now

$$\Delta_{n_c 1} + \sum_{i=1}^{n_c-1} \Delta_{i,i+1} = \sum_{i=1}^{n_c} (\theta_i - \theta_{i+1} + 2\pi k_i) = 2\pi q(\vec{\theta}), \quad (2.24)$$

where $q \in \mathbb{Z}$ is a well-defined integer called **winding number**. It counts the number of times the angle winds around the origin in the complex plane as one travels around the cycle.

According to the definition of the angle differences $\Delta_{ij} \in (-\pi, \pi]$, the winding number q on a cycle of length n is necessarily bounded

$$-n/2 \leq q \leq n/2. \quad (2.25)$$

Remark. Eq. (2.24) is the natural discretization of the degree [55] of the continuous map

$$\begin{aligned} \gamma: \mathbb{S}^1 &\longrightarrow \mathbb{S}^1 \\ x &\longmapsto y, \end{aligned} \quad (2.26)$$

where x is the position on the cycle \mathcal{C} and y is the angle θ at location x . Parametrizing \mathbb{S}^1 as the interval $[0, 1]$ where 0 and 1 are identified, we position the vertices $i = 1, \dots, n$ at $x_i = i/n$ respectively. The function γ then takes value $[\theta_i]$ at x_i , where $[\cdot]: \mathbb{R} \rightarrow \mathbb{S}^1$ is the natural projection of the real line on the circle $\mathbb{S}^1 \simeq \mathbb{R}/2\pi\mathbb{Z}$. We then extend γ to the whole circle by linear interpolation between x_i and x_{i+1} ,

$$\gamma((1-\alpha)x_i + \alpha x_{i+1}) = (1-\alpha)[\theta_i] + \alpha[\theta_{i+1}], \quad (2.27)$$

with $\alpha \in [0, 1]$ and $i = 1, \dots, n$.

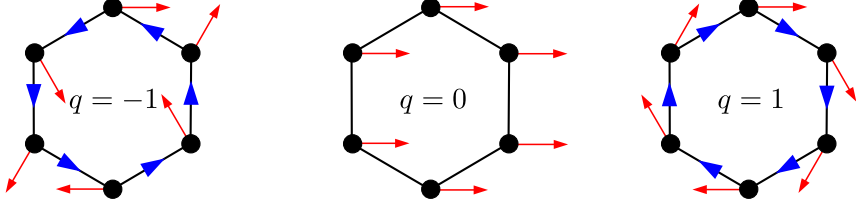


Figure 3: Three different loop flows on the same network, with identical frequencies. The red arrows represent the angles of the oscillators, and the blue arrows indicate the flows on the edges. Left: the winding number is $q = -1$ and the loop flow rotates counterclockwise. Center: the winding number is zero and there is no loop flow. Right: the winding number is $q = 1$ and the loop flow rotates clockwise.

Tavora and Smith [39] showed how loop flows are related to winding numbers. If the winding number of a state is non-zero on a cycle, $q > 0$ (resp. $q < 0$), then the average angle difference on the edges of the cycle is $\bar{\Delta} = 2\pi q/n$ and thus for most, if not all the edges of the cycle, we have a flow from i to $i + 1$ (resp. from $i + 1$ to i). Figure 3 illustrates an example of network with three different loop flow and how they are related to winding numbers. The correspondence between loop flows and winding numbers becomes clear when considering a fixed point on a cycle with identical frequencies. In this case, if $q \neq 0$, we have $\Delta_{i,i+1} = 2\pi q/n \neq 0$ for all i and the flow from i to $i + 1$ is

$$P_{i,i+1} = K \sin(2\pi q/n) \neq 0, \quad (2.28)$$

and we have a loop flow of magnitude $K \sin(2\pi q/n)$.

2.3 Linear and nonlinear stability

Most work on the stability of fixed points of dynamical systems rely on the seminal work of Aleksandr Lyapunov [56, 57] at the end of the XIXth century. Lyapunov first investigated *linear stability*, by linearizing the dynamics around a given fixed point. However, linear stability analysis is only valid locally. To overcome this limitation, Lyapunov came up with his second method, based on *Lyapunov functions*.

Linear stability. Consider a dynamical system in \mathbb{R}^n defined by the ordinary differential equation

$$\dot{\vec{x}} = f(\vec{x}), \quad (2.29)$$

where $\vec{x} \in \mathbb{R}^n$ and $f: \mathbb{R}^n \rightarrow \mathbb{R}^n$ is a vector field.

Remark. For the sake of brevity, we restrict our analysis to dynamical systems on Euclidean spaces, but all stability analysis naturally extend to dynamical systems on differentiable manifolds. Considering $\tilde{f}: \mathcal{M} \rightarrow T\mathcal{M}$ a vector field on a differentiable manifold \mathcal{M} , the dynamical system

$$\dot{y} = \tilde{f}(y), \quad (2.30)$$

can be locally mapped to a dynamical system on a Euclidean space through coordinate charts φ ,

$$\mathbb{R}^n \xrightarrow{\varphi^{-1}} \mathcal{M} \xrightarrow{\tilde{f}} T\mathcal{M} \xrightarrow{\text{id}} \mathbb{R}^n, \quad (2.31)$$

where $\text{id}: T\mathcal{M} \rightarrow \mathbb{R}^n$ trivially identifies each tangent space $T_y\mathcal{M}$ with \mathbb{R}^n . Defining $f := \text{id} \circ \tilde{f} \circ \varphi^{-1}$, the local stability properties of the dynamical system of Eq. (2.29) are the same as for the system Eq. (2.30).

An equilibrium of Eq. (2.29) is a point $\vec{x}^* \in \mathbb{R}^n$ such that $f(\vec{x}^*) = 0$. For small perturbation δx around a fixed point \vec{x}^* , we obtain

$$\frac{d}{dt}(\vec{x}^* + \delta x) = f(\vec{x}^* + \delta x) = f(\vec{x}^*) + \mathcal{J}_f(\vec{x}^*) \cdot \delta x + \mathcal{O}(\delta x^2) \approx \mathcal{J}_f(\vec{x}^*) \cdot \delta x, \quad (2.32)$$

where $\mathcal{J}_f(\vec{x}^*)$ is the Jacobian matrix of f at \vec{x}^* and its eigenvalues, $\lambda_1, \dots, \lambda_n$ ordered by decreasing real part, are called **Lyapunov exponents**. Rewriting the perturbation δx in the basis of eigenvectors of the Jacobian $\{\vec{u}_i\}$ as $\delta x = \sum_i \delta_i \cdot \vec{u}_i$, its time evolution can be analyzed component-wise

$$\frac{d}{dt} (\delta_i \cdot \vec{u}_i) \approx \mathcal{J}_f(\vec{x}^*) \cdot (\delta_i \cdot \vec{u}_i) = \lambda_i \delta_i \cdot \vec{u}_i , \quad (2.33)$$

which yields

$$\delta_i(t) = \begin{cases} e^{\lambda_i t}, & \text{if } \lambda_i \neq 0, \\ \delta_i(0), & \text{if } \lambda_i = 0, \end{cases} \quad (2.34)$$

and the magnitude of the perturbation in direction \vec{u}_i decreases exponentially fast if and only if λ_i has negative real part. The equilibrium \vec{x}^* is then linearly stable if and only if all Lyapunov exponent have non-positive real part. This guarantees that small enough deviations go exponentially fast to zero.

The dynamics of the Kuramoto model are governed by Eq. (2.5), which allows to determine the linear stability of solutions of Eq. (2.9), which are fixed points of Eq. (2.5). Under small perturbations about such a synchronous solution, $\theta_i^* \rightarrow \theta_i^* + \delta\theta_i$, the linearized dynamics reads

$$\delta\dot{\theta}_i = -K \sum_{j=1}^n a_{ij} \cos(\theta_i^* - \theta_j^*)(\delta\theta_i - \delta\theta_j), \quad i = 1, \dots, n. \quad (2.35)$$

The linear stability of the fixed point $\vec{\theta}^*$ is therefore determined by the spectrum of the Jacobian matrix $\mathcal{J}(\vec{\theta}^*)$ (denoted \mathcal{J} below),

$$\mathcal{J}_{ij} := \begin{cases} K a_{ij} \cos(\theta_i^* - \theta_j^*), & \text{if } i \neq j, \\ -K \sum_k a_{ik} \cos(\theta_i^* - \theta_k^*), & \text{if } i = j, \end{cases} \quad (2.36)$$

which depends on the angle differences at the synchronous fixed point. Because $\sum_j \mathcal{J}_{ji} = \sum_j \mathcal{J}_{ij} = 0$, for all i , the constant vector is an eigenvector of \mathcal{J} with eigenvalue $\lambda_1 = 0$. This follows from the invariance under constant angle shift mentioned at Eq. (2.6), where only angle differences between oscillators matter. Furthermore, as \mathcal{J} is real symmetric, all its eigenvalues are real. Thus the synchronous state is stable if \mathcal{J} is negative semidefinite and unstable otherwise. In other words, the synchronous fixed point remains stable as long as the largest nonvanishing eigenvalue λ_2 of \mathcal{J} remains negative.

To the best of our knowledge, it was first mentioned in [39] that as long as all angle differences are in $[-\pi/2, \pi/2]$, Gershgorin's Circle Theorem (see Section 2.4) guarantees that \mathcal{J} is negative semidefinite. Then all Lyapunov exponents are non-positive, which implies that any fixed point of Eq. (2.5) with $\theta_i^* - \theta_j^* \in [-\pi/2, \pi/2]$ for all $\langle ij \rangle \in \mathcal{E}_G$ is linearly stable. The same theorem allows to conclude that if $|\theta_i^* - \theta_j^*| > \pi/2$ on all edges, the fixed point is linearly unstable. Recent works have investigated fixed points with a single angle difference larger than $\pi/2$ in a Kuramoto model on a cycle network [40, 51]. However, little is known analytically if some of the angle differences are smaller and some are larger than $\pi/2$, except on cycle networks with unidirectional nearest-neighbor coupling [44]. In Section 3, we fill this gap and show that at most one angle difference is larger than $\pi/2$ in a stable fixed point of Eq. (2.5) and that a stable fixed point with one angle difference exceeding $\pi/2$ is a continuation of a fixed point at larger K with all angle differences smaller than $\pi/2$.

Nonlinear stability. Linear stability is a local concept and gives no information about the stability of the system against large perturbations. Lyapunov went beyond linear stability with his second method, which assesses stability based on the existence of what is now called a *Lyapunov function* [56, 57]. The latter generalizes the concept of energy for the states of a dynamical system.

Without loss of generality, we assume that the origin of the state space is a fixed point, applying a change of coordinates if necessary. The function $V: \mathbb{R}^n \rightarrow \mathbb{R}$ is a **Lyapunov function** if it is continuous, its first derivatives are continuous, and both functions V and $-\nabla V \cdot f$ vanish at the origin and are positive in a neighborhood of the origin. In this neighborhood, following the

dynamics $\dot{x} = f(x)$, the value of a Lyapunov function then decreases until it reaches its minimal value at the fixed point, where it remains constant. The system then converges towards the fixed point.

In particular, if f can be written as a gradient, i.e. there is a function $\mathcal{U}: \mathbb{R}^n \rightarrow \mathbb{R}$ such that $f = -\nabla \mathcal{U}$, up to addition of a constant, then \mathcal{U} is a Lyapunov function. By assumption \mathcal{U} and its derivatives are continuous, and adding the appropriate constant to \mathcal{U} , it can be positive in the neighborhood of any fixed point and vanish at the fixed point. By definition, f vanishes at all fixed points, thus $-\nabla \mathcal{U} \cdot f$ as well, and away from fixed points,

$$-\nabla \mathcal{U} \cdot f = -\nabla \mathcal{U} \cdot (-\nabla \mathcal{U}) = \|\nabla \mathcal{U}\|_2^2 > 0. \quad (2.37)$$

The existence of a Lyapunov function guarantees stability of the fixed point and the domain where the positivity conditions above are satisfied is an inner approximation of the domain of \mathbb{R}^n where the system stabilizes to the origin. The Lyapunov function of a system can be used to determine the **basin of attraction** of a given fixed point [58, 59], which is the set of all initial conditions converging dynamically to this fixed point. A global measure of the stability of a fixed point is given by the volume of its basin of attraction – this has been called *basin stability* [52, 60, 61]. Clearly, the larger the basin of attraction, the more likely the system is to reach the corresponding fixed point dynamically. This gives a global measure of the stability of a fixed point.

The function

$$\begin{aligned} \mathcal{U}: \mathbb{R}^n &\longrightarrow \mathbb{R} \\ \vec{\theta} &\longmapsto -\sum_{i=1}^n P_i \theta_i + \frac{1}{2} \sum_{i,j=1}^n K_{ij} [1 - \cos(\theta_i - \theta_j)], \end{aligned} \quad (2.38)$$

is a Lyapunov function for the system defined by Eq. (1.3). Furthermore, the set of fixed points of Eq. (1.3) coincides exactly with the set of points where $\dot{\mathcal{U}}(\vec{\theta})$ vanishes. But if $P_i \neq 0$ for some i , the value of \mathcal{U} is not lower bounded and convergence to a fixed point cannot be guaranteed in general. If we were able to fully analyze \mathcal{U} , we would get all information about the basins of attraction of the fixed points of Eq. (1.3). But in general, due to the nonlinearity of \mathcal{U} and the complex interaction graph, such an analysis is complicated.

2.4 Toolbox of linear algebra

We recall here some standard definitions and results of linear algebra [62].

Definition 2.4. A square matrix M is **diagonal dominant** if for all i ,

$$|M_{ii}| \geq \sum_{j \neq i} |M_{ij}|. \quad (2.39)$$

The **principal minors** of a matrix M are the determinants of the square submatrices of M with the same row and column indices.

Theorem 2.5 (Sylvester's criterion). A matrix is positive semidefinite if and only if all its principal minors are non-negative.

Theorem 2.6 (Gershgorin's Circle Theorem). Let M be a square matrix with elements $M_{ij} \in \mathbb{C}$. Define the **Gershgorin discs**

$$D_i := \left\{ z \in \mathbb{C} \mid |z - M_{ii}| \leq \sum_{j \neq i} |M_{ij}| \right\}. \quad (2.40)$$

Then each eigenvalue of M lies in the union of the Gershgorin discs $\bigcup_i D_i$.

Corollary 2.7. Let M be a diagonal dominant matrix with positive (resp. negative) diagonal elements. Then all eigenvalues of M have non-negative (resp. non-positive) real part.

3 The number of stable equilibria in locally coupled Kuramoto models on single-cycle networks

In this chapter, we investigate single-cycle networks and show that the bound on the number of stable fixed points obtained by Rogge and Aeyels [44], and by Ochab and Góra [45] is generically valid for the Kuramoto model on a nonoriented cycle with nearest-neighbor interactions. We furthermore demonstrate that, for such networks, at most one angle difference can exceed $\pi/2$. According to the fixed point classification scheme of [51], where fixed points are characterized by their winding number q and the number ℓ of angle differences larger than $\pi/2$, stable fixed points are then restricted to $\ell \in \{0, 1\}$. We show that the number of stable fixed points decreases monotonically as the coupling strength is reduced, and that stable fixed points with $\ell = 1$ emerge continuously at lower coupling from stable fixed points with $\ell = 0$.

Theorem 2.3 connects the existence of multiple solutions to Eq. (2.9) to the presence of loop flows. The number of solutions is thus related to the number of acceptable loop flows, which will be shown to be discrete. In this chapter, we focus on this problem in cycle graphs with nearest neighbor coupling. Eq. (2.5) then simplifies to

$$\dot{\theta}_i = P_i - K \sin(\theta_i - \theta_{i-1}) - K \sin(\theta_i - \theta_{i+1}), \quad i = 1, \dots, n, \quad (3.1)$$

where indices are taken modulo n .

We first treat the case of large coupling $K \rightarrow \infty$ (which is equivalent to the identical frequency case), where stable fixed points necessarily have all angle differences in $[-\pi/2, \pi/2]$. We then consider the situation for finite K , where we show that the number of stable fixed points decreases with K , that the angle difference along some of the edges can exceed $\pi/2$, but that it can happen on a single edge at most.

Most of the results presented in this section were published in [48].

3.1 Angle differences and sum of angle differences

A fixed point is fully characterized by the angle differences Δ_{ij} , defined in Eq. (2.23), along the edges. These can be written as functions of the loop flow parameter ε ,

$$P_{i,i+1} = P_{i,i+1}^* + K\varepsilon = K \sin(\Delta_{i,i+1}) \implies \Delta_{i,i+1} = h_i(\varepsilon), \quad (3.2)$$

where there are two possible choices for each h_i ,

$$h_i(\varepsilon) = \begin{cases} \arcsin(\varepsilon + P_{i,i+1}^*/K) & \implies \Delta_{i,i+1} \in [-\pi/2, \pi/2], \\ \pm\pi - \arcsin(\varepsilon + P_{i,i+1}^*/K) & \implies \Delta_{i,i+1} \in \mathcal{I}, \end{cases} \quad (3.3)$$

where we defined $\mathcal{I} := (-\pi, -\pi/2) \cup (\pi/2, \pi]$ and the sign in front of π is chosen such that h_i belongs to $(-\pi, \pi]$. Since the flow along any edge is bounded by K , we obtain the following bounds on ε ,

$$-K \leq P_{i,i+1} \leq K \iff -1 - P_{i,i+1}^*/K \leq \varepsilon \leq 1 - P_{i,i+1}^*/K, \quad i = 1, \dots, n. \quad (3.4)$$

Thus defining $P_{\min}^* := \min_i P_{i,i+1}^*$ and $P_{\max}^* := \max_i P_{i,i+1}^*$, we have $\varepsilon \in [\varepsilon_{\min}, \varepsilon_{\max}]$, with

$$\varepsilon_{\min} := -1 - P_{\min}^*/K, \quad \varepsilon_{\max} := 1 - P_{\max}^*/K. \quad (3.5)$$

Note that as soon as the P_i 's are not all equal to zero, $P_{\min}^* \neq P_{\max}^*$. We add an appropriate constant to the reference flow to make sure that $P_{\min}^* < 0$ and $P_{\max}^* > 0$, which will facilitate our discussion without restricting its generality.

As seen previously, a fixed point is stable if all angle differences belong to $[-\pi/2, \pi/2]$. In this situation, we can write the sum of angle differences around the cycle as a function of the parameter ε ,

$$\mathcal{A}(K, \varepsilon) := \sum_{i=1}^n \Delta_{i,i+1} = \sum_{i=1}^n \arcsin(\varepsilon + P_{i,i+1}^*/K). \quad (3.6)$$

As the arcsine is continuous and monotonically increasing, the function \mathcal{A} is also continuous and increasing with respect to ε . Thus for fixed K_0 , the function $\mathcal{A}(K_0, \varepsilon)$ defines a one-to-one correspondence between the intervals

$$[\varepsilon_{\min}(K_0), \varepsilon_{\max}(K_0)] \longleftrightarrow [\mathcal{A}(K_0, \varepsilon_{\min}(K_0)), \mathcal{A}(K_0, \varepsilon_{\max}(K_0))]. \quad (3.7)$$

The sum of angle differences around the cycle has to be an integer multiple of 2π , thus defining ε_q such that $\mathcal{A}(K_0, \varepsilon_q) = 2\pi q$, $q \in \mathbb{Z}$, and

$$\Delta_{i,i+1} = \arcsin(\varepsilon_q + P_{i,i+1}^*/K_0), \quad i = 1, \dots, n, \quad (3.8)$$

gives a solution of Eq. (2.9) corresponding to a stable fixed point, constructed as

$$\theta_1 = 0, \quad \text{and} \quad \theta_i = -\sum_{j=1}^{i-1} \Delta_{j,j+1}, \quad i = 2, \dots, n. \quad (3.9)$$

Therefore, the number of fixed points with $|\Delta_{i,i+1}| < \pi/2$ for all i is straightforwardly given by the number of q 's such that $\mathcal{A}(K_0, \varepsilon_q) = 2\pi q$.

3.2 Infinite coupling

The case $K \rightarrow \infty$ is equivalent to the identical frequencies case with $P_i = 0$, for all i , because the finite value of the P_i 's has then no influence on the dynamics of Eq. (3.1). In this limit, the bounds on ε are

$$\lim_{K \rightarrow \infty} \varepsilon_{\min}(K) = -1, \quad \lim_{K \rightarrow \infty} \varepsilon_{\max}(K) = 1, \quad (3.10)$$

and thus

$$\lim_{K \rightarrow \infty} \mathcal{A}(K, \varepsilon_{\min}(K)) = -n\pi/2, \quad \lim_{K \rightarrow \infty} \mathcal{A}(K, \varepsilon_{\max}(K)) = n\pi/2. \quad (3.11)$$

An ε_q is associated to each integer multiple of 2π in $(-n\pi/4, n\pi/4)$ corresponding to a solution of Eq. (2.9) related to a stable fixed point. There are

$$\mathcal{N} = 2 \cdot \text{Int}[(n-1)/4] + 1 \quad (3.12)$$

such integers. This is illustrated in Figure 4.

Remark. In [48], we obtained $\mathcal{N} = 2 \cdot \text{Int}(n/4) + 1$ which differs from Eq. (3.12) if n is a multiple of 4. When n is a multiple of 4, we considered the fixed points with winding numbers $q = \pm n\pi/4$ as stable. In such fixed points, all angle differences are $\pm\pi/2$ and the Jacobian matrix \mathcal{J} is full of zeros, and thus linearizing the dynamics gives no information about stability. It has been reported in [63], based on [64], that such fixed points are unstable, we then removed them from our count.

Theorem 3.1. For $K \rightarrow \infty$, any stable fixed point of Eq. (3.1) on a cycle network has all angle differences in $[-\pi/2, \pi/2]$. Furthermore all angle differences are equal to $2\pi q/n$, where $q \in \mathbb{Z}$ is the winding number of the fixed point.

Remark. The result of Theorem 3.1 was already known for unidirectional coupling [44]. Here we extend this result to bidirectional interactions. Furthermore, our approach allows to relate the finite K situation to the infinite K situation.

Proof. The flow along edge $\langle i, i+1 \rangle$ is

$$P_{i,i+1} = K \sin(\Delta_{i,i+1}) = P_{i,i+1}^* + K\varepsilon, \quad (3.13)$$

where $\{P_{i,i+1}^*\}$ is a reference flow constructed from finite natural frequencies. Thus when $K \rightarrow \infty$, the sine of the angle difference along every edge of the cycle tends to the same value,

$$\lim_{K \rightarrow \infty} \sin(\Delta_{i,i+1}) = \varepsilon. \quad (3.14)$$

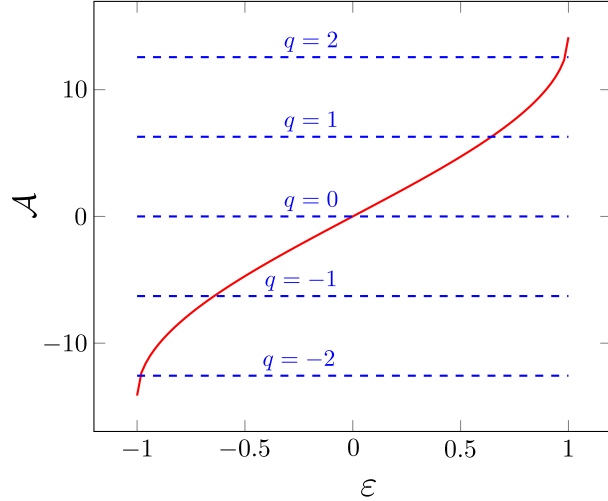


Figure 4: (Figure taken from [48]) Plot of $A(K, \varepsilon)$ as a function of ε (red), for a cycle network of length $n = 9$, with $K \rightarrow \infty$. Horizontal dashed lines correspond to $A = 2\pi q$ with q values indicated. Each intersection of the red line with a blue dashed line gives a solution of Eq. (2.9), corresponding to a stable fixed point.

This implies that the angle difference along each edge of the cycle belongs to the set $\{\arcsin(\varepsilon), \pi - \arcsin(\varepsilon)\}$ and thus the cosine of the angle differences along all the edges takes the same absolute value with either positive or negative sign. First of all, if all angle differences are $\arcsin(\varepsilon)$, the Jacobian matrix defined in Eq. (2.36) is easily expressed as

$$\mathcal{J} = K c_0 \begin{pmatrix} -2 & 1 & & 1 \\ 1 & -2 & \ddots & \\ & \ddots & \ddots & 1 \\ 1 & & 1 & -2 \end{pmatrix}, \quad (3.15)$$

where $c_0 := \cos(\arcsin(\varepsilon)) = \sqrt{1 - \varepsilon^2}$. This matrix is negative semidefinite and has only non-positive eigenvalues by Gershgorin's Circle Theorem (Corollary 2.7). Thus the fixed point is stable. Now, if all angle differences are $\pi - \arcsin(\varepsilon)$, then all cosines are negative and the Jacobian matrix is obviously positive semidefinite. The fixed point is then unstable. Let us now consider the mixed case where at least one angle difference is $\arcsin(\varepsilon)$ and at least one is $\pi - \arcsin(\varepsilon)$. In this case, there exists at least one vertex i such that $\Delta_{i-1,i} = \arcsin(\varepsilon)$ and $\Delta_{i,i+1} = \pi - \arcsin(\varepsilon)$ and the corresponding Jacobian matrix has the form

$$\mathcal{J}' = K c_0 \begin{pmatrix} \ddots & \ddots & & \\ \ddots & x & 1 & 0 \\ & 1 & 0 & -1 \\ 0 & -1 & y & \ddots \\ & & & \ddots \end{pmatrix}. \quad (3.16)$$

The principal minor (Definition 2.4) of $-\mathcal{J}'$ with row and column indices i and $i + 1$ is

$$\begin{vmatrix} 0 & +1 \\ +1 & -y \end{vmatrix} = -1, \quad (3.17)$$

which, by Sylvester's criterion (Theorem 2.5), implies that \mathcal{J}' is not negative semidefinite. In other words, \mathcal{J}' has at least one positive eigenvalue and thus the fixed point is unstable. From this we conclude that all stable fixed points for sufficiently large K have angle differences in $[-\pi/2, \pi/2]$.

They are captured by finding the intersections of $\mathcal{A}(K, \varepsilon)$ with integer multiples of 2π as illustrated in Figure 4.

Let q be the winding number of a stable fixed point for $K \rightarrow \infty$. As all angle differences have the same value $\Delta \in [-\pi/2, \pi/2]$, we have

$$2\pi q = \sum_{i=1}^n \Delta_{i,i+1} = n\Delta \implies \Delta = 2\pi q/n. \quad (3.18)$$

The corresponding angles are $\theta_i = -2\pi q i / n$. □

3.3 Finite coupling

We now consider finite values for K and heterogeneous values of P_i . We first show that the number of fixed points to Eq. (3.1) with all angle differences in $[-\pi/2, \pi/2]$ decreases with K . Second, we show that for finite K , there exist stable fixed points with one angle difference in \mathcal{I} , and we relate them to fixed points at larger K with all angle differences in $[-\pi/2, \pi/2]$. Such behavior of stable fixed points with respect to K were observed numerically in [40, 51], which we confirm here analytically.

Proposition 3.2. *For a cycle network with n vertices, if K decreases, then $\mathcal{A}(K, \varepsilon_{\min})$ increases and $\mathcal{A}(K, \varepsilon_{\max})$ decreases.*

Proof. From Eqs. (3.5) and (3.6) the derivative of \mathcal{A} with respect to K at $\varepsilon = \varepsilon_{\min}$ reads

$$\frac{d\mathcal{A}(K, \varepsilon_{\min})}{dK} = \sum' \left[1 - \left(-1 + \frac{P_{i,i+1}^* - P_{\min}^*}{K} \right)^2 \right]^{-\frac{1}{2}} \frac{P_{\min}^* - P_{i,i+1}^*}{K^2}, \quad (3.19)$$

where \sum' indicates that the sum is taken over indices j such that $P_{j,j+1}^* > P_{\min}^*$. This sum is obviously non-positive. In the same way one sees that

$$\frac{d\mathcal{A}(K, \varepsilon_{\max})}{dK} = \sum'' \left[1 - \left(1 + \frac{P_{i,i+1}^* - P_{\max}^*}{K} \right)^2 \right]^{-\frac{1}{2}} \frac{P_{\max}^* - P_{i,i+1}^*}{K^2} \geq 0. \quad (3.20)$$

□

Proposition 3.2 implies that as K decreases, the interval of values of \mathcal{A} gets smaller and contains fewer and fewer multiples of 2π , and thus less winding numbers are realizable. We show now that for finite couplings, the stable fixed points are directly related to the stable fixed points for $K \rightarrow \infty$, even if some of them have angle differences in \mathcal{I} . First we define

$$\mathcal{A}^{(j)}(K, \varepsilon) := \pi - \arcsin(\varepsilon + P_{j,j+1}^*/K) + \sum_{i \neq j} \arcsin(\varepsilon + P_{i,i+1}^*/K), \quad j = 1, \dots, n. \quad (3.21)$$

The function \mathcal{A} is the sum of angle differences all taken in the interval $[-\pi/2, \pi/2]$ and for $j = 1, \dots, n$, the function $\mathcal{A}^{(j)}$ is this sum with one angle difference, the j^{th} , taken in \mathcal{I} . We also introduce the following notation

$$c_i := \cos(\Delta_{i,i+1}), \quad i = 1, \dots, n. \quad (3.22)$$

The sign of c_i depends on our choice of h_i for the angle difference $\Delta_{i,i+1}$,

$$c_i = \begin{cases} \cos[\arcsin(\varepsilon + P_{i,i+1}^*/K)] &= \sqrt{1 - (\varepsilon + P_{i,i+1}^*/K)^2}, \\ \cos[\pi - \arcsin(\varepsilon + P_{i,i+1}^*/K)] &= -\sqrt{1 - (\varepsilon + P_{i,i+1}^*/K)^2}, \end{cases} \quad (3.23)$$

but its absolute value is the same in both cases.

Let \mathcal{D} be the subdomain of the (K, ε) -plane where the functions $\mathcal{A}^{(j)}$ are defined, i.e. such that each arcsine is well-defined,

$$\mathcal{D} = \{(K, \varepsilon) \mid \varepsilon + P_{\min}^*/K \geq -1 \text{ and } \varepsilon + P_{\max}^*/K \leq 1\} . \quad (3.24)$$

By definition, in the interior of \mathcal{D} , the c_i 's are nonzero. Let us define the upper and lower boundaries of \mathcal{D} ,

$$\mathcal{D}_\dagger := \{(K, \varepsilon) \mid \varepsilon + P_{\max}^*/K = 1\} , \quad \mathcal{D}_\ddagger := \{(K, \varepsilon) \mid \varepsilon + P_{\min}^*/K = -1\} . \quad (3.25)$$

We next denote by j_\dagger and j_\ddagger the indices such that $P_{j_\dagger, j_\dagger+1}^* = P_{\max}^*$ and $P_{j_\ddagger, j_\ddagger+1}^* = P_{\min}^*$ respectively. Note that for $(K, \varepsilon) \in \mathcal{D}_\dagger$ [resp. $(K, \varepsilon) \in \mathcal{D}_\ddagger$], the functions $\mathcal{A}(K, \varepsilon)$ and $\mathcal{A}^{(j_\dagger)}(K, \varepsilon)$ [resp. $\mathcal{A}^{(j_\ddagger)}(K, \varepsilon)$] have the same value.

Remark. *It is possible that multiple edges carry the same maximal or minimal flow. In this case the indices j_\dagger and j_\ddagger are not uniquely defined, but we are free to choose any j_\dagger and j_\ddagger satisfying $P_{j_\dagger, j_\dagger+1}^* = P_{\max}^*$ and $P_{j_\ddagger, j_\ddagger+1}^* = P_{\min}^*$.*

For any choice of h_i 's in Eq. (3.3), any point $(K, \varepsilon) \in \mathcal{D}$ such that $\sum_i h_i = 2\pi q$ is a solution of Eq. (2.9). Hence we now investigate the $2\pi q$ -level sets of \mathcal{A} and $\mathcal{A}^{(j)}$, for $q \in \mathbb{Z}$ and $j = 1, \dots, n$. Note first that as $\mathcal{A}^{(j)}$ is smooth in the interior of the domain \mathcal{D} for any j , the Implicit Function Theorem [65] implies that its level sets are level curves. For any K , we define $\mathcal{N}(K)$ the number of stable fixed points of Eq. (3.1). The main results of this section are the following theorem on the properties of $\mathcal{N}(K)$ and its corollary.

Theorem 3.3. *The number, $\mathcal{N}(K)$, of stable equilibria of Eq. (3.1) is a monotonically increasing function of K .*

Corollary 3.4. *The value*

$$\mathcal{N}_\infty := \lim_{K \rightarrow \infty} \mathcal{N}(K) = 2 \cdot \text{Int}[(n-1)/4] + 1 , \quad (3.26)$$

is an upper bound on the number of stable fixed points of Eq. (3.1) on a cycle network, independently of K and \vec{P} .

The proof of Theorem 3.3 relies on five lemmas. A major ingredient of the proof is that the functions $\mathcal{A}^{(j)}(K, \varepsilon)$, for $j = 1, \dots, n$, have no critical points. This fact and Lemma 3.7 give precise informations about the shape of the level curves of $\mathcal{A}^{(j)}$.

Lemma 3.5. *For $j \in \{1, \dots, n\}$, the function $\mathcal{A}^{(j)}$ has no critical point in the interior of \mathcal{D} .*

Proof. For $j \in \{1, \dots, n\}$, we have

$$\frac{\partial \mathcal{A}^{(j)}}{\partial \varepsilon} = \sum_{k=1}^n c_k^{-1} , \quad (3.27)$$

which is well-defined because in the interior of \mathcal{D} , $c_k \neq 0$, for all k . Assume first that at some point (K, ε) in the interior of \mathcal{D} , $\partial \mathcal{A}^{(j)}/\partial \varepsilon = 0$. In the definition of $\mathcal{A}^{(j)}$ we chose

$$\Delta_{j, j+1} = \pi - \arcsin(\varepsilon + P_{j, j+1}^*/K) , \quad (3.28)$$

thus we have $c_j < 0$ and

$$\frac{\partial \mathcal{A}^{(j)}}{\partial \varepsilon} = 0 \iff \sum_k c_k^{-1} = 0 \iff \sum_{k \neq j} c_k^{-1} = -c_j^{-1} \iff \sum_{k \neq j} -c_j/c_k = 1 . \quad (3.29)$$

It is then easy to check that for any $k \neq j$

$$\begin{aligned} 0 < -c_j/c_k < 1 &\implies 0 < -c_j < c_k \implies \sqrt{1 - (\varepsilon + P_{j, j+1}^*/K)^2} < \sqrt{1 - (\varepsilon + P_{k, k+1}^*/K)^2} \\ &\implies (\varepsilon + P_{j, j+1}^*/K)^2 > (\varepsilon + P_{k, k+1}^*/K)^2 . \end{aligned} \quad (3.30)$$

There are now two possible cases:

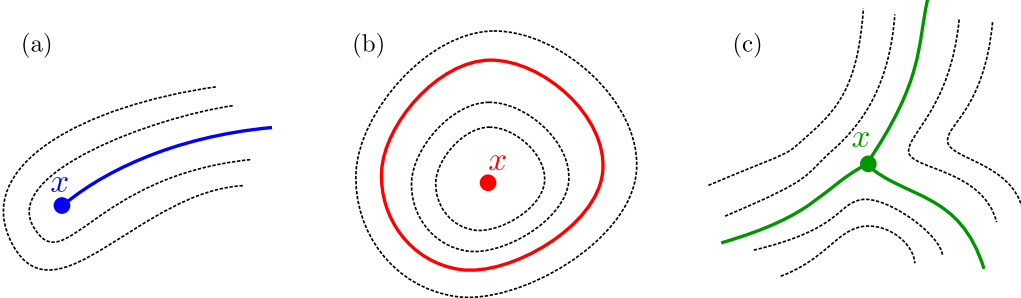


Figure 5: Three types of level curves that cannot occur in the domain \mathcal{D} . By smoothness of $\mathcal{A}^{(j)}$, in each case, at least one point, denoted x , is a critical point, which is impossible by Corollary 3.6

1. If $\varepsilon + P_{j,j+1}^*/K > 0$, then for all $k \neq j$,

$$\begin{aligned} \varepsilon + P_{j,j+1}^*/K > \varepsilon + P_{k,k+1}^*/K &\iff P_{j,j+1}^* > P_{k,k+1}^* \\ &\implies P_{j,j+1}^* = P_{\max}^*; \end{aligned} \quad (3.31)$$

2. If $\varepsilon + P_{j,j+1}^*/K < 0$, then for all $k \neq j$,

$$\begin{aligned} \varepsilon + P_{j,j+1}^*/K < \varepsilon + P_{k,k+1}^*/K &\iff P_{j,j+1}^* < P_{k,k+1}^* \\ &\implies P_{j,j+1}^* = P_{\min}^*. \end{aligned} \quad (3.32)$$

Thus if $j \notin \{j_\dagger, j_\ddagger\}$, Eq. (3.29) cannot hold and $\mathcal{A}^{(j)}$ has no critical point in \mathcal{D} . Let now $j \in \{j_\dagger, j_\ddagger\}$ and assume that

$$\frac{\partial \mathcal{A}^{(j)}}{\partial \varepsilon} = \sum_k c_k^{-1} = 0. \quad (3.33)$$

We calculate

$$\begin{aligned} \frac{\partial \mathcal{A}^{(j)}}{\partial K} &= \frac{\partial}{\partial K} [\pi - \arcsin(\varepsilon + P_{j,j+1}^*/K)] + \sum_{k \neq j} \frac{\partial}{\partial K} \arcsin(\varepsilon + P_{k,k+1}^*/K) \\ &= -c_j^{-1} P_{j,j+1}^*/K^2 - \sum_{k \neq j} c_k^{-1} P_{k,k+1}^*/K^2 = \sum_{k \neq j} c_k^{-1} P_{j,j+1}^*/K^2 - \sum_{k \neq j} c_k^{-1} P_{k,k+1}^*/K^2 \\ &= \sum_{k \neq j} (P_{j,j+1}^* - P_{k,k+1}^*) / (K^2 c_k), \end{aligned} \quad (3.34)$$

which is non zero as every term is non-negative (resp. non-positive) if $j = j_\ddagger$ (resp. $j = j_\dagger$). Thus the partial derivatives of $\mathcal{A}^{(j)}$ are never simultaneously zero implying that $\mathcal{A}^{(j)}$ has no critical point in the domain \mathcal{D} . \square

Corollary 3.6. *For any $j \in \{1, \dots, n\}$, the level sets of $\mathcal{A}^{(j)}$ are continuous lines that: (a) cannot end in the interior of \mathcal{D} , (b) are not closed and (c) have no trifurcation.*

Proof. By smoothness of $\mathcal{A}^{(j)}$, any of these situations (shown in Figure 5) would imply at least one critical point of $\mathcal{A}^{(j)}$ in the interior of \mathcal{D} , which would contradict Lemma 3.5. \square

Lemma 3.7. *Let $L \in \mathbb{R}$. If there exists $K_0 \in \mathbb{R}$ such that $\mathcal{A}^{(j_\dagger)}(K_0, \varepsilon_{\max}(K_0)) = L$, then there is a single level curve of $\mathcal{A}^{(j_\dagger)} = L$ starting at $(K_0, \varepsilon_{\max}(K_0))$. The same holds for level curves of $\mathcal{A}^{(j_\ddagger)} = L$ starting at $(K_0, \varepsilon_{\min}(K_0))$.*

Remark. *This lemma means that the plain red curve in Figure 6 is unique.*

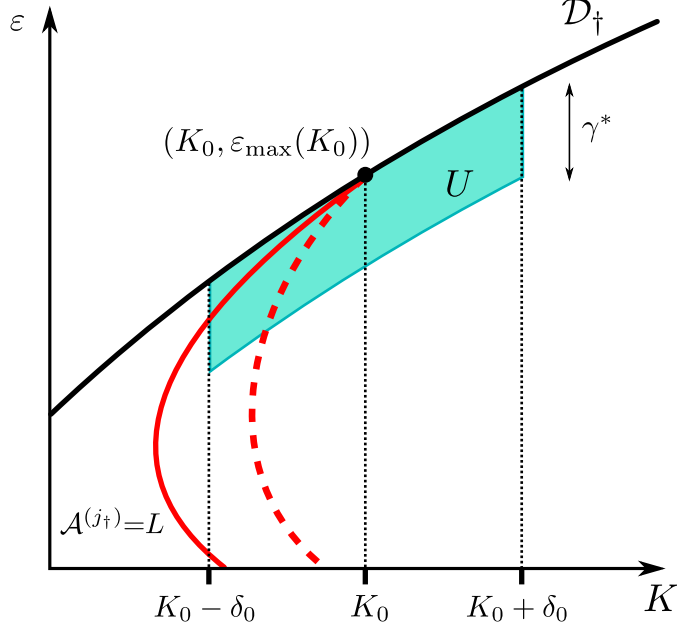


Figure 6: (Figure adapted from [48]) Sketch of the level curve $A^{(j\dagger)} = L$ (red curve) and of the neighborhood U of $(K_0, \varepsilon_{\max}(K_0))$ where the partial derivative of $A^{(j\dagger)}$ with respect to K always has the same non-zero sign. The neighborhood U , defined in Eq. (3.39), is bounded from above by the boundary of the domain D , left and right by the bounds of the interval K and is of height γ^* . The dashed red line sketches another level curve that cannot exist by Lemma 3.7.

Proof. We assume that there is a single index j such that $P_{j,j+1}^* = P_{\max}^*$, but the argument can be adapted if there are multiple such indices.

We first remark that

$$\frac{\partial A^{(j\dagger)}}{\partial K} = \left[1 - \left(\varepsilon + \frac{P_{\max}^*}{K} \right)^2 \right]^{-1/2} \frac{P_{\max}^*}{K^2} - \sum_{k \neq j\dagger} \left[1 - \left(\varepsilon + \frac{P_{k,k+1}^*}{K} \right)^2 \right]^{-1/2} \frac{P_{k,k+1}^*}{K^2}. \quad (3.35)$$

Consider now a small interval around K_0 , $\mathcal{K} = [K_0 - \delta_0, K_0 + \delta_0]$, $\delta_0 > 0$. For any $K \in \mathcal{K}$, it is clear that

$$\lim_{\varepsilon \rightarrow \varepsilon_{\max}} \frac{\partial}{\partial K} A^{(j\dagger)}(K, \varepsilon) = \pm\infty. \quad (3.36)$$

By continuity, there exists $\gamma_K > 0$ such that for all $\varepsilon \in (\varepsilon_{\max}(K) - \gamma_K, \varepsilon_{\max}(K))$,

$$\left| \left[1 - (\varepsilon + P_{\max}^*/K)^2 \right]^{-1/2} P_{\max}^*/K^2 \right| > \left| \sum_{k \neq j\dagger} \left[1 - (\varepsilon + P_{k,k+1}^*/K)^2 \right]^{-1/2} P_{k,k+1}^*/K^2 \right|, \quad (3.37)$$

and thus the partial derivative $\partial A^{(j\dagger)} / \partial K$ has the same sign as P_{\max}^* , which we chose positive [see discussion below Eq. (3.5)]. Thus defining

$$\gamma^* := \min_{K \in \mathcal{K}} \{\gamma_K\} > 0, \quad (3.38)$$

allows us to define a neighborhood $U \subset D$ of $(K_0, \varepsilon_{\max}(K_0))$,

$$U := \{(K, \varepsilon) \mid |K - K_0| < \delta_0, 0 \leq \varepsilon_{\max}(K) - \varepsilon \leq \gamma^*\}, \quad (3.39)$$

where the partial derivative $\partial A^{(j\dagger)} / \partial K$ is always positive. This neighborhood is sketched in Figure 6. But if there is more than one level curve (see red dashed line in Figure 6) with value L

starting at $(K_0, \varepsilon_{\max}(K_0))$ and since $\mathcal{A}^{(j_\dagger)}$ is not constant, this partial derivative has to change sign in any neighborhood of $(K_0, \varepsilon_{\max}(K_0))$, which leads to a contradiction. There is therefore at most one such level curve.

The proof of the second statement is similar, substituting the indices \ddagger for \dagger and ε_{\min} for ε_{\max} . \square

We next investigate how the linear stability of the fixed points of Eq. (3.1) varies along the level curves $\mathcal{A}^{(j)} = 2\pi q$. The two following lemmas show that the only functions leading to stable fixed points are \mathcal{A} , $\mathcal{A}^{(j_\ddagger)}$ and $\mathcal{A}^{(j_\dagger)}$.

Lemma 3.8. *For any choice of h_i 's in Eq. (3.3) and any point (K, ε) in the interior of \mathcal{D} , the Jacobian matrix \mathcal{J} has a second null eigenvalue λ_2 if and only if*

$$\sum_k c_k^{-1} = 0. \quad (3.40)$$

Proof. Consider the characteristic polynomial of the Jacobian matrix \mathcal{J} ,

$$\chi_{\mathcal{J}}(\lambda) = \begin{vmatrix} -c_1 - c_n - \lambda & c_1 & \cdots & 0 & \cdots & c_n \\ c_1 & -c_1 - c_2 - \lambda & c_2 & & & \vdots \\ \vdots & c_2 & \ddots & \ddots & & 0 \\ 0 & & \ddots & & & \vdots \\ \vdots & & & & & c_{n-1} \\ c_n & \cdots & 0 & \cdots & c_{n-1} & -c_{n-1} - c_n - \lambda \end{vmatrix}. \quad (3.41)$$

Adding all rows to the first one it can be written $\chi_{\mathcal{J}}(\lambda) = \det(\tilde{\mathcal{J}}(\lambda))$ with

$$\tilde{\mathcal{J}}(\lambda) = \begin{pmatrix} -\lambda & \cdots & -\lambda & \cdots & -\lambda \\ c_1 & -c_1 - c_2 - \lambda & c_2 & & \vdots \\ \vdots & c_2 & \ddots & \ddots & 0 \\ 0 & & \ddots & & \vdots \\ \vdots & & & & c_{n-1} \\ c_n & \cdots & 0 & \cdots & c_{n-1} & -c_{n-1} - c_n - \lambda \end{pmatrix}. \quad (3.42)$$

Expanding the determinant along the first row one obtains

$$\begin{aligned} \chi_{\mathcal{J}}(\lambda) &= (-\lambda) \sum_{i=1}^n (-1)^{i-1} \det([\tilde{\mathcal{J}}(\lambda)]_{1,i}) \\ &=: (-\lambda)\tilde{\chi}(\lambda), \end{aligned} \quad (3.43)$$

where $\det([M]_{ij})$ stands for the (i, j) -cofactor of the matrix M . One eigenvalue obviously vanishes and a second eigenvalue, λ_2 , is zero if and only if $\tilde{\chi}(0) = 0$.

We show now that for $i = 2, \dots, n$,

$$\det([\tilde{\mathcal{J}}(0)]_{1,i}) = -\det([\tilde{\mathcal{J}}(0)]_{1,i-1}). \quad (3.44)$$

Let \mathcal{C}_k denote the k^{th} column of the matrix $\tilde{\mathcal{J}}(0)$ with the first row removed,

$$\mathcal{C}_k := \begin{cases} (c_1, 0, \dots, 0, c_n)^\top, & \text{if } k = 1, \\ (-c_1 - c_2, c_2, 0, \dots, 0)^\top, & \text{if } k = 2, \\ (\dots, 0, c_{k-1}, -c_{k-1} - c_k, c_k, 0, \dots)^\top, & \text{if } 2 < k < n, \\ (\dots, 0, c_{n-1}, -c_{n-1} - c_n)^\top, & \text{if } k = n. \end{cases} \quad (3.45)$$

We obtain

$$\begin{aligned}
\det([\tilde{\mathcal{J}}(0)]_{1i}) &= \left| \begin{array}{ccccccc} \mathcal{C}_1 & \cdots & \mathcal{C}_{i-2} & \mathcal{C}_{i-1} & \mathcal{C}_{i+1} & \cdots & \mathcal{C}_n \end{array} \right| \\
&= \left| \begin{array}{ccccccc} \mathcal{C}_1 & \cdots & \mathcal{C}_{i-2} & \sum_{j \neq i} \mathcal{C}_j & \mathcal{C}_{i+1} & \cdots & \mathcal{C}_n \end{array} \right| \\
&= \left| \begin{array}{ccccccc} \mathcal{C}_1 & \cdots & \mathcal{C}_{i-2} & -\mathcal{C}_i & \mathcal{C}_{i+1} & \cdots & \mathcal{C}_n \end{array} \right| = -\det([\tilde{\mathcal{J}}(0)]_{1,i-1}),
\end{aligned} \tag{3.46}$$

where in the second line we used that the determinant is not changed by adding a linear combination of columns to any column, and in the third line, we used the fact that the sum of the elements of any row is zero. We conclude

$$\det([\tilde{\mathcal{J}}(0)]_{1i}) = (-1)^{i-1} \det([\tilde{\mathcal{J}}(0)]_{11}). \tag{3.47}$$

Therefore, to calculate $\tilde{\chi}(0)$ we only have to compute $\det([\tilde{\mathcal{J}}(0)]_{11})$. Since $[\tilde{\mathcal{J}}(0)]_{11}$ is tridiagonal we compute its *LU*-factorization using Thomas algorithm [66],

$$\begin{aligned}
[\tilde{\mathcal{J}}(0)]_{11} &= \begin{pmatrix} -c_1 - c_2 & c_2 & & & & \\ c_2 & -c_2 - c_3 & \ddots & & & \\ & \ddots & \ddots & & & \\ & & c_{n-1} & -c_{n-1} - c_n & & \end{pmatrix} \\
&= \begin{pmatrix} 1 & 0 & \cdots & 0 \\ c_2/\beta_1 & 1 & \ddots & \vdots \\ 0 & \ddots & \ddots & 0 \\ 0 & c_{n-1}/\beta_{n-2} & 1 \end{pmatrix} \cdot \begin{pmatrix} \beta_1 & c_2 & 0 & & \\ 0 & \beta_2 & \ddots & 0 & \\ \vdots & \ddots & \ddots & c_{n-1} & \\ 0 & \cdots & 0 & \beta_{n-1} & \end{pmatrix},
\end{aligned} \tag{3.48}$$

where

$$\beta_i := \begin{cases} -(c_1 + c_2), & \text{if } i = 1, \\ -(c_i + c_{i+1} + c_i^2/\beta_{i-1}), & \text{if } i = 2, \dots, n-1. \end{cases} \tag{3.49}$$

This factorization is only valid for non-singular matrices, but by continuity it can be computed arbitrarily close to points where the determinant vanishes. Computing the determinant of the matrix $[\tilde{\mathcal{J}}(0)]_{11}$ then reduces to computing the product of the β_i 's. Let us define

$$\mu_i := \begin{cases} 1, & \text{if } i = 0, \\ \sum_{j=1}^{i-1} \prod_{\substack{k=1 \\ k \neq j}}^{i+1} c_k, & \text{if } i = 1, \dots, n-1, \end{cases} \tag{3.50}$$

which, by Lemma 3.9 below, satisfies

$$\mu_{i-1} \cdot \beta_i = -\mu_i, \quad i = 1, \dots, n-1. \tag{3.51}$$

We can now compute the determinant of $[\tilde{\mathcal{J}}(0)]_{11}$,

$$\det([\tilde{\mathcal{J}}(0)]_{11}) = \prod_{i=1}^{n-1} \beta_i = (-1)^{n-1} \frac{\mu_{n-1}}{\mu_0} = (-1)^{n-1} \sum_{j=1}^n \prod_{\substack{k=1 \\ k \neq j}}^n c_k = (-1)^{n-1} \prod_{j=1}^n c_j \cdot \sum_{k=1}^n c_k^{-1}, \tag{3.52}$$

where the last equality holds as long as all c_k 's are nonzero, which is true in the interior of \mathcal{D} .

Finally, combining Eqs. (3.43), (3.47) and (3.52) we have

$$\tilde{\chi}(0) = (-1)^{n-1} n \prod_{j=1}^n c_j \sum_{k=1}^n c_k^{-1}, \quad (3.53)$$

and thus

$$\lambda_2 = 0 \iff \tilde{\chi}(0) = 0 \iff \sum_{k=1}^n c_k^{-1} = 0, \quad (3.54)$$

which completes the proof. \square

In the previous proof we used the following lemma.

Lemma 3.9. *For all $i = 1, \dots, n-1$, the values β_i and μ_i satisfy*

$$\mu_{i-1} \cdot \beta_i = -\mu_i. \quad (3.55)$$

Proof. We prove this by induction. For $i = 1$,

$$\mu_0 \cdot \beta_1 = 1 \cdot (-c_1 - c_2) = -\mu_1. \quad (3.56)$$

Assume now that $\mu_{i-1} \cdot \beta_i = -\mu_i$, $i > 1$ and let us prove that $\mu_i \cdot \beta_{i+1} = -\mu_{i+1}$,

$$\begin{aligned} \mu_i \cdot \beta_{i+1} &= \mu_i \left(-c_{i+1} - c_{i+2} - \frac{c_{i+1}^2}{\beta_i} \right) = -c_{i+1}\mu_i - c_{i+2}\mu_i - c_{i+1}^2\mu_{i-1} \\ &= -c_{i+1} \sum_{j=1}^{i+1} \prod_{\substack{k=1 \\ k \neq j}}^i c_k - c_{i+2} \sum_{j=1}^{i+1} \prod_{\substack{k=1 \\ k \neq j}}^{i+1} c_k + c_{i+1}^2 \sum_{j=1}^i \prod_{\substack{k=1 \\ k \neq j}}^i c_k \\ &= -c_{i+1} \left(c_{i+1} \sum_{j=1}^i \prod_{\substack{k=1 \\ k \neq j}}^i c_k + \prod_{k=1}^i c_k \right) - c_{i+2} \sum_{j=1}^{i+1} \prod_{\substack{k=1 \\ k \neq j}}^{i+1} c_k + c_{i+1}^2 \sum_{j=1}^i \prod_{\substack{k=1 \\ k \neq j}}^i c_k \\ &= -c_{i+1} \prod_{k=1}^i c_k - c_{i+2} \sum_{j=1}^{i+1} \prod_{\substack{k=1 \\ k \neq j}}^{i+1} c_k = -\sum_{j=1}^{i+2} \prod_{\substack{k=1 \\ k \neq j}}^{i+2} c_k = -\mu_{i+1}. \end{aligned} \quad (3.57)$$

\square

We show now that Eq. (3.40) is satisfied at most for one point of the level curves $\mathcal{A}^{(j_\dagger)}$ or $\mathcal{A}^{(j_\ddagger)}$.

Lemma 3.10. *For a given value $L \in \mathbb{R}$ and $j \in \{j_\dagger, j_\ddagger\}$, there is at most one point where $\sum_k c_k^{-1} = 0$ along a connected component of the level curve $\mathcal{A}^{(j)} = L$.*

Remark. *From Lemma 3.5 we already know that if $j \notin \{j_\dagger, j_\ddagger\}$, $\sum_k c_k^{-1}$ never vanishes.*

Proof. We recall Eq. (3.27),

$$\sum_k c_k^{-1} = \frac{\partial \mathcal{A}^{(j)}}{\partial \varepsilon}. \quad (3.58)$$

Hence the sum $\sum_k c_k^{-1}$ equals zero if and only if the level curve of $\mathcal{A}^{(j)}$ is parallel to the ε axis. Let us now differentiate the sum $\sum_k c_k^{-1}$ with respect to ε at such a point, to see how it varies along the level curve of $\mathcal{A}^{(j)}$. Using the fact that $c_j^{-1} = -\sum_{k \neq j} c_k^{-1}$ we have

$$\begin{aligned} \frac{\partial}{\partial \varepsilon} \sum_{k=1}^n c_k^{-1} &= \sum_{k \neq j} \frac{\partial}{\partial \varepsilon} \left[1 - (\varepsilon + P_{k,k+1}^*/K)^2 \right]^{-\frac{1}{2}} - \frac{\partial}{\partial \varepsilon} \left[1 - (\varepsilon + P_{j,j+1}^*/K)^2 \right]^{-\frac{1}{2}} \\ &= \sum_{k \neq j} \left[1 - (\varepsilon + P_{k,k+1}^*/K)^2 \right]^{-\frac{3}{2}} \left[1 - (\varepsilon + P_{j,j+1}^*/K)^2 \right]^{-1} \\ &\quad \times \left[1 + (\varepsilon + P_{j,j+1}^*/K) (\varepsilon + P_{k,k+1}^*/K) \right] (P_{k,k+1}^* - P_{j,j+1}^*) / K. \end{aligned} \quad (3.59)$$

The only term in the last expression that is not necessarily positive is $(P_{k,k+1}^* - P_{j,j+1}^*)/K$. But if $j = j_\dagger$ (resp. $j = j_\ddagger$), this term is always negative (resp. positive) for $k \neq j$, and consequently the whole sum is positive (resp. negative). Thus, following a connected component of the level curve $\mathcal{A}^{(j)} = L$, whenever $\sum_k c_k^{-1}$ hits zero, its derivative always has the same sign, therefore, by continuity, it cannot cross zero more than once. This completes the proof. \square

The proof of Theorem 3.3 finally relies on Taylor's lemma [37, Lemma 2.1], which we recall here.

Lemma 3.11 (Taylor [37]). *Let $\vec{\theta}^*$ be a stable fixed point of Eq. (2.5) on any network. Then for any non-empty vertex subset N ,*

$$\sum_{\substack{\langle ij \rangle : \\ i \in N, j \notin N}} \cos(\theta_i^* - \theta_j^*) \geq 0. \quad (3.60)$$

In other words, if we can partition the vertices of the network in two sets N and $\mathcal{V}_G \setminus N$, such that the sum of cosines of the angle differences on all the edges between these two sets is negative, then the fixed point is unstable. In the case of a cycle, if the angle differences on two edges are larger than $\pi/2$ or less than $-\pi/2$, removing these two edges splits the network in two parts, N and $\mathcal{V}_G \setminus N$, such that

$$\sum_{\substack{\langle ij \rangle : \\ i \in N, j \notin N}} \cos(\Delta_{ij}^*) < 0, \quad (3.61)$$

and the fixed point is unstable. We conclude that there is at most a single $|\Delta_{i,i+1}| > \pi/2$. We are now ready to prove Theorem 3.3.

Proof of Theorem 3.3. Since for any K_0 , $\mathcal{A}(K_0, \varepsilon)$ is a monotonically increasing function of ε , we know that for any integer $q \in [-(n-1)/4, (n-1)/4] \cap \mathbb{Z}$, the level set of $\mathcal{A} = 2\pi q$ is a single level curve. Furthermore, any point on such a level curve corresponds to a stable fixed point of Eq. (3.1). Starting from large values of K and following this level curve while decreasing K , Corollary 3.6 implies that it meets the boundary of \mathcal{D} at some point. Assume that it meets the upper boundary \mathcal{D}_\dagger at $x = (K^*, \varepsilon^*)$ as shown in Figure 7 (the case of the lower boundary \mathcal{D}_\ddagger is treated in the same way, interchanging j_\ddagger and j_\dagger in what follows). We know that $\mathcal{A}(K^*, \varepsilon^*) = \mathcal{A}^{(j_\dagger)}(K^*, \varepsilon^*)$. As \mathcal{A} and $\mathcal{A}^{(j_\dagger)}$ coincide on \mathcal{D}_\dagger , Proposition 3.2 implies that $\mathcal{A}^{(j_\dagger)}$ is monotonic on \mathcal{D}_\dagger . It is as well smooth in the interior of the domain \mathcal{D} . There is then a level curve of $\mathcal{A}^{(j_\dagger)} = 2\pi q$ starting at x (the dashed red line in Figure 7), and by Lemma 3.7, it is unique. Furthermore, at x , the corresponding fixed point is stable.

According to Corollary 3.6, the level curve of $\mathcal{A}^{(j_\dagger)}$ either meets the boundary of \mathcal{D} or goes to $K \rightarrow \infty$. First, it cannot meet \mathcal{D}_\dagger because the value of $\mathcal{A}^{(j_\dagger)}$ is strictly increasing with K on \mathcal{D}_\dagger and the level curve cannot be closed by Corollary 3.6. Second, if it goes to $K \rightarrow \infty$, we know from Section 3.2 that for K large enough, the fixed point is unstable. Third, if it meets \mathcal{D}_\ddagger , at this point, $|\Delta_{j_\dagger, j_\dagger+1}| > \pi/2$ because we consider the level curve of $\mathcal{A}^{(j_\dagger)}$ and $|\Delta_{j_\dagger, j_\dagger+1}| = \pi/2$ because it is on the boundary \mathcal{D}_\ddagger . Lemma 3.11 then implies that the corresponding fixed point is unstable. Thus along the level curve considered, the eigenvalue λ_2 has to change sign. Following Lemmas 3.8 and 3.10, this happens only once, at point y shown in Figure 7 where the level curve changes direction with respect to K .

Assume now that there is another connected component of the level set of $\mathcal{A}^{(j_\dagger)} = 2\pi q$. From Corollary 3.6 it cannot be closed and by monotonicity of $\mathcal{A}^{(j_\dagger)}$ along \mathcal{D}_\dagger and Lemma 3.7, it cannot meet the upper boundary \mathcal{D}_\dagger . Thus the corresponding fixed points are unstable at both ends of this level curve and as, by Lemmas 3.8 and 3.10, λ_2 changes sign at most once along a level curve, then the corresponding fixed points are unstable all along this level curve.

We conclude that the number of ε values corresponding to stable fixed points of Eq. (3.1) increases with K , because a fixed point appears at point y and exists for any larger K . \square

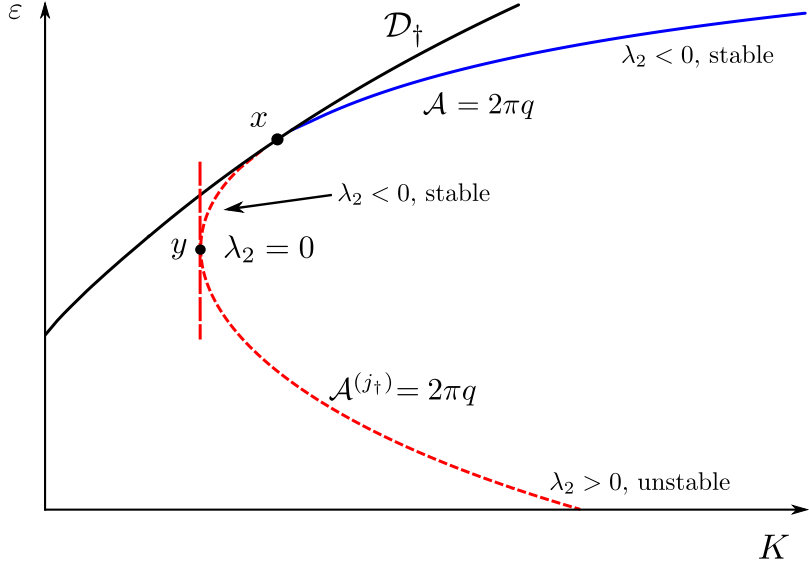


Figure 7: (Figure adapted from [48]) Level curves $\mathcal{A}(\varepsilon, K) = 2\pi q$ (blue line) and $\mathcal{A}^{(j\dagger)}(\varepsilon, K) = 2\pi q$ (dashed red line). Both functions are undefined above the boundary \mathcal{D}_\dagger (black line). The corresponding fixed points are stable ($\lambda_2 < 0$) along the blue curve and between points x and y on the dashed red curve, and unstable ($\lambda_2 > 0$) along the dashed red curve, from y to $K \rightarrow \infty$.

Remark. If there are two indices i_1 and i_2 such that $P_{i_1, i_1+1}^* = P_{i_2, i_2+1}^* = P_{\min}^*$ (the same works with P_{\max}^*), then $\sum_k c_k^{-1} > 0$ for $h_{i_2} \in \mathcal{I}$ and all other h_i 's in $[-\pi/2, \pi/2]$, because $c_{i_1} = -c_{i_2}$ and then

$$\sum_k c_k^{-1} = \sum_{k \neq i_1, i_2} c_k^{-1} > 0. \quad (3.62)$$

Hence, inside \mathcal{D} , λ_2 never changes sign along the level curves of $\mathcal{A}^{(i_1)}$ and $\mathcal{A}^{(i_2)}$. This result together with the fact that for $K \rightarrow \infty$ the fixed points corresponding to the level curves $\mathcal{A}^{(i_1)}$ and $\mathcal{A}^{(i_2)}$ are known to be unstable, implies that such fixed points remain unstable also for finite values of K . Which implies that, in this case, no fixed point having one angle difference outside the interval $[-\pi/2, \pi/2]$ can be locally stable.

To summarize, we showed that while decreasing K , the number of stable fixed points $\mathcal{N}(K)$ also decreases, and that any stable fixed point of Eq. (3.1) for finite K is a continuation of a fixed point for $K \rightarrow \infty$. We also showed that for finite K , stable fixed points have at most one angle difference outside $[-\pi/2, \pi/2]$, and that such fixed points are continuations of fixed points with all angle differences in $[-\pi/2, \pi/2]$. Figure 8 illustrates the whole situation. The domain \mathcal{D} is bounded from above by the curve \mathcal{D}_\dagger and from below by \mathcal{D}_\ddagger . The blue lines are the $2\pi q$ -level curves of \mathcal{A} for $q \in \{-1, 0, 1\}$, i.e. any point on a blue curve gives a pair (K, ε) corresponding to a stable fixed point of Eq. (3.1) with all angle differences in $[-\pi/2, \pi/2]$. The red dashed lines and the green dash-dotted line are the $2\pi q$ -level curves of $\mathcal{A}^{(j\dagger)}$ and $\mathcal{A}^{(j\dagger)}$ respectively. The points on the red dashed curves correspond to fixed points (not necessarily stable) where the angle difference on the edge carrying P_{\max}^* is in \mathcal{I} and the points on the green dash-dotted curve correspond to fixed points where the angle difference along the edge carrying P_{\min}^* is in \mathcal{I} . Any blue line meets either a red dashed line on \mathcal{D}_\dagger (a zoom-in of this is depicted in Figure 7) or a green dash-dotted line on \mathcal{D}_\ddagger . While increasing K , stable fixed points appear on the level curves of $\mathcal{A}^{(j\dagger)}$ and $\mathcal{A}^{(j\dagger)}$ (at point y in Figure 7), thus with one angle difference larger than $\pi/2$ (or less than $-\pi/2$). This angle difference then enters $[-\pi/2, \pi/2]$ while K increases. This happens at point x in Figure 7. Then the stable fixed point persists for larger K along the corresponding level curve of \mathcal{A} .

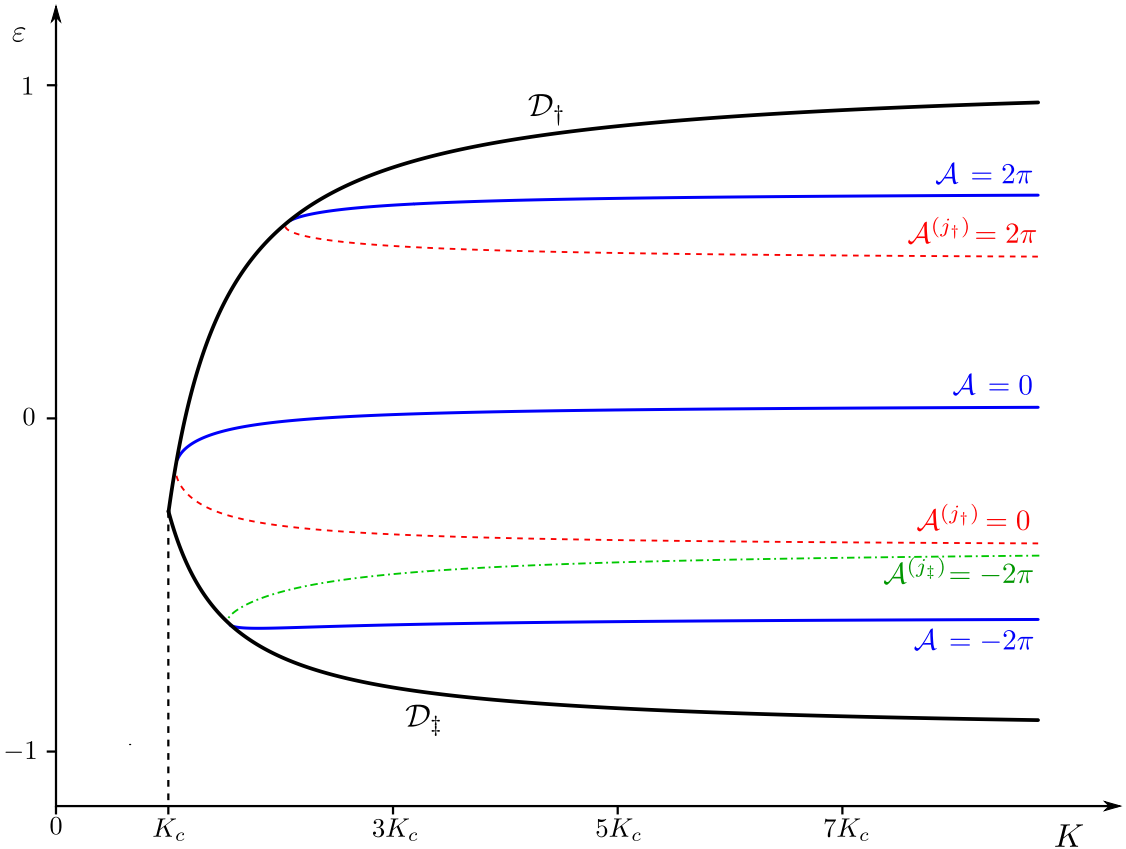


Figure 8: (Figure adapted from [48]) Level curves $\mathcal{A} = 2\pi q$ (blue), $\mathcal{A}^{(j\dagger)} = 2\pi q$ (dashed red) and $\mathcal{A}^{(j\dagger)} = 2\pi q$ (dash-dotted green), for different q -values, in the (K, ε) -plane. The level curves of \mathcal{A} and $\mathcal{A}^{(j\dagger)}$ meet on the upper boundary \mathcal{D}_\dagger of the domain \mathcal{D} defined in Eq. (3.24), and the level curves of \mathcal{A} and $\mathcal{A}^{(j\dagger)}$ meet on the lower boundary \mathcal{D}_\ddagger . The two boundaries \mathcal{D}_\ddagger and \mathcal{D}_\dagger meet at $K_c = (P_{\max}^* - P_{\min}^*)/2$. A zoom-in of the region where the level curves $\mathcal{A} = 2\pi$ and $\mathcal{A}^{(j\dagger)} = 2\pi$ meet is depicted in Figure 7.

4 The number of stable equilibria in equal-frequency Kuramoto models on planar graphs

We amplify on the results of Section 3 by generalizing the upper bound on the number of stable fixed points of Eq. (1.3) on a single-cycle network of length n , to the case of planar networks with identical natural frequencies. The problem here is threefold. First, one must account for an effective coupling between neighboring cycles with common edges. Along the latter, loop flows are superimposed, which couples two conditions as expressed in Eq. (2.24) for two different cycles, as the winding number on both cycles has to be an integer. Second, this superposition leads to increased or decreased angle differences, which sometimes jeopardizes the stability of the resulting fixed point solutions, or sometimes stabilizes some of them. Third, in meshed networks, one has to revisit the one-to-one relation between number of stable fixed points and number of possible winding numbers on which the strategy of Section 3 is based. Below, we present a method that overcomes these obstacles, which allows us to generalize the bound found in [44, 45] and in Section 3. Most of the results presented in this section were published in [49].

From now on, we consider planar networks with identical frequencies, Eq. (2.5) then simplifies to

$$\dot{\theta}_i = -K \sum_{j=1}^n a_{ij} \sin(\theta_i - \theta_j), \quad i = 1, \dots, n. \quad (4.1)$$

For any connected graph \mathcal{G} with n vertices and m edges, we can define a set of **fundamental cycles**. Let $\mathcal{T} \subset \mathcal{G}$ be a spanning tree of \mathcal{G} and r an arbitrary vertex of \mathcal{G} which we call the **root**. Each edge of $\mathcal{W} := \mathcal{E}_{\mathcal{G}} \setminus \mathcal{E}_{\mathcal{T}}$ closes a cycle of \mathcal{G} . The fundamental cycle associated to an edge $\langle ij \rangle \in \mathcal{W}$ is the set of edges obtained by concatenation of the unique path in \mathcal{T} from r to i , the edge $\langle ij \rangle$ and the unique path in \mathcal{T} from j to r , with the prescription that, if the resulting path goes twice through an edge, then we remove the latter from the path. This gives us $c = m - n + 1$ fundamental cycles which form together a cycle basis. Any cycle of \mathcal{G} is a linear combination of fundamental cycles (see [54] for more details). If the graph \mathcal{G} is planar, a wise choice of the spanning tree \mathcal{T} gives a set of fundamental cycles defined by the edges surrounding each face of the embedding of \mathcal{G} in \mathbb{R}^2 . From now on, we focus on connected planar graphs and choose this fundamental cycle basis. We do not consider tree-like parts on \mathcal{G} , since angle differences on such parts are uniquely defined and have no influence on the stability of the rest of the network. Tree-like parts can therefore be absorbed in the vertex that connects them to the meshed part of \mathcal{G} , which is why we neglect them in the following.

Let $\mathcal{L}_1, \dots, \mathcal{L}_c$ be the sets of edges composing each fundamental cycle. For $k = 1, \dots, c$, we define m_k as the number of edges exclusively in cycle k and for $k \neq \ell$, $m_{k\ell}$ is the number of edges common to the two cycles k and ℓ . Because we restrict ourselves to planar graphs and with our choice of fundamental cycle, no edge is common to more than two cycles. We then define $n_k := m_k + \sum_{\ell \neq k} m_{k\ell}$ the number of elements in \mathcal{L}_k . When there are more than one cycle in a network, we index the loop flow parameter on each cycle with the corresponding cycle index, $\varepsilon_k \in \mathbb{R}$ is the loop flow parameter on the fundamental cycle k . Any loop flow can be uniquely written as a linear combination of loop flows on fundamental cycles.

Connection with Algebraic Topology. The fundamental cycles $\mathcal{L}_1, \dots, \mathcal{L}_c$ are linearly independent elements of $C_1(\mathcal{G}; \mathbb{R})$, defined in Eq. (2.14). Furthermore they are in the kernel of the boundary map ∂ defined in Eq. (2.18), which is the first homology group of the graph \mathcal{G} . These fundamental cycle then form a basis of $\ker(\partial)$ and each of them is then a different non-trivial element of the first homology group of \mathcal{G} , seen as a CW complex.

We arbitrarily fix an orientation to each edge and each cycle independently. We can now define the **edge-cycle incidence matrix**, $\mathcal{S} \in \mathbb{R}^{m \times c}$ as follows

$$\mathcal{S}_{ek} := \begin{cases} +1 & \text{if } e \in \mathcal{L}_k \text{ with the same orientation,} \\ -1 & \text{if } e \in \mathcal{L}_k \text{ with opposite orientation,} \\ 0 & \text{if } e \notin \mathcal{L}_k, \end{cases} \quad (4.2)$$

where e is an edge index and k a cycle index. As the columns of \mathcal{S} are the edge vectors of the fundamental cycles, the flow amplitude on any edge $e = \langle ij \rangle$ can be written as

$$P_{ij} = \sum_{k: e \in \mathcal{L}_k} K \mathcal{S}_{ek} \varepsilon_k, \quad (4.3)$$

where the sum is taken over all cycles containing edge e . Note that here the reference flow defined in Eq. (2.13) is zero everywhere. The magnitude of the interaction strength on each edge is bounded by the coupling on that edge, therefore, for every edge $e = \langle ij \rangle$,

$$-K \leq P_{ij} \leq K \implies -1 \leq \sum_{k: e \in \mathcal{L}_k} \mathcal{S}_{ek} \varepsilon_k \leq 1, \quad (4.4)$$

which defines a compact parameter domain $\mathcal{D}_G \subset \mathbb{R}^c$ of possible values for the vector of loop flows $\vec{\varepsilon} := (\varepsilon_1, \dots, \varepsilon_c)$.

From now on, we consider stable fixed points of Eq. (4.1) with all angle differences in the interval $[-\pi/2, \pi/2]$. Let $\vec{\varepsilon} \in \mathcal{D}_G$ be the loop flow vector of a fixed point of Eq. (4.1). The angle difference on edge $e = \langle ij \rangle$ is $\Delta_{ij} \in [-\pi/2, \pi/2]$, and is given by

$$\Delta_{ij}(\vec{\varepsilon}) = \arcsin(P_{ij}(\vec{\varepsilon})/K) = \arcsin\left(\sum_{k: e \in \mathcal{L}_k} \mathcal{S}_{ek} \varepsilon_k\right). \quad (4.5)$$

The definition of winding number, Eq. (2.24), applies to any cycle in a network. Defining $q_k \in \mathbb{Z}$ the winding number on the fundamental cycle \mathcal{L}_k ,

$$\sum_{e \in \mathcal{L}_k} \Delta_e(\vec{\varepsilon}) = 2\pi q_k, \quad k = 1, \dots, c, \quad (4.6)$$

and recalling that any cycle of \mathcal{G} is a combination of fundamental cycles, it is straightforward that the winding number on any cycle of \mathcal{G} is fully determined by the winding number on the fundamental cycles. Note that we can associate a point $\vec{\varepsilon} \in \mathcal{D}_G$ to any fixed point of Eq. (4.1), but Eq. (4.6) implies that not any $\vec{\varepsilon} \in \mathcal{D}_G$ gives a fixed point of Eq. (4.1).

Remark. If a fixed point has all angle differences in $[-\pi/2, \pi/2]$, then its Jacobian matrix is diagonal dominant. According to Corollary 2.7, the Jacobian matrix is then negative semidefinite and the fixed point is stable. This was previously noted in [39].

Define the **quantization function**

$$\vec{\mathcal{A}} = (\mathcal{A}_1, \dots, \mathcal{A}_c): \mathcal{D}_G \rightarrow \mathbb{R}^c, \quad (4.7)$$

whose components are the sums of angle differences around the corresponding fundamental cycles,

$$\mathcal{A}_k(\vec{\varepsilon}) := \sum_{e \in \mathcal{L}_k} \Delta_e(\vec{\varepsilon}) = \sum_{e \in \mathcal{L}_k} \arcsin\left(\sum_{\ell: e \in \mathcal{L}_\ell} \mathcal{S}_{e\ell} \varepsilon_\ell\right), \quad k = 1, \dots, c. \quad (4.8)$$

Remark. We call $\vec{\mathcal{A}}$ quantization function because Eq. (4.6) leads to $\mathcal{A}_k = 2\pi q_k$, which is analogous to quantization conditions in quantum mechanics such as quantization of circulation around vortices in superfluids or of fluxes through superconducting rings. Note however that there is no quantum mechanics in the Kuramoto model.

Define next the level sets $\mathcal{Q}_k^q := \{\vec{\varepsilon} \in \mathcal{D}_G \mid \mathcal{A}_k(\vec{\varepsilon}) = 2\pi q\}$, for $k = 1, \dots, c$ and $q \in \mathbb{Z}$. It is easy to check that for any k , there are at most

$$\mathcal{N}_k = 2 \cdot \text{Int}(n_k/4) + 1 \quad (4.9)$$

distinct such level sets for \mathcal{A}_k in the domain \mathcal{D}_G (see Section 3). For a given **winding vector** $\vec{q} = (q_1, \dots, q_c) \in \mathbb{Z}^c$, giving a winding number on each fundamental cycle, define finally the intersection of level sets

$$\mathcal{Q}(\vec{q}) := \bigcap_{k=1}^c \mathcal{Q}_k^{q_k}. \quad (4.10)$$

These definitions bring us to the following proposition, which we will need below.

Proposition 4.1. *Stable fixed point solutions of Eq. (4.1) with winding vectors $\vec{q} = (q_1, \dots, q_c)$ and angle differences in $[-\pi/2, \pi/2]$ are in a one-to-one correspondence with loop flow vectors $\vec{\varepsilon} \in \mathcal{Q}(\vec{q})$.*

Proof. For a given winding vector $\vec{q} = (q_1, \dots, q_c)$, we define $\mathcal{F}(\vec{q})$ the set of stable fixed points of Eq. (4.1) with winding vector \vec{q} . Let us define the map $\Theta: \mathcal{Q}(\vec{q}) \rightarrow \mathcal{F}$ that associates a fixed point $\Theta(\vec{\varepsilon})$ to each point $\vec{\varepsilon} \in \mathcal{Q}(\vec{q})$ as follows. For every edge $\langle ij \rangle \in \mathcal{E}_G$, the flow P_{ij} is defined by Eq. (4.3), and the angle difference $\Delta_{ij}(\vec{\varepsilon})$ is defined by Eq. (4.5). We then consider the spanning tree \mathcal{T} chosen to construct the fundamental cycles of \mathcal{G} and its root r , and construct the fixed point $\Theta(\vec{\varepsilon})$ iteratively. We fix the angle at the root to zero $\Theta_r(\vec{\varepsilon}) = 0$ and all other angles as

$$\Theta_i(\vec{\varepsilon}) = - \sum_{e \in \mathcal{P}_{ri}} \Delta_e(\vec{\varepsilon}), \quad i = 1, \dots, n, \quad (4.11)$$

where \mathcal{P}_{ri} is the unique path in \mathcal{T} from r to i . We show now that this is a fixed point. For any edge $\langle ij \rangle \in \mathcal{W} = \mathcal{E}_G \setminus \mathcal{E}_{\mathcal{T}}$, the angle difference obtained this way is

$$\Theta_i(\vec{\varepsilon}) - \Theta_j(\vec{\varepsilon}) = \sum_{e \in \mathcal{P}_{ij}} \Delta_e, \quad (4.12)$$

where \mathcal{P}_{ij} is the unique path in \mathcal{T} from i to j , and by definition of $\mathcal{Q}(\vec{q})$,

$$\sum_{e \in \mathcal{P}_{ij} \cup \langle ji \rangle} \Delta_e = 2\pi q \iff \Delta_{ij} + 2\pi q = \sum_{e \in \mathcal{P}_{ij}} \Delta_e = \Theta_i(\vec{\varepsilon}) - \Theta_j(\vec{\varepsilon}) \quad (4.13)$$

$$\implies \sin(\Theta_i(\vec{\varepsilon}) - \Theta_j(\vec{\varepsilon})) = \sin(\Delta_{ij}(\vec{\varepsilon})). \quad (4.14)$$

The sum of flows at vertex i for the state $\vec{\theta}^*$ is then

$$\sum_{j: \langle ij \rangle \in \mathcal{E}_G} K \sin(\Delta_{ij}(\vec{\varepsilon})) = \sum_{j: \langle ij \rangle \in \mathcal{E}_G} \sum_{k: \langle ij \rangle \in \mathcal{L}_k} K \mathcal{S}_{\langle ij \rangle, k} \varepsilon_k = \sum_{j: \langle ij \rangle \in \mathcal{E}_G} K (\mathcal{S} \vec{\varepsilon})_{\langle ij \rangle} = K (\mathcal{B} \mathcal{S} \vec{\varepsilon})_i = 0, \quad (4.15)$$

where one obtains the last equality by remarking that the columns of \mathcal{S} are cycles, which are exactly the null-space of \mathcal{B} . The state $\vec{\theta}^*$ is then a fixed point of Eq. (4.1), and by definition, all its angle differences taken modulo 2π are in $[-\pi/2, \pi/2]$, and it is then stable. The map Θ is then well defined.

Let $\vec{\theta}^*$ be a stable fixed point of Eq. (4.1) with winding vector \vec{q} . As the vector of identical angles is a fixed point as well, according to Theorem 2.3, the flows of $\vec{\theta}^*$ are a collection of loop flows. We then construct the vector $\vec{\varepsilon}$, such that $K \varepsilon_k$ is the amplitude of the loop flow of $\vec{\theta}^*$ on the k^{th} fundamental cycle. By construction, there exist $\phi \in \mathbb{R}$ and $k_i \in \mathbb{Z}$, $i = 1, \dots, n$ such that $\Theta_i(\vec{\varepsilon}) = \theta_i^* + 2\pi k_i + \phi$ for all i . According to the discussion around Eq. (2.6), the states $\vec{\theta}^*$ and $\Theta(\vec{\varepsilon})$ are then the same fixed point and the map Θ is then surjective.

Assume that $\mathcal{Q}(\vec{q})$ is not empty and let $\vec{\eta}, \vec{\rho} \in \mathcal{Q}(\vec{q})$, such that $\Theta(\vec{\eta}) = \Theta(\vec{\rho})$. This means that $\Delta_e(\vec{\eta}) = \Delta_e(\vec{\rho})$ for all edges $e \in \mathcal{E}_{\mathcal{T}}$, and then

$$\sum_{k=1}^c \mathcal{S}_{ek} \eta_k = \sum_{k=1}^c \mathcal{S}_{ek} \rho_k, \quad (4.16)$$

and in matricial form

$$\mathcal{S} \cdot (\vec{\eta} - \vec{\rho}) = 0. \quad (4.17)$$

As the columns of \mathcal{S} correspond to the fundamental cycles of \mathcal{G} , they are linearly independent, implying $\vec{\eta} = \vec{\rho}$. The map Θ is then injective, which concludes the proof of the one-to-one correspondence. \square

4.1 Bound on the number of stable fixed points

We show that for a given winding vector, $\vec{q} \in \mathbb{Z}^c$, the corresponding level sets $\mathcal{Q}_k^{q_k}$, $k = 1, \dots, c$ intersect at most at one point. We then derive some bounds on the number of stable fixed points of Eq. (4.1) with all angle differences less than $\pi/2$. The following theorem is key to obtain this bound, which we later derive in Corollary 4.3.

Theorem 4.2. *Let \mathcal{G} be a planar graph and $\vec{\mathcal{A}}: \mathcal{D}_{\mathcal{G}} \rightarrow \mathbb{R}^c$ the quantization function associated with its fundamental cycle basis defined on the faces of the embedding of \mathcal{G} in \mathbb{R}^2 . For a given winding vector $\vec{q} \in \mathbb{Z}^c$, the intersection, Eq. (4.10), of its level sets is either a single point or empty.*

Remark. *The hypothesis of planar graphs is key to Theorem 4.2. It guarantees in particular that any edge of \mathcal{G} belongs to at most two different fundamental cycles, which is necessary for the proof.*

Proof. For a planar network composed of c fundamental cycles, Eq. (4.6) reads

$$\mathcal{A}_k(\vec{\varepsilon}) := m_k \arcsin(\varepsilon_k) + \sum_{i \neq k} m_{ki} \arcsin(\varepsilon_k - \varepsilon_i) = 2\pi q_k, \quad k = 1, \dots, c. \quad (4.18)$$

For each k , Eq. (4.18) defines a level set, $\mathcal{Q}_k^{q_k} \subset \mathcal{D}_{\mathcal{G}}$ of possible values for $\vec{\varepsilon}$. Assume that these level sets intersect in two distinct points of $\mathcal{D}_{\mathcal{G}}$, $\vec{\eta}$ and $\vec{\rho}$, and let $\vec{\xi} := \vec{\rho} - \vec{\eta}$. Because $\vec{\eta}$ and $\vec{\rho}$ are assumed distinct, $\vec{\xi}$ has at least one non-zero component. Without loss of generality, we assume this component to be positive. We then order the cycles such that $\xi_1 = \max_{\ell} \{\xi_{\ell}\} > 0$. We now consider the directional derivative of \mathcal{A}_k for $k = 1, \dots, c$ in the direction of $\vec{\xi}$,

$$\nabla \mathcal{A}_k(\vec{\varepsilon}) \cdot \vec{\xi} = \frac{m_k \xi_k}{\sqrt{1 - \varepsilon_k^2}} + \sum_{i \neq k} \frac{m_{ki} (\xi_k - \xi_i)}{\sqrt{1 - (\varepsilon_k - \varepsilon_i)^2}}. \quad (4.19)$$

At each end of the segment defined by $\vec{\eta} + \alpha \vec{\xi}$, $\alpha \in [0, 1]$, the function \mathcal{A}_k takes the same value. Thus the directional derivative either is constant and equal to zero or changes sign for some $\alpha \in (0, 1)$. Consider Eq. (4.19) with $k = 1$,

$$\nabla \mathcal{A}_1(\vec{\varepsilon}) \cdot \vec{\xi} = \frac{m_1 \xi_1}{\sqrt{1 - \varepsilon_1^2}} + \sum_{i \neq 1} \frac{m_{1i} (\xi_1 - \xi_i)}{\sqrt{1 - (\varepsilon_1 - \varepsilon_i)^2}}. \quad (4.20)$$

First if $m_1 > 0$, then the sum of terms on the right-hand-side is strictly positive. Thus the directional derivative of \mathcal{A}_1 is never zero for $\alpha \in (0, 1)$. Second, if $m_1 = 0$ and there exist a cycle ℓ such that $m_{1\ell} > 0$ and $\xi_{\ell} < \xi_1$, then the right-hand-side of Eq. (4.20) is positive, because at least the term $i = \ell$ is positive and no term is negative. Third, if $m_1 = 0$ and for all ℓ such that $m_{1\ell} > 0$, $\xi_1 = \xi_{\ell}$, then either $\xi_k = \xi_1$ for all $k = 1, \dots, c$, in which case there exist k_0 such that $m_{k_0} > 0$, or there exist k_0 and k_1 such that $\xi_1 = \xi_{k_0} > \xi_{k_1}$ and $m_{k_0 k_1} > 0$. In both cases, considering \mathcal{A}_{k_0} instead of \mathcal{A}_1 in Eq. (4.20), we obtain that the right-hand-side is strictly positive.

Therefore, the directional derivative on the left-hand-side of Eq. (4.20) does not vanish along $\vec{\varepsilon} = \vec{\eta} + \alpha \vec{\xi}$ for any α . This contradicts the assumption that $\vec{\eta}$ and $\vec{\rho}$ are distinct points of the intersection of level sets $\mathcal{Q}(\vec{q})$ and concludes the proof. \square

Theorem 4.2 implies that the set of stable fixed points of Eq. (4.1) with angle differences in $[-\pi/2, \pi/2]$ injects in the set of possible winding vectors. In other words, two distinct fixed points with angle differences in $[-\pi/2, \pi/2]$ have distinct winding vectors. The number of stable fixed points of Eq. (4.1) is then bounded from above by the number of possible winding vectors.

Corollary 4.3. *For any planar graph \mathcal{G} , the number \mathcal{N}^* of stable fixed points of Eq. (4.1) with angle differences in $[-\pi/2, \pi/2]$ is bounded from above as*

$$\mathcal{N}^* \leq \prod_{k=1}^c [2 \cdot \text{Int}(n_k/4) + 1]. \quad (4.21)$$

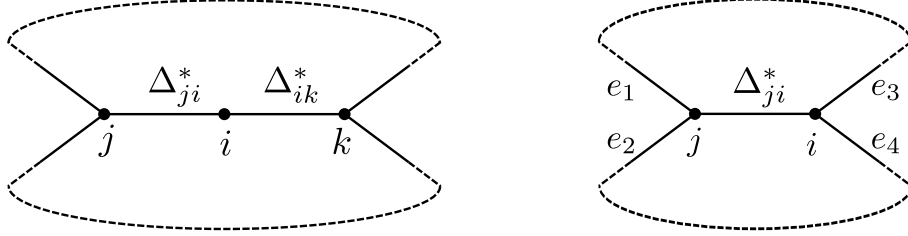


Figure 9: (Figure adapted from [49]) Neighboring cycles separated by two consecutive edges (left panel) and a single edge (right panel). In the left panel, the angle differences Δ_{ji}^* and Δ_{ik}^* must both be in the interval $[-\pi/2, \pi/2]$ for a fixed point solution to be stable. In the right panel, however, the angle difference Δ_{ji}^* may be larger than $\pi/2$.

Proof. For all $k = 1, \dots, c$, the function \mathcal{A}_k takes value in $[-n_k\pi/2, n_k\pi/2]$ and thus

$$q_k \in [-\text{Int}(n_k/4), \dots, \text{Int}(n_k/4)] \cap \mathbb{Z}. \quad (4.22)$$

There are then at most $\prod_{k=1}^c [2 \cdot \text{Int}(n_k/4) + 1]$ possible winding vectors \vec{q} . According to Theorem 4.2, for each of these winding vectors, the corresponding level sets $\mathcal{Q}_k^{q_k}$ intersect at most at a single point. The one-to-one correspondence between fixed points of Eq. (4.1) and intersections of these level sets expressed in Proposition 4.1 concludes the proof. \square

Remarks. (i) Note that in Corollary 4.3 we restrict ourselves to stable fixed points with all angle differences in $[-\pi/2, \pi/2]$ whose number \mathcal{N}^* is, in general, lower than the total number of stable fixed points \mathcal{N} .

(ii) The bound on \mathcal{N}^* is algebraic in the length of the cycles. This is a significant improvement on the previously known bounds which are exponential in the number of vertices. Nevertheless, the bound of Corollary 4.3 is not yet tight, because some choices of $\vec{q} = (q_1, \dots, q_c)$ are not realizable.

The following lemma characterizes network topologies whose stable fixed points necessarily have angle differences in $[-\pi/2, \pi/2]$ and thus satisfy $\mathcal{N} = \mathcal{N}^*$. In networks where adjacent cycles share at least two consecutive edges, as in the left panel of Figure 9, all stable fixed points have all angle differences in the interval $[-\pi/2, \pi/2]$. If however, two cycles share a single edge only, as in the right panel of Figure 9, some stable fixed points may have angle differences larger than $\pi/2$.

Lemma 4.4. On a graph \mathcal{G} where no pair of vertices with degree larger or equal to 3 are connected by a single-edge path, all angle differences of any stable fixed point of Eq. (4.1) are in $[-\pi/2, \pi/2]$.

Proof. Let $\vec{\theta}^*$ be a stable fixed point of Eq. (4.1) on \mathcal{G} . First, according to Lemma 3.11, the two edges connected to a vertex of degree 2 cannot both carry an angle difference whose cosines are negative. Thus in the left panel of Figure 9, Δ_{ji}^* and Δ_{ik}^* cannot be both larger than $\pi/2$. Without loss of generality, we assume Δ_{ji}^* and Δ_{ik}^* to be both positive, otherwise we consider Δ_{ij}^* and Δ_{ki}^* instead. Now if $\Delta_{ji}^* < \pi/2 < \Delta_{ik}^*$, according to Eq. (2.11),

$$\sin(-\Delta_{ji}^*) + \sin(\Delta_{ik}^*) = 0 \iff \Delta_{ik}^* = \pi - \Delta_{ji}^* \implies \cos(\Delta_{ik}^*) = -\cos(\Delta_{ji}^*) =: -c_0. \quad (4.23)$$

Consider the Jacobian matrix \mathcal{J} defined in Eq. (2.36). The principal minor (Definition 2.4) of $-\mathcal{J}$ with row and column indices j and i is

$$\det \begin{pmatrix} x & -\cos(\Delta_{ji}^*) \\ -\cos(\Delta_{ji}^*) & \cos(\Delta_{ji}^*) + \cos(\Delta_{ik}^*) \end{pmatrix} = \det \begin{pmatrix} x & -c_0 \\ -c_0 & 0 \end{pmatrix}, \quad (4.24)$$

which is negative. According to Sylvester's criterion (Theorem 2.5), \mathcal{J} is not negative semidefinite, implying that the fixed point is unstable. We conclude that a stable fixed point of Eq. (4.1) has all angle differences in $[-\pi/2, \pi/2]$. \square

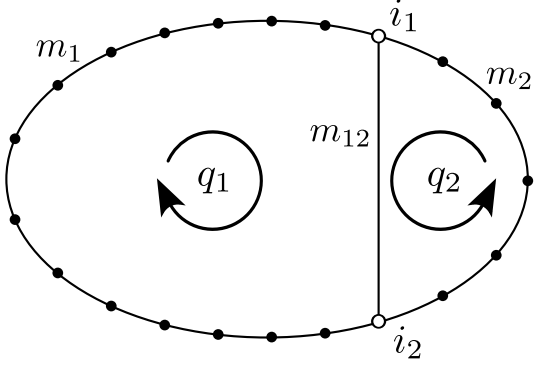


Figure 10: (Figure taken from [49]) Example of a network having a stable fixed point solution of Eq. (4.1) with one angle difference larger than $\pi/2$. The number of edges along the three paths from i_1 to i_2 are $m_1 = 15$, $m_2 = 6$ and $m_{12} = 1$, the coupling constant is $K = 1$. The angle difference in the middle path is $\Delta_{i_1 i_2} \approx \pi/2 + 0.149$ for a stable fixed point solution with $q_1 = -1$ and $q_2 = 1$.

Lemma 4.4 allows to apply Corollary 4.3 to a well-defined class of networks. The next corollary gives a bound on the number of stable fixed points of Eq. (4.1) depending on the topology of the network.

Corollary 4.5. *On a planar graph \mathcal{G} where no pair of vertices with degree larger or equal to 3 are connected by a single-edge path, the number \mathcal{N} of stable fixed points of Eq. (4.1) is bounded from above by*

$$\mathcal{N} \leq \prod_{k=1}^c [2 \cdot \text{Int}(n_k/4) + 1]. \quad (4.25)$$

Corollary 4.5 covers a large class of networks. The bound (4.25) is valid for any planar network with any number of cycles, as long as two cycles share either two or more edges, or no edge. When two cycles share a single edge, as in the right panel of Figure 9, we cannot identify a negative principal minor of $-\mathcal{J}$ as in Eq. (4.24), which invalidates the proof for such network topologies. In the next section, we discuss some examples where the Jacobian matrix \mathcal{J} is negative semidefinite even though some angle differences are larger than $\pi/2$, meaning that all principal minors of $-\mathcal{J}$ are non-negative. What happens in these situations, is that angle differences on edges e_1, e_2, e_3 and e_4 , in the right panel of Figure 9, may be small enough to stabilize an angle difference larger than $\pi/2$ on edge $\langle ij \rangle$.

Remark. *The bounds Eq. (4.21) and (4.25) both depend on the choice of fundamental cycles. Both remain true for any choice of the fundamental cycles such that any edge of the interaction graph belongs to at most two fundamental cycles. If multiple such choices of fundamental cycles are possible, the sharper bound is obviously the minimum among all choices of fundamental cycles,*

$$\mathcal{N} \leq \min_{\mathcal{L}_1, \dots, \mathcal{L}_c} \prod_{k=1}^c [2 \cdot \text{Int}(n_k/4) + 1], \quad (4.26)$$

where the minimum is taken among the choices of fundamental cycles such that every edge belongs to at most two fundamental cycles.

4.2 Angle differences exceeding $\pi/2$

The results of the previous section do not give a bound on the number of stable fixed points of Eq. (4.1) for any planar network. There exist some examples of networks admitting a stable fixed point with some angle differences larger than $\pi/2$. We discuss two such examples here. These networks have at least one pair of cycles sharing only one edge and consequently they do not satisfy the hypothesis of Lemma 4.4.

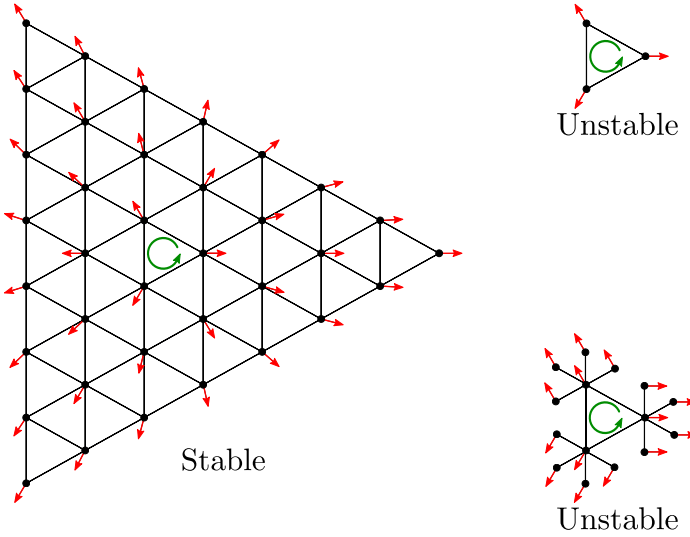


Figure 11: (Figure taken from [49]) Left: Stable fixed point on a triangular lattice with three angle differences of $2\pi/3$, here $\lambda_2 \approx -0.0974 < 0$. The red arrows indicate the angle at each vertex and the green arrow indicates a loop flow with $q = 1$ on the central triangle. The lattice shown is the smallest one we found numerically that stabilizes this loop flow. Top right: Fixed point on the triangular network with winding number $q = 1$. This fixed point is unstable, $\lambda_2 = 1.5 > 0$, which agrees with the results of [39] and Section 3. Bottom right: Fixed point on the hairy triangle network with a loop flow $q = 1$. As for the simple triangle, the fixed point is unstable, $\lambda_2 \approx 0.386$, even if its vertices have higher degree. For all these three examples, $K = 1$.

Example 1. Consider the network of Figure 10 with $K = 1$, where the left path from i_1 to i_2 is of length $m_1 = 15$, the right path is of length $m_2 = 6$ and the center path is of length $m_{12} = 1$. We checked numerically that there exists a stable fixed point of Eq. (4.1) with one angle difference larger than $\pi/2$. This fixed point has winding numbers $q_1 = -1$ and $q_2 = 1$, a large angle difference on the central edge $\langle i_1 i_2 \rangle$, $\Delta_{i_1 i_2} \approx \pi/2 + 0.149$ and negative Lyapunov exponents, $\lambda_2 \approx -0.0194$, implying that it is stable.

The right-hand-side of Eq. (4.25) give here 27. To obtain this value, we assumed that the possible values for the winding number q_1 (resp. q_2) are $\{-4, \dots, 4\}$ (resp. $\{-1, 0, 1\}$), which encompass the case $q_1 = -1$ and $q_2 = 1$ considered here. From this point of view, there is then hope that our bound is valid for any planar graph, even if we are not able to prove it yet. The following example is a counterexample to this idea.

Example 2. Consider now the triangular lattice shown in the left panel of Figure 11 with $K = 1$. The fixed point with winding number $q = 1$ on the central triangle has three angle differences of $2\pi/3$, but we checked numerically that it is stable nevertheless, $\lambda_2 \approx -0.0974$. According to [39] and to Section 3, the fixed point with a loop flow on the 3-vertex network (top right panel of Figure 11) is unstable. The largest eigenvalue of its Jacobian matrix can be analytically computed, $\lambda_2 = 1.5$. In the triangular lattice, the structure of the network surrounding the central triangle stabilizes these large angle differences, thanks to an increased connectivity. It should be noted however that increasing the connectivity with only tree-like graph extensions is not enough. For the *hairy triangle* shown on the bottom right panel of Figure 11, the fixed point with winding number $q = 1$ is unstable, as for the triangle of the top right panel, $\lambda_2 \approx 0.386$. It therefore cannot carry a loop flow.

All fundamental cycles in the triangular lattice of the left panel of Figure 11 are triangles. In the bound of Eq. (4.25), each of them contributes as a factor 1 in the product, the right-hand-side takes then value 1. But as we showed, there are strictly more than one fixed point. This implies that the class of networks where our bound, Eq. (4.25), is valid cannot be extended to any planar networks. In the conclusive discussion, we conjecture a more general bound that encompasses any planar network.

5 Protected loop flows

Knowing that multiple stable fixed points of Eq. (2.5) can exist, we now investigate how a system at a given stable fixed point can be brought to another stable fixed point. This question is hard to tackle analytically and we offer here some numerical simulations showing some modifications of the networks at hand, that lead the system from a fixed point to another. Even if our approach is numerical, the choice of networks and the perturbations that lead to a change of stable fixed point are guided by our knowledge of the characteristics of different fixed points, namely their different winding numbers.

We present here simulations of three mechanisms leading to a change of fixed point for given networks. The networks considered are very specific and simple networks, but they capture the fundamental ingredients needed to observe the phenomena of interest. All presented mechanisms need a drastic change in the network. Namely, either a change of topology of the network or a perturbation of natural frequencies sufficiently large to lead to destabilization of a fixed point. We show as well that coming back continuously to the initial configuration of the system does not bring the system back to its initial fixed point, in general. We relate this to the fact that winding numbers are discrete quantities, and thus continuous changes of the network's parameters cannot change this value. Most of the results of this section were published in [67].

To perform our simulations, we implemented the dynamics of the Kuramoto model, Eq. (1.3), with a 4th-order Runge-Kutta method.

5.1 Process 1: Creating Loop Flows via Change of Natural Frequencies

Consider first a cycle network as illustrated in Figure 12(d), with natural frequencies P and $-P$ on the vertices x and y respectively, and almost zero otherwise (see Remark below). The flows around the ring are governed by Eq. (2.9). From Section 3, the system carries at most nine stable fixed points differing by loop flows, when $K \rightarrow \infty$. Figure 12(b) shows seven of these fixed points, each characterized by its winding number $q = -3, -2, \dots, 3$. As mentioned in Section 2.3, the stability of each fixed point is determined by the spectrum of the Jacobian matrix \mathcal{J} and in particular by the sign of λ_2 . Figure 12(a) shows, together with Figure 12(b), how stable fixed points disappear as they lose their stability, $\lambda_2 \rightarrow 0$, as P is increased. The fixed point with $q = 0$ has the smallest λ_2 at small P . Remarkably enough, the $q = 0$ fixed point loses its stability at $P/K \approx 1.6$, before the $q = -1$ fixed point, which remains stable until $P/K \approx 1.85$. Starting from the $q = 0$ fixed point and increasing P beyond $1.6K$, we observe a loss of stability followed by a short transient after which the operating state has been transferred to the $q = -1$ state. This transient is illustrated in Figures 12(c) and (d), which show that mostly one angle, corresponding to the negative natural frequency, rotates while all other angles move very little (a movie of this transient can be found in [67, Supplemental Material]). The rotation of this angle changes q which oscillates between $q = 0$ and $q = -1$, eventually stabilizing at $q = -1$. These oscillations of winding number happen during the transient each time an angle difference gets larger than π or smaller than $-\pi$, because of the definition of the angle difference $\Delta_{i,i+1}$ in Eq. (2.23) used to compute the winding number in Eq. (2.24). In the case considered here, the angle represented by the black line in Figure 12(c) is the only one to contribute to this modification of winding number. During the transient, it slips away from the other angles, from a value of approximately $-\pi$ to -8π . Along the way, when it gets further than π from its next neighbor (according to the ordering of the cycle), the winding number jumps from 0 to -1 , and when it gets further than $-\pi$ from its previous neighbor, the winding number jumps from -1 to 0.

Reducing then P starting from the $q = -1$ fixed point at $P/K > 1.6$, one remains on the $q = -1$ fixed point. This hysteretic behavior is indicated by arrows in Figures 12(a) and (b) and illustrates the topological protection brought about by the integer winding number q .

We showed that by increasing natural frequencies' absolute values, depending on the network's topology, leads to a flow reaching its maximum value and a temporary dynamical instability, eventually driving the system to a new, stable stationary state.

Remark. *In all simulations, small random natural frequencies at all vertices are introduced to remove a mirror symmetry along grey dashed line in the inset of Figure 12(d). If the angles are distributed symmetrically with respect to this axis, which is the case for the $q = 0$ stable fixed point,*

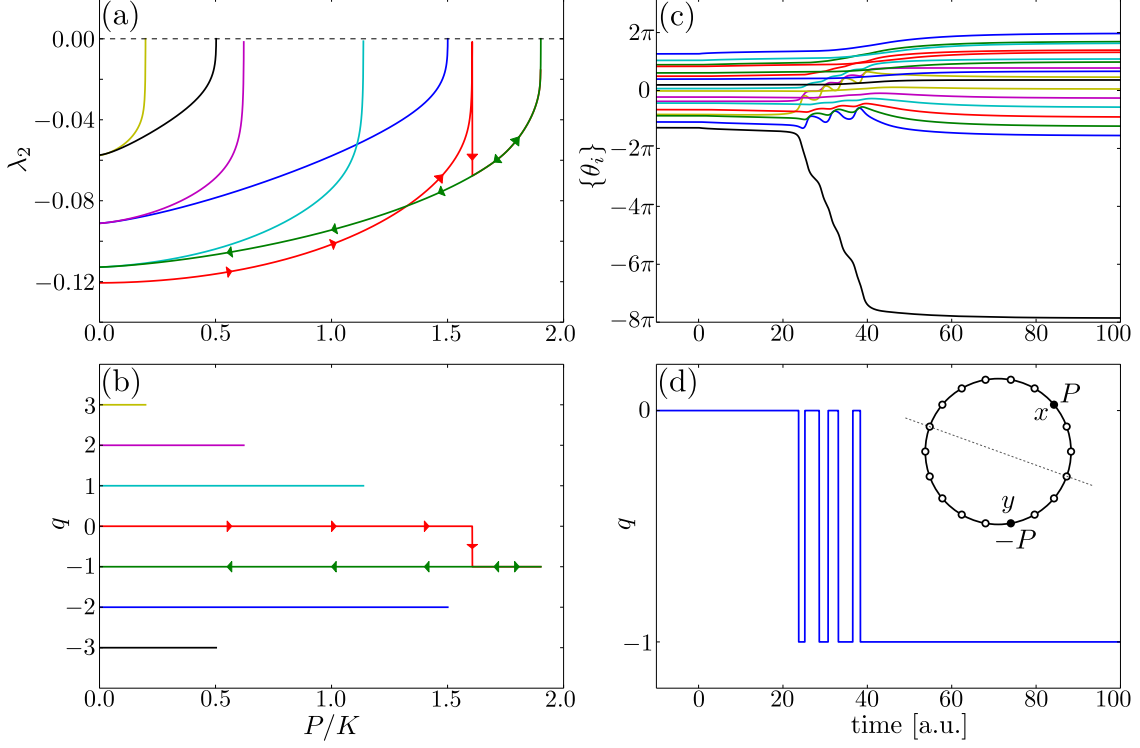


Figure 12: (Figure adapted from [67]) Loop flow formation for a cycle with $n = 18$ vertices. Locations of the non-zero natural frequencies are indicated by the black vertices in the inset of panel (d), while all white vertices have small random natural frequencies summing to zero, to make the model not too specific. Panels (a) and (b): stability diagram for fixed points with different winding numbers q , showing (a) the Lyapunov exponent λ_2 and (b) the range of stability of the solution. Each spike with $\lambda_2 \rightarrow 0$ in panel (a) indicates the loss of stability of a fixed point. The red arrows in (a) and (b) indicate jumps from the $q = 0$ fixed point to that with $q = -1$ as P increases. The path is not retraced, however, as one reverses P back to $P = 0$ (green arrows). Panels (c) and (d): transient dynamics of the change of stable fixed point as P/K is changed from 1.575 to 1.65 at $t = 0$. The $q = 0$ fixed point loses its stability and Eq. (2.5) induces a transient behavior where the angle on the oscillator with negative natural frequency rotates until the system reaches the $q = -1$ fixed point.

and if the changes of natural frequencies are as well symmetric, then this results in $\dot{\theta}_i = -\dot{\theta}_{-i}$ at all time, where $-i$ indicates the mirror symmetric of vertex i . Analytically, this forbids transitions to other q -values starting from any stationary $q = 0$ states, because the dynamics Eq. (2.5) preserve the symmetry of angles. Numerically it results in very long transients with anomalously long angle rotations. Small random frequencies break this symmetry without modifying the dynamics we are interested in.

We now consider a slightly different model to corroborates our conclusions. We consider a single cycle of $n = 12$ vertices and edges with coupling K . Instead of increasing the natural frequency of one oscillator, we fix the natural frequency of the first oscillator [x in the inset of Figure 13(b)] and add another positive natural frequency at oscillator y . These two positive natural frequencies are both balanced by oscillator z , whose natural frequency is $-(P_x + P_y)$. Initially, oscillators x and z have natural frequencies $P_x = K$ and $P_z = -P_x = -K$ respectively. There are two paths from x to z , and the sum of flows on these two paths is P_x . Next, the natural frequency at z is decreased from $-P_x$ to $-P_x - P_y$, while the natural frequency of oscillator y is increased to $P_y > 0$. This increase in natural frequencies increases the flow on the edge between y and z . This process can be seen as a weakening of this path. The flow on the left path from x to z then increases to maintain the balance at oscillator x . The fixed point with $q = 0$ loses stability when the increase of natural frequency reaches $P_y \approx 0.45K$, which drives the system to the $q = -1$ fixed point, and

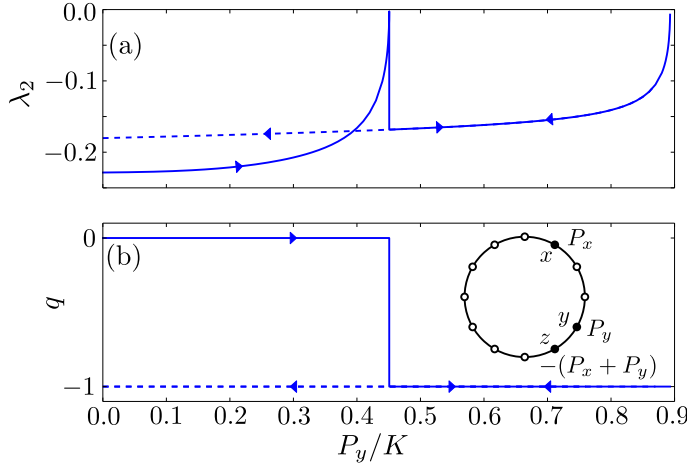


Figure 13: (Figure adapted from [67]) Dynamical generation of loop flow by increase of natural frequencies absolute values for a cycle with $n = 12$ vertices and edges with coupling K . Locations of the main natural frequencies are indicated by the black vertices in the inset of panel (b), while all white vertices have small random natural frequencies summing to zero, to make the model more generic. As the negative natural frequency decreases from $-P_x$ to $-P_x - P_y$, the path connecting y to z carries an increasing flow, forcing a larger flow on the path around the other side of the cycle. As the natural frequency is increased beyond $P_y \approx 0.45K$, the $q = 0$ fixed point becomes unstable [panel (a)], driving the system into a state with winding number $q = -1$.

that fixed point remains stable until $P_y \approx 0.9K$. The arrows indicate the hysteretic behavior where decreasing P_y from the $q = -1$ stable fixed point does not bring the system back to the $q = 0$ fixed point.

Non-zero winding numbers at weak coupling

It is expected in general that for large natural frequencies (in absolute value), which is equivalent to weak coupling K , only fixed points with winding number $q = 0$ can exist. This makes sense if we realize that large natural frequencies induce large flows on the edges of the interaction graph. As large flows require large angle differences, the Jacobian matrix \mathcal{J} of the system in such a state is more likely to have small or even negative off-diagonal values. The system is then closer to instability with larger flows. Furthermore, a non-zero winding number on a cycle is related to a loop flow, which increases the flow on some of the edges of the network. We then expect fixed point with larger winding number to lose stability for smaller natural frequencies (in absolute value).

However, as seen previously, this is not true for some networks. As shown in Figure 12(b), for the network in the inset of Figure 12(d), with $P > 1.65K$, the only stable fixed point has winding number $q = -1$. We explain here what happens in this situation.

Consider a cycle network with two non-zero natural frequencies $P > 0$ at oscillators x and $-P$ at oscillator y . There are two paths from x to y of length n_1 on the left in Figure 14 and n_2 on the right, and we assume without loss of generality that $n_2 \leq n_1$. At a fixed point of Eq. (2.5) on this network, the angle differences along the left path (resp. the right path) are all identical equal to Δ_1 (resp. Δ_2). Note that for convenience, angle differences are counted here in the direction from x to y , regardless of the path considered. The winding number (computed clockwise) of a fixed point is computed as

$$n_2\Delta_2 - n_1\Delta_1 = 2\pi q. \quad (5.1)$$

From the results of Sections 2 and 3, we know that a fixed point is stable if and only if $|\Delta_1|, |\Delta_2| < \pi/2$. Starting at a fixed point with winding number $q \in \mathbb{Z}$ at small P , the absolute angle differences $|\Delta_1|$ and $|\Delta_2|$ will increase until one of them reaches $\pi/2$, which implies loss of stability. Assuming

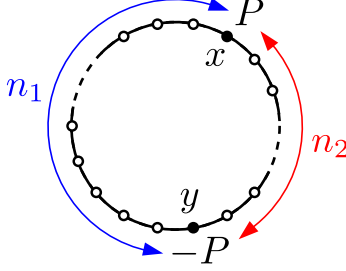


Figure 14: Cycle network with n_1 edges on the left path from x to y and n_2 edges on the right path. Natural frequencies are P at oscillator x , $-P$ at oscillator y and zero at other oscillators. In such a network, the last stable fixed point for large values of natural frequency P can have any winding number depending on the respective values of n_1 and n_2 .

that instability is triggered by Δ_2 being $\pi/2$, at some value $P = P_q$, Eq. (5.1) yields

$$\Delta_1 = \frac{n_2 - 4q}{2n_1} \pi \leq \frac{\pi}{2}, \quad (5.2)$$

which is smaller than $\pi/2$ because otherwise the fixed point would have lost stability at smaller P . The same reasoning can be done if it is $|\Delta_1|$ that reaches $\pi/2$. The limiting natural frequency P_q can as well be computed

$$P_q = K \sin\left(\frac{\pi}{2}\right) + K \sin\left(\frac{n_2 - 4q}{2n_1} \pi\right), \quad (5.3)$$

which is larger for smaller q .

Thus, for given n_1 and n_2 , the fixed point remaining stable for the largest P is the one with the smallest winding number q satisfying Eq. (5.2). In particular, we see that the network presented in the inset of Figure 12(d) has $n_1 = 12$ and $n_2 = 6$, which gives

$$\Delta_1(q=0) = \frac{\pi}{4} < \Delta_1(q=-1) = \frac{5\pi}{12} < \frac{\pi}{2} < \Delta_1(q=-2) = \frac{7\pi}{12}. \quad (5.4)$$

The fixed point remaining stable for the largest value of P is then the one with winding number $q = -1$ as seen in our simulations in Figure 12. We see furthermore that for any winding number q , we can find a pair (n_1, n_2) such that the fixed point with winding number q is the last stable one for large natural frequency P .

5.2 Process 2: Creating Loop Flows via Edge Removing

We next investigate the second mechanism for loop flow generation, by removing an edge. Consider the model shown in the inset of Figure 15(a), where an oscillator with positive natural frequency P is connected to an oscillator with negative natural frequency $-P$, via three different paths. Assume then that an edge on the middle path is removed. The contribution of this path to the balance of Eq. (2.9) has then to be redistributed on the two remaining paths, and if P is relatively large, the angle differences $\Delta_{L,R}$ on each remaining path increase significantly. When one of these two paths, say the left one, goes through many more edges than the other one, $n_L \gg n_R$, it is then possible that $n_L \Delta_L - n_R \Delta_R = 2\pi q$ with $q > 0$, even if the system had only zero winding numbers initially. This simple example shows how one edge removing in an asymmetric double-cycle system can generate a loop flow.

Figure 15 illustrates how a $q \neq 0$ state emerges from a $q = 0$ state after an edge removing. The initial state is a stationary state of the double-cycle system with zero winding number on both cycles. The red edge in the inset of Figure 15(a) is then removed, which induces a transient driving the system to a stationary state of the resulting single-cycle system. Figure 15(a) shows the obtained winding number. One sees that for small P , the final state has $q = 0$, while for larger P , a $q = 1$ state is reached. In other words, when P is large enough, the amount to redistribute

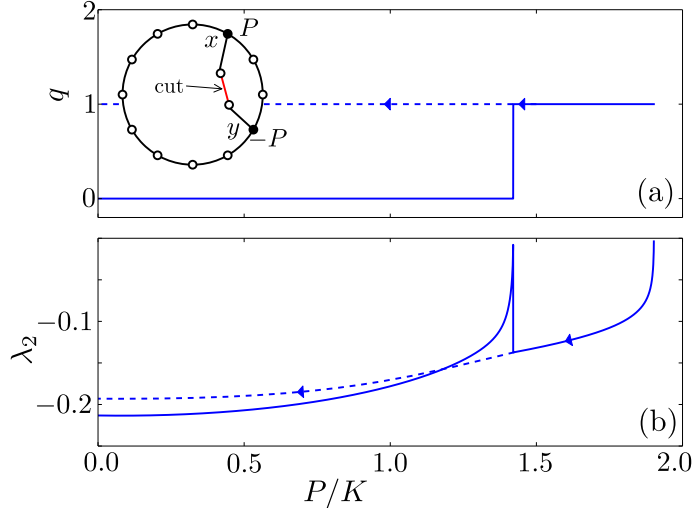


Figure 15: (Figure adapted from [67]) Loop flow creation by edge removing in a double cycle network with $n = 14$ vertices and constant coupling K . Locations of the vertices with non-zero natural frequencies are indicated by the black vertices in the inset of panel (a), while all white vertices have small random natural frequencies summing to zero, to make the model not too specific. The initial state corresponds to a $q = 0$ state on both the cycles of the double-cycle system. The edge indicated in red in the inset of panel (a) is then removed, generating a transient to a stable fixed point of the new network. Panels (a) and (b) show the winding number and the Lyapunov exponent of the new stationary state with respect to the amplitude P of the natural frequencies. Arrows on all panels indicate that once created, a loop flow does not disappear when reducing P/K .

is large, such that the increase of Δ_L brings the system to $q \neq 0$ state. We have found that this behavior is generic of sufficiently asymmetric double-cycle systems. Again, once a loop flow is created, reducing the natural frequencies does not remove it, as show the arrows and the dashed line in Figure 15

The reason for the non-zero winding number in this case is the same as in the previous mechanism. It is basically due to the asymmetry of the non-zero natural frequencies on the cycle. The difference here is in the mechanism, where instead of modifying the natural frequencies, we modify the interaction network by itself.

5.3 Process 3: Creating Loop Flows via Edge Addition

We have just showed that removing an edge can lead to a loop flow. In this section, we finally consider loop flow creation via addition of an edge. We consider again the single-cycle model sketched in the inset of Figure 12(d). We start from the cycle system with an synchronous state with $q = 0$. There is a clockwise flow from x to y (via the right path) and a counterclockwise one (via the left path). One edge along the right path is then removed, which forces the left path to account for the whole natural frequency P . The angle difference Δ_L between any two vertices along the left path increases, while angle differences along the right path vanish, $\Delta_R = 0$. This gives an angle difference $\Delta_0 = n_L \Delta_L$ between the two vertices on each side of the removed edge.

Upon adding back that edge, the system will evolve according to the dynamics of Eq. (2.5), starting with initial condition given by the stable fixed point of the network with the edge removed. The winding number of the final state of the system depends on the basin of attraction of the Lyapunov function Eq. (2.38) in which the initial condition lies. The Lyapunov function Eq. (2.38) can be rewritten as a function of angle differences $\Delta_{i,i+1}$ as

$$\mathcal{U}(\{\Delta_{i,i+1}\}) = - \sum_{i=1}^n P_{i,i+1}^* \Delta_{i,i+1} + \sum_{i=1}^n K [1 - \cos(\Delta_{i,i+1})] , \quad (5.5)$$

where $P_{i,i+1}^*$ is defined in Eq. (2.13). The single-cycle model we consider here can be split in two

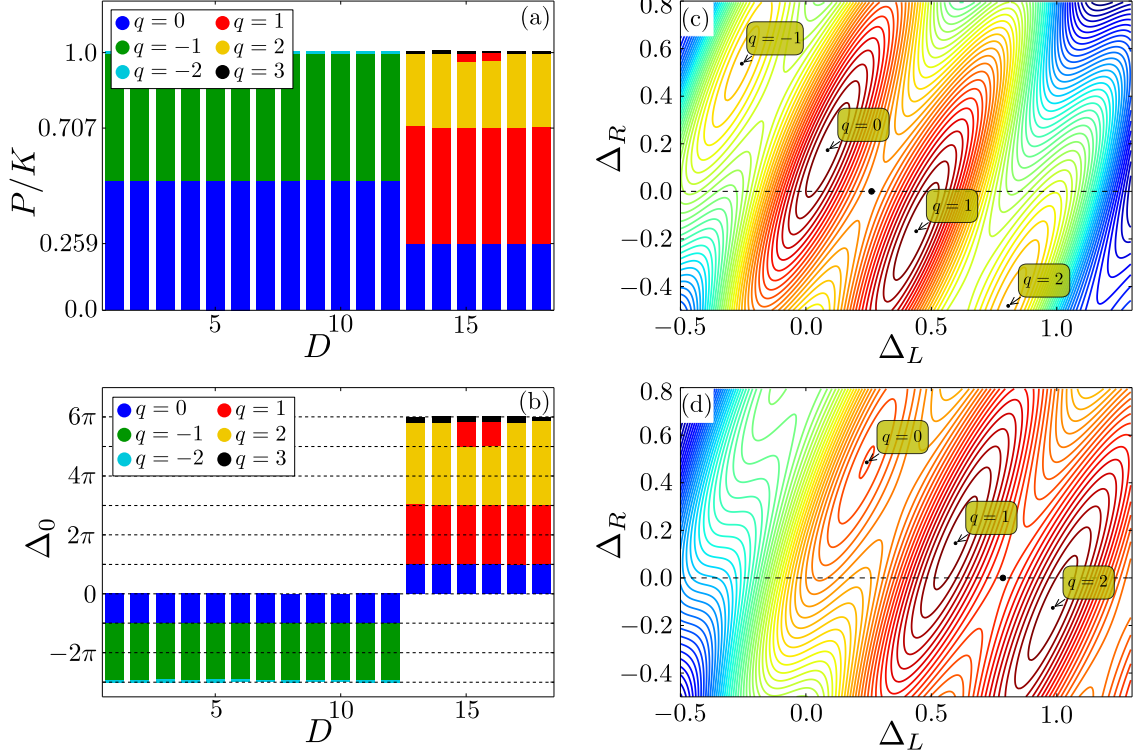


Figure 16: (Figure adapted from [67]) Loop flow generation and basins of attraction for the single-cycle model shown in the inset of Figure 12(d) under the edge removing adding mechanism. Panels (a) and (b): final winding numbers as a function of the position of the removed edge and (a) the rescaled natural frequency P/K , (b) the corresponding angle differences Δ_0 between the two ends of the removed edge. Panels (c) and (d): Contour plots of the Lyapunov function for a removed edge at $13 \leq D \leq 18$ (on the right path), (c) $P = K \sin(\pi/12)$ and (d) $P = K \sin(\pi/4)$. Local minima with different values of q are indicated. When the edge is removed, $\Delta_R = 0$ and $\Delta_0 = 12\Delta_L$, and black dots show the operating states right before adding back the removed edge. For the chosen values of P/K they are located precisely on saddle points at the boundary between the basins of attraction of $q = 0$ and $q = 1$ [panel (c)], and $q = 1$ and $q = 2$ [panel (d)].

paths (left and right) from vertex x to vertex y . We have

$$P_{i,i+1}^* = \begin{cases} P & \text{if the edge from } i \text{ to } i+1 \text{ is on the left path,} \\ 0 & \text{if the edge from } i \text{ to } i+1 \text{ is on the right path.} \end{cases} \quad (5.6)$$

Furthermore, any fixed point of Eq. (2.5) on the cycle network considered, has the same angle differences, $\Delta_{i,i+1} = \Delta_L$, along each edge on the left path and $\Delta_{i+1,i} = \Delta_R$ on the right path.

Before adding back the removed edge, the angle difference Δ_0 between its two ends can be written as a function of Δ_L and Δ_R ,

$$\Delta_0 = n_L \Delta_L - (n_R - 1) \Delta_R - 2\pi q, \quad (5.7)$$

where $n_L > n_R \geq 2$ are the number of edges on the left and right paths. Then we can project the Lyapunov function on the (Δ_L, Δ_R) -plane, which yields

$$\mathcal{U}(\Delta_L, \Delta_R) = Kn - n_L P \Delta_L - n_L K \cos \Delta_L - (n_R - 1) K \cos \Delta_R - K \cos(n_L \Delta_L - (n_R - 1) \Delta_R), \quad (5.8)$$

where $n = n_L + n_R$ is the number of vertices which equals the number of edges.

Figures 16(c) and (d) show contour plots of $\mathcal{U}(\Delta_L, \Delta_R)$. Local minima are indicated, together with the corresponding integer winding numbers. To each minimum corresponds a basin of attraction containing the set of initial states that converge towards that minimum under Eq. (2.5).

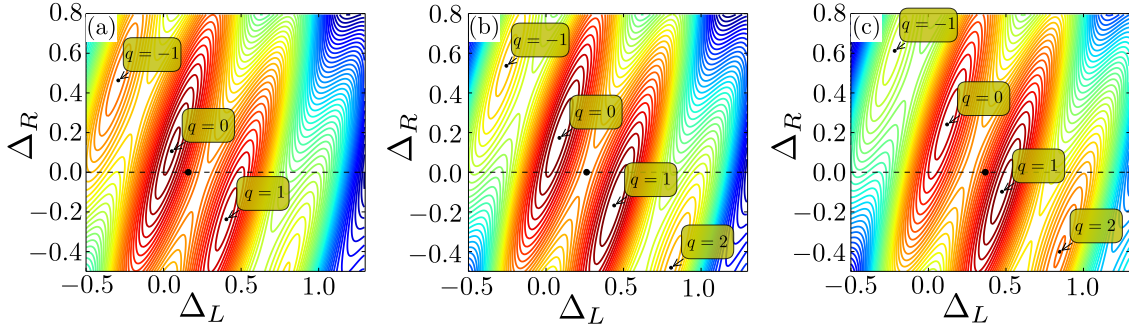


Figure 17: (Figure adapted from [67]) Contour plots of the projected Lyapunov function for the $n = 18$ vertices cycle network described in the inset of Figure 12(d) and natural frequency $P \approx 0.159K$ in panel (a), $P = K \sin(\pi/12) \approx 0.259K$ in panel (b), and $P \approx 0.359K$ in panel (c). Local minima at different values of q are indicated. The operating state obtained by removing one edge on the shortest path between the positive and negative natural frequencies [$\Delta_R = 0, \Delta_L = \arcsin(P/K)$, and $\Delta_0 = 12\Delta_L$] is indicated by the black dot on each panel. It lies in the basin of attraction of the $q = 0$ state for $P < 0.259K$ [case (a)], in the basin of attraction of the $q = 1$ state for $P > 0.259K$ [case (c)], and at the saddle point separating the two basins for $P = 0.259K$ [case (b)].

All points around a minimum belong to that basin, until one reaches a saddle point or a ridge, beyond which, points belong to another basin of attraction. Cutting the right path projects Δ_R to zero. Right before adding back the edge, the system is at $\Delta_L = \arcsin(P/K)$ on the dashed lines in Figures 16(c) and (d) which correspond to $P/K = 0.259$ and $P/K = 0.707$ respectively. The fixed point towards which the system converges after adding back the edge depends on the basin of attraction to which the initial state belongs. For P such that $n_L \Delta_L = \Delta_0 = (2p+1)\pi$ with $p \in \mathbb{Z}$, the point $(\Delta_L, \Delta_R) = (\arcsin(P/K), 0)$ lies right on a saddle point at the boundary between two basins of attraction, as we show below. Tuning the value of P allows then to control in which basin of attraction the system lies at the time where the edge is added back, and thus the winding number of the final state. This is illustrated in Figure 17, where the projected Lyapunov function is represented for three different values of P . In panel (a) [resp. panel (c)], the initial state is clearly in the basin of attraction of the $q = 0$ (resp. $q = 1$) fixed point, and in panel (b) it is precisely at the boundary. The only change from one panel to another is the value of P .

Let us show now that if $n_L \arcsin(P/K) = (2p+1)\pi$, with integer p , then $(\Delta_L, \Delta_R) = (\arcsin(P/K), 0)$ is a saddle point of the projected Lyapunov function Eq. (5.8). The gradient of the Lyapunov function \mathcal{U} in the (Δ_L, Δ_R) -plane is given by

$$\nabla \mathcal{U} = \begin{pmatrix} -n_L P + n_L K \sin \Delta_L + n_L K \sin(n_L \Delta_L - (n_R - 1) \Delta_R) \\ (n_R - 1) K \sin \Delta_R - (n_R - 1) K \sin(n_L \Delta_L - (n_R - 1) \Delta_R) \end{pmatrix}. \quad (5.9)$$

It is easy to check that $\nabla \mathcal{U} = 0$ at $(\Delta_L, \Delta_R) = (\arcsin(P/K), 0)$, which is thus a critical point. The nature of this critical point is determined by the two eigenvalues of $H_{\mathcal{U}}$, the Hessian of \mathcal{U} . At our critical point, we obtain

$$H_{\mathcal{U}}(\arcsin(P/K), 0) = K \begin{pmatrix} n_L \cos \Delta_L - n_L^2 & n_L(n_R - 1) \\ n_L(n_R - 1) & (n_R - 1) - (n_R - 1)^2 \end{pmatrix} =: \begin{pmatrix} a & b \\ b & c \end{pmatrix}. \quad (5.10)$$

The two eigenvalues of $H_{\mathcal{U}}$ are then the two roots of

$$\chi(\lambda) = \lambda^2 - (a+c)\lambda + ac - b^2 \implies \lambda^{\pm} = \left(a + c \pm \sqrt{(a+c)^2 - 4(ac-b^2)} \right) / 2. \quad (5.11)$$

Then λ^+ is always positive and λ^- is negative if and only if $ac - b^2 < 0$. Replacing a , b and c we have

$$ac - b^2 = -K^2 n_L (n_R - 1) [n_L + (n_R - 2) \cos \Delta_L], \quad (5.12)$$

which is necessarily negative since first, at the moment of the edge addition, $\Delta_L = \arcsin(P/K)$ implying that $\cos \Delta_L > 0$, and second $n_R \geq 2$. We conclude that $(\Delta_L, \Delta_R) = (\arcsin(P/K), 0)$

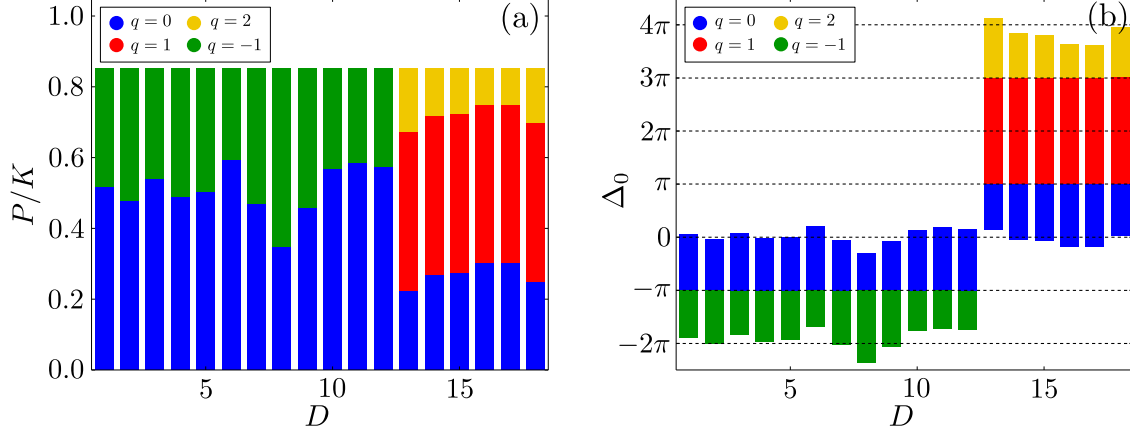


Figure 18: (Figure adapted from [67]) Loop flow generation under the edge addition mechanism, for the single-cycle model shown in the inset of Figure 12(d) in the main text, with additional random natural frequencies at the intermediate vertices. The final winding numbers, after adding back the edge, are color-coded and plotted as a function of the position D of the removed edge and (a) the rescaled natural frequency P/K , (b) the angle differences Δ_0 between the two ends of the removed edge. Loop flow generation occurs as soon as $\Delta_0 \geq \pi$ and higher winding numbers q are reached each time Δ_0 crosses an odd integer multiple of π . This shows that the argument presented holds even in the more general situation with non-zero natural frequencies between the main natural frequencies.

for $n_L \arcsin(P/K) = (2p + 1)\pi$ is a saddle point of the projected Lyapunov function. As there is one direction with positive curvature and one direction with negative curvature in the projected (Δ_L, Δ_R) -plane, this point is a saddle point for the full Lyapunov function as well. One concludes that loop flow generation by this mechanism occurs for $\Delta_0 > \pi$, and that the final winding number increases by one each time Δ_0 crosses an odd integer multiple of π . The same line of argument swapping L and R indices, applies when the edge to be removed is on the left path.

The above argument is based on the projected Lyapunov function. It neglects the fact that, after adding back the edge, the transient dynamics leaves the (Δ_L, Δ_R) -plane until a new stationary state is reached. We therefore check its validity numerically. Figure 16 shows what final winding number is obtained upon edge adding depending on the location $D = 1, \dots, n$ of the removed edge (counted counterclockwise, starting from the positive natural frequency) and the rescaled natural frequency P/K [Figure 16(a)] and Δ_0 [Figure 16(b)]. Figure 16(b) confirms that the final winding number changes by one each time Δ_0 crosses an odd integer multiple of π , except when the natural frequency P gets close to its maximal allowed value, $P \nearrow K$. We attribute this change of behavior to a more complicated transient in this case.

We performed the same simulation with additional small random natural frequencies at all oscillators. In Figure 18, we reproduce Figures 16(a) and (b) in this situation. This confirms that our findings are generic. Compared to Figure 16, the presence of random natural frequencies strongly modifies the borders between fixed points after adding back the edge, with different q in the P/K vs. D plane [panel (a)] but not in the Δ_0 vs. D plane [panel (b)]. This is so because the small random natural frequencies change the value of P necessary for $\Delta_0 = (2p + 1)\pi$. One sees that, despite the presence of random natural frequencies, loop flows are generated by edge addition as soon as $|\Delta_0| > \pi$, but not earlier, and that the created loop flow has a winding number increasing/decreasing by one each time Δ_0 crosses an odd integer multiple of π with good precision. This confirms that the findings presented are generic and not restricted to the a priori ideal situation considered there.

6 The size of the sync basin revisited

Our aim is now to estimate the nonlinear stability of an equilibrium of Eq. (1.3) based on the volume of its basin of attraction. In networks of all-to-all coupled oscillators, tight estimates of the volume of the basin of attraction of the synchronous state are known [68]. Much less is known about the basins of attraction of cycle networks. Most of the results presented in this section were published in [69].

In [52], Wiley et al. consider such network topology, with identical natural frequencies and investigate how the volume of the basin of attraction of a stable fixed point is related to its winding number. In particular, they are interested in the likelihood of the system to reach the phase synchronous state [i.e. $\theta_i(t) = \theta_j(t)$ for all $i, j \in \mathcal{V}_G$ and all $t \geq 0$]. This likelihood is directly related to the volume of the basin of attraction of the phase synchronous state, which they call “sync basin”. Starting from random initial conditions, they numerically evolve the system until it converges to a stable fixed point. The volume of the basin of attraction of every fixed point is then estimated by the proportion of initial conditions that converged to it. It is found that the volume of the basins of attraction follows a Gaussian distribution with respect to the winding numbers q , as shown in Figure 19 (red dots). One issue with that procedure is that the winding numbers of randomly chosen initial conditions also follow a Gaussian distribution,

$$p(q) = (\sqrt{2\pi}\sigma)^{-1} \exp(-q^2/2\sigma^2). \quad (6.1)$$

From the data shown in Figure 19, we obtain a standard deviation of $\sigma = 2.63$ for the distribution of winding numbers of the initial conditions and a narrower distribution with $\sigma = 1.63$ for the converged fixed points (the latter value in agreement with [52]). The Gaussian distribution for the initial conditions can easily be understood once one realizes that picking an initial condition is similar to a random walk [70]. The vertex index along the cycle corresponds to a time step index and the angle on each vertex gives by how much and in what direction the random walk progresses. Large winding numbers correspond then to random walks with large excursions. This analogy explains the obtained Gaussian distribution for initial winding numbers.

We also observe that the winding number of the initial conditions and of the converged fixed points are significantly correlated, with a correlation coefficient of 0.47. Therefore, if one does not have enough resolution for the initial conditions, the distribution of the winding numbers of the final states may, at least partially, reflect the initial distribution of q instead of the volume of the basins of attraction. Due to the high dimensionality of the state space ($n = 83$ in Figure 19 and $n = 80$ in [52]), simulations with random initial conditions would need an unfeasible number of runs to representatively cover the whole state space.

To the best of our knowledge, the only paper, beside [52], focusing specifically on the basins of attraction of the Kuramoto model on cycle network is [71], which analytically obtains lower bounds on the volume of the basins of attraction for a cycle of Kuramoto oscillators with unidirectional coupling.

We therefore revisit this issue by constructing a new systematic numerical method. Our approach is first to find all the stable fixed points of Eq. (1.3) describing all the possible synchronous states, and second to perturb them in random directions with an increasing magnitude to assess the volume of their basins of attraction. The volume is estimated from the magnitude of the largest perturbation still converging to the initial fixed point. In the case of a single cycle with identical natural frequencies, one can analytically identify all stable fixed points and the problem is sufficiently tractable to obtain an analytical estimate of the volume of the basins of attraction, which we confirm numerically. We show that for $n \gg 1$ and q not too small, the volume of the basins of attraction scales as $\text{Vol}_q \sim (1 - 4q/n)^n$ instead of the Gaussian law of Wiley et al. [Eq. (6.1)]. We then extend our perturbation procedure to cycle networks with non-identical frequencies and to meshed networks with identical frequencies. Our numerical method guarantees that we investigate every basin of attraction with a representative number of initial conditions. It is based on (i) a numerical procedure to systematically find stable fixed points of Eq. (1.3) on any meshed network and (ii) the perturbation procedure described above.

We give here analytical and numerical insight into the volume of the basins of attraction of the dynamical system Eq. (1.3). We first restrict ourselves to the case of cyclic couplings and identical

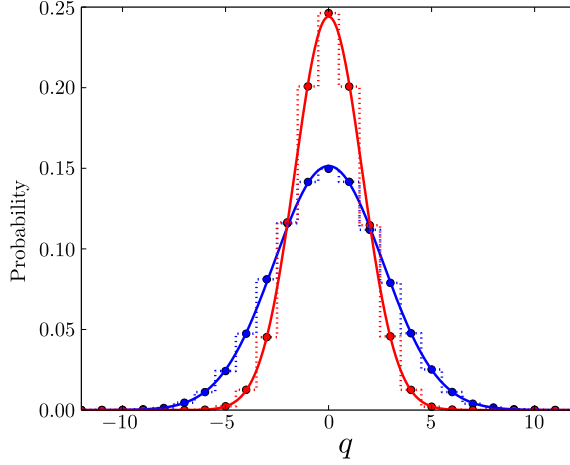


Figure 19: (Figure taken from [69]) Distributions of the initial (blue) and final (red) winding numbers for the equal frequency Kuramoto model on a cycle [Eq. (3.1)] with $n = 83$ vertices. Initial states have been chosen randomly. Continuous curves are Gaussian fits with $\sigma = 2.63$ (blue) and $\sigma = 1.63$ (red).

frequencies,

$$\dot{\theta}_i = -K \sin(\theta_i - \theta_{i-1}) - K \sin(\theta_i - \theta_{i+1}), \quad i = 1, \dots, n, \quad (6.2)$$

where indices are taken modulo n . Fixed points of Eq. (6.2) satisfy either

$$\Delta_{i,i+1} = \Delta_{i-1,i} \quad \text{or} \quad \Delta_{i,i+1} = \pm\pi - \Delta_{i-1,i}, \quad (6.3)$$

where the sign in front of π in the right-hand side is chosen to ensure that $\Delta_{i,i+1} \in (-\pi, \pi]$.

According to Section 3, any stable fixed point of Eq. (6.2) must have all angle differences between neighboring oscillators in $[-\pi/2, \pi/2]$. Eq. (6.3) then implies that there is a unique stable fixed point, $\vec{\theta}^{(q)}$, with winding number q ,

$$\Delta = 2\pi q/n \iff \theta_i^{(q)} = 2\pi q i/n + \phi, \quad (6.4)$$

for all $i = 1, \dots, n$, where ϕ is an arbitrary uniform angle shift. This implies that for a fixed point to be stable, the winding number cannot be larger than $q_{\max} := \text{Int}[(n-1)/4]$. Angle differences would be larger than $\pi/2$ otherwise. Winding numbers for stable fixed points then range from $-q_{\max}$ to $+q_{\max}$, which gives $2q_{\max} + 1$ stable fixed points (see Section 3).

A fixed point of Eq. (6.2) is unstable if one (see Section 3) or more [37] angle differences are larger than $\pi/2$. In this case, a fixed point has $n-j$ angle differences $\Delta_{k+1,k} \equiv \Delta \in [-\pi/2, \pi/2]$ and j angle differences $\Delta_{k+1,k} \equiv \pm\pi - \Delta$, with $j > 0$, and $\sum_k \Delta_{k+1,k} = 2\pi q$.

6.1 Identical frequencies: Analytical approach

For a cycle network of length n with identical frequencies, we derive an analytical expression for the volume of the basins of attraction. Our approach is to approximate the basin of attraction of a given stable fixed point by the hypercube centered at the fixed point and whose radius is the distance to the closest unstable fixed point.

As Eq. (6.2) is invariant under a constant shift of all angles ϕ , we will work in the hyperplane \mathcal{H}_{n-1} orthogonal to the vector $(1, \dots, 1)^T$. The angle vector $\vec{\theta}^{(q)}$ of Eq. (6.4) projected on \mathcal{H}_{n-1} has components

$$\theta_i^{(q)} = \frac{2\pi q}{n} i - \frac{n-1}{n} q\pi. \quad (6.5)$$

According to [72], a fixed point of Eq. (6.2) has a unique unstable direction in angle space if and only if it has a single angle difference, between neighboring oscillators, which is larger than

$\pi/2$. Such an unstable fixed point is called a *1-saddle* point. Consider then a 1-saddle point with winding number q' , where the angle difference between i and $i+1$, $i \neq k$ is $\Delta' \in [-\pi/2, \pi/2]$ and the angle difference between k and $k+1$ is $\pm\pi - \Delta' \in \mathcal{I}$. Combining Eqs. (6.3) and (2.24), its winding number q' is given by

$$(n-1) \cdot \Delta' + \pi - \Delta' = 2\pi q' \iff \Delta' = \frac{2q' - 1}{n-2}\pi. \quad (6.6)$$

This allows to compute the components of the 1-saddle angle vector, $\vec{\varphi}^{(q')}$ where k can be any index, projected on \mathcal{H}_{n-1} ,

$$\varphi_i^{(q')} = \begin{cases} i\Delta' - s_k, & \text{if } i < k, \\ (i-2)\Delta' + \pi - s_k, & \text{if } i \geq k, \end{cases} \quad (6.7)$$

where s_k is a constant angle shift guaranteeing that the sum of components is zero,

$$s_k := n^{-1} \sum_{j=0}^{k-1} j\Delta' + n^{-1} \sum_{j=k}^{n-1} [(j-2)\Delta' + \pi]. \quad (6.8)$$

Massaging Eqs. (6.7) and (6.8) together gives

$$\varphi_i^{(q')} = \pi \left[\frac{2q' - 1}{n-2} i + \frac{-2n^2k + 2nk - 8q'k - n}{2n(n-2)} + t_i^{(k)} \right], \quad (6.9)$$

where

$$t_i^{(k)} = \begin{cases} \frac{10nq' - n^2}{2n(n-2)}, & \text{if } i < k, \\ \frac{2nq' + n^2}{2n(n-2)}, & \text{if } i \geq k. \end{cases} \quad (6.10)$$

Remark. We have found numerically that:

- (i) the 1-saddles are the closest unstable fixed points to the stable fixed points;
- (ii) stable fixed points and 1-saddles are the closest if they have the same winding number.

We denote by $\vec{\varphi}_N^{(q,\ell)}$ the unstable fixed points with winding number q and ℓ angle differences larger than $\pi/2$, where N is the set of edges with angle differences larger than $\pi/2$.

The left panel of Figure 20 shows that the 1-saddles are the closest unstable fixed points to stable fixed points. The right panel of Figure 20 shows that stable fixed points and 1-saddles are the closest if they have the same winding number. We computed these distances numerically, constructing each $\vec{\varphi}_N^{(q,\ell)}$ as follows. For a given pair (q, ℓ) , the number of different fixed points with winding number q and ℓ angle differences larger than $\pi/2$ is $\binom{n}{\ell}$, each of them corresponding to a different choice of locations for the angle differences larger than $\pi/2$. Such a choice of locations is given by a partition of edges in the set N (resp. $\mathcal{V}_G \setminus N$) of edges with angle differences larger (resp. smaller) than $\pi/2$. Given such a partition, we construct recursively the angle vector

$$\left(\varphi_N^{(q,\ell)} \right)_i = \begin{cases} 0, & \text{if } i = 1, \\ \left(\varphi_N^{(q,\ell)} \right)_{i-1} + \frac{2q-\ell}{n-2\ell}\pi, & \text{if } i > 1 \text{ and } \langle i-1, i \rangle \in \mathcal{V}_G \setminus N, \\ \left(\varphi_N^{(q,\ell)} \right)_{i-1} + \pi - \frac{2q-\ell}{n-2\ell}\pi, & \text{if } i > 1 \text{ and } \langle i-1, i \rangle \in N, \end{cases} \quad (6.11)$$

and we compute the geodesic distance on the torus.

Note that according to this notation, the fixed point $\vec{\varphi}^{(q')}$ is the same as $\vec{\varphi}_{\{k\}}^{(q',1)}$ for some $k = 1, \dots, n$.

Following the remark above, we investigate the case $q = q'$. The difference between angle vectors is easily obtained as

$$\theta_i^{(q)} - \varphi_i^{(q)} = \begin{cases} \frac{(1+2i-2k+n)(n-4q)}{2(n-2)n}\pi, & \text{if } i < k, \\ \frac{(1+2i-2k-n)(n-4q)}{2(n-2)n}\pi, & \text{if } i \geq k, \end{cases} \quad (6.12)$$

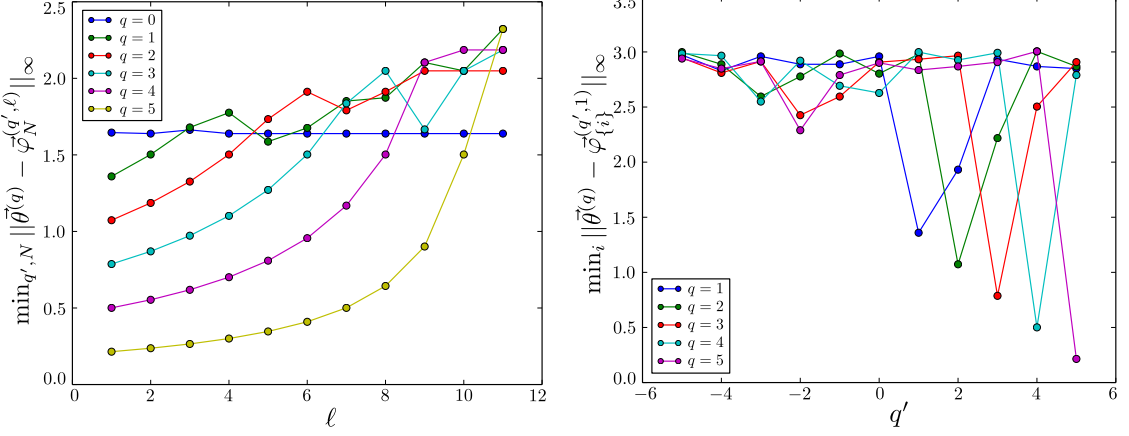


Figure 20: (Figures adapted from [69]) Left panel: Distance between $\vec{\theta}^{(q)}$, the stable fixed point with winding number q , and the closest unstable fixed point with ℓ angle differences larger than $\pi/2$, as a function of ℓ , for a cycle of length $n = 23$. Minimum is taken over all possible winding numbers q' and all possible partitions $\mathcal{E}_G = N \cap (\mathcal{V}_G \setminus N)$ such that $|N| = \ell$. Right panel: Distance between $\vec{\theta}^{(q)}$, the stable fixed point with winding number q , and the closest 1-saddle with winding number q' , with respect to q' , for a cycle of length $n = 23$. Minimum is taken over all possible choices of $N = \{i\}$.

which gives the distance between the stable fixed point and the unstable 1-saddle point

$$\|\vec{\theta}^{(q)} - \vec{\varphi}^{(q)}\|_\infty = \frac{(n-1)(n-4q)}{2(n-2)n} \pi. \quad (6.13)$$

In particular, the large n limit is

$$\lim_{n \rightarrow \infty} \|\vec{\theta}^{(q)} - \vec{\varphi}^{(q)}\|_\infty = \frac{\pi}{2} \left(1 - \frac{q}{q_{\max}}\right). \quad (6.14)$$

We remark that we lost the dependence on k , meaning that the stable fixed point $\vec{\theta}^{(q)}$ is equidistant to all 1-saddles with the same winding number. This indicates that the basins of attraction are isotropic in the directions of the 1-saddle points.

Since $\vec{\theta}^{(q)}$ is equidistant to all 1-saddles, one expect, for $n \gg 1$, that the volume Vol_q of the basin of attraction is well approximated by an hypercube of side $\|\vec{\theta}^{(q)} - \vec{\varphi}^{(q)}\|_\infty$, up to a constant factor, i.e.

$$\text{Vol}_q \sim \|\vec{\theta}^{(q)} - \vec{\varphi}^{(q)}\|_\infty^n \sim (1 - q/q_{\max})^n. \quad (6.15)$$

As $q_{\max} = \text{Int}[(n-1)/4]$, $\text{Vol}_q \rightarrow e^{-4q}$ in the limit $n \rightarrow \infty$ for fixed q . Note that the numerical results presented in the previous remark suggest that Eq. (6.15) underestimates the volumes of the basins of attraction.

Remark. In our convention, angle differences are taken in the interval $(-\pi, \pi]$. Trying to construct a 1-saddle with $q' = 0$, one obtains

$$\Delta' = -\frac{\pi}{n-2} \iff \pi - \Delta' = \frac{n-1}{n-2}\pi > \pi. \quad (6.16)$$

The angle vector obtained in this way has winding number $q' = -1$. This means that there is no 1-saddle with winding number zero. Eq. (6.12) then applies to $q > 0$. It can be checked that there is no k -saddle with winding number $q = 0$ for any $k \geq 1$.

6.2 Identical frequencies: Numerical approach

To validate the scaling of Eq. (6.15), we numerically estimate the volume of the basin of attraction of each stable fixed point of Eq. (6.2). For a cycle network of length n with identical frequencies,

all stable fixed points are known and given by Eq. (6.5). To estimate the volume of the basin of attraction of each $\vec{\theta}^{(q)}$, we randomly choose d normalized perturbation vectors $\vec{e}_j \in \mathcal{H}_{n-1} \subset \mathbb{R}^n$, for $j = 1, \dots, d$, $\|\vec{e}_j\|_\infty = 1$. We then consider perturbed states

$$\vec{\eta}_{q,j,\alpha} := \vec{\theta}^{(q)} + \pi\alpha \vec{e}_j, \quad (6.17)$$

as initial conditions for the dynamics of Eq. (6.2), with $\alpha \geq 0$. The parameter α is increased from zero to $\alpha_{q,j}$ which we define as the largest value such that $\vec{\eta}_{q,j,\alpha}$ converges back to $\vec{\theta}^{(q)}$ under the dynamics of Eq. (6.2). The distance between the stable fixed point $\vec{\theta}^{(q)}$ and the boundary of its basin of attraction in the direction \vec{e}_j is given by $\pi\alpha_{q,j}$.

We performed 4th-order Runge-Kutta simulations of the dynamics of Eq. (6.2) for $n = 23, 43, 83, 163, 323$. These values are chosen to maximize the volume of the basin of attraction for the largest winding number $q_{\max} = \text{Int}[(n-1)/4]$. We took $d = 1000$ randomly chosen perturbation directions and increased α by steps of 0.01. For each q , we can then estimate the proportion of the hypercube of side α centered at $\vec{\theta}^{(q)}$ which belongs to its basin of attraction as

$$p_q(\alpha) := \frac{\text{Card} \left\{ \vec{\eta}_{q,j,\alpha} \mid \vec{\theta}(0) = \vec{\eta}_{q,j,\alpha}, \vec{\theta}(t \rightarrow \infty) = \vec{\theta}^{(q)} \right\}}{d}, \quad (6.18)$$

where $\text{Card}(\cdot)$ stands for the cardinality of the ensemble. In Figure 21 we see that this proportion stays close to 1 for small values of α and quickly drops to zero around some q -dependent value of α . Given a threshold $\tau \in [0, 1]$ we can then define

$$\alpha_\tau(q) := \sup \{ \alpha \mid p_q(\alpha) \geq \tau \}, \quad (6.19)$$

as a typical linear size of the basin of attraction. The abrupt drop of the curves in Figure 21 implies that the precise value of τ is not too significant to understand the behavior of $\alpha_{q,j}$ with respect to q , provided that τ is neither too close to 1, nor to 0. We arbitrarily chose $\tau = 0.7$, but checked that similar conclusions follow for $\tau = 0.6$ and 0.8.

In Figure 22, we plot $\alpha_\tau(q)$ for various system sizes. Except a saturation for small q 's, we observe a linear behavior of α_τ with respect to q . Furthermore, curves for different values of n varying by more than one order of magnitude are rescaled almost on top of one another when plotting them against q/q_{\max} . Both findings corroborate Eq. (6.13). Figure 23, shows for each q , the quartiles of the values of $\alpha_{q,j}$ [defined by $\alpha_\tau(q)$ for $\tau = 0.25, 0.5, 0.75$] and the extreme values $\min_j \alpha_{q,j}$ and $\max_j \alpha_{q,j}$, for $n = 323$, as well as the distance between the stable fixed point $\vec{\theta}^{(q)}$ and the 1-saddle $\vec{\varphi}^{(q)}$ given by Eq. (6.13) (dashed line). All curves have linear behavior, except for small q . The discrepancy between numerics and Eq. (6.13) comes from the fact that the random perturbations are not aligned with the direction of shortest distance to a 1-saddle. In other words, Eq. (6.13) is a lower bound on the distance between the stable fixed point $\vec{\theta}^{(q)}$ and the boundary of its basin of attraction. As mentioned above, 1-saddles are closer to the stable fixed points than other saddle points, which are also on the boundary of the basins of attraction. Our approach of using the 1-saddles to evaluate the volume of the basins of attraction underestimates it, but clearly gives its right parametric dependence in n and q .

6.3 The size of the sync basin revisited

The scaling obtained in Eq. (6.15), for large values of n , is different from the Gaussian scaling postulated in [52]. The numerical method used there took initial conditions at random in the angle space $(-\pi, \pi]^n$, which would need a huge number of runs to reach a resolution allowing a fair estimate of the volumes of the basins of attraction. Even for a moderate resolution of 0.5 in each angle direction, one would need approximately $(2\pi/0.5)^{83} \approx 10^{91}$ different initial conditions, which is obviously unfeasible numerically. Hence, estimates based on brute-force numerical methods cannot catch the scaling behavior in dynamical systems with large dimensionality, especially for large winding numbers, which have very small basins of attractions.

Our approach overcomes this difficulty. Taking advantage of our knowledge of the stable fixed points, we are able to restrict the exploration of the basins of attraction to the neighborhood of the stable fixed points. We avoid scanning the whole angle space which significantly reduces the computation time and increase the accuracy of the method.

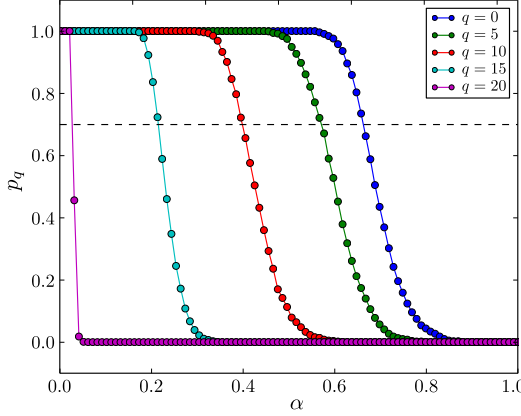


Figure 21: (Figure taken from [69]) Proportion of perturbed states converging back to their reference stable fixed point with respect to the parameter α of Eq. (6.17), for the equal-frequency Kuramoto model on a single cycle with $n = 83$ vertices and winding numbers $q = 0, 5, 10, 15, 20$ from right to left.

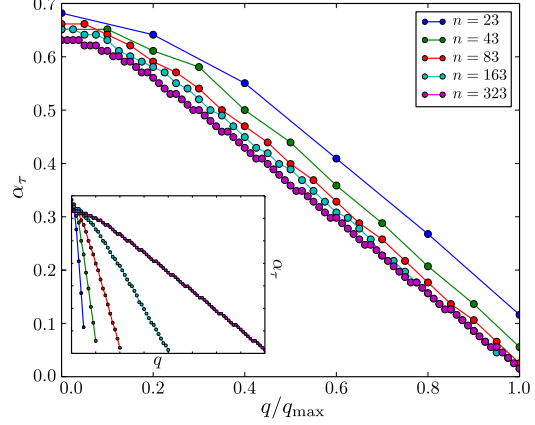


Figure 22: (Figure taken from [69]) Typical linear size of the basins of attraction with respect to the winding number for the model of Eq. (3.1). Threshold values α_τ defined such that 70% of the 1000 perturbed states $\vec{\eta}_{q,j,\alpha}$ converge to $\vec{\theta}^{(q)}$, are plotted as a function of q/q_{\max} (main panel) and q (inset), for $n = 23, 43, 83, 163, 323$.

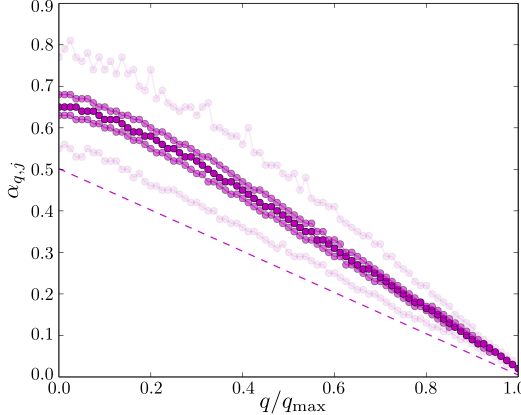


Figure 23: (Figure taken from [69]) Quartiles of the values of $\alpha_{q,j}$ obtained from 1000 random directions \vec{e}_j (purple dots), for $n = 323$. A quarter of the $\alpha_{q,j}$'s are between two vertically consecutive points. Dashed line: distance between the stable fixed point $\vec{\theta}^{(q)}$ and the 1-saddles $\vec{\varphi}^{(q)}$ calculated in Eq. (6.13).

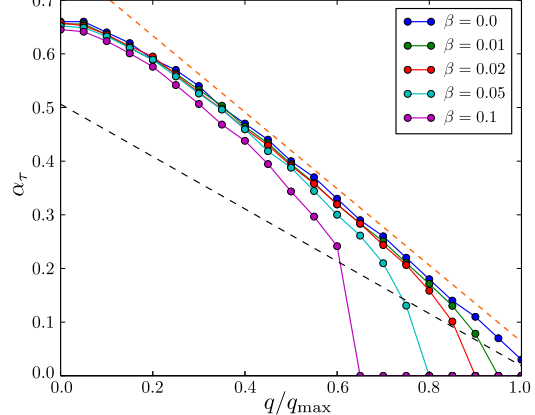


Figure 24: (Figure taken from [69]) Typical linear size of the basins of attraction with respect to the winding number for the model of Eq. (6.20). Threshold values α_τ defined such that 70% of the 1000 perturbed states $\vec{\eta}_{q,j,\alpha}$ converge to $\vec{\theta}^{(q)}$, are plotted as a function of q/q_{\max} for $n = 83$ and frequency distribution in $[-\beta, \beta]$ with $\beta = 0, 0.01, 0.02, 0.05, 0.1$. The black dashed line is Eq. (6.13) and the orange dashed line is a linear guide to the eye.

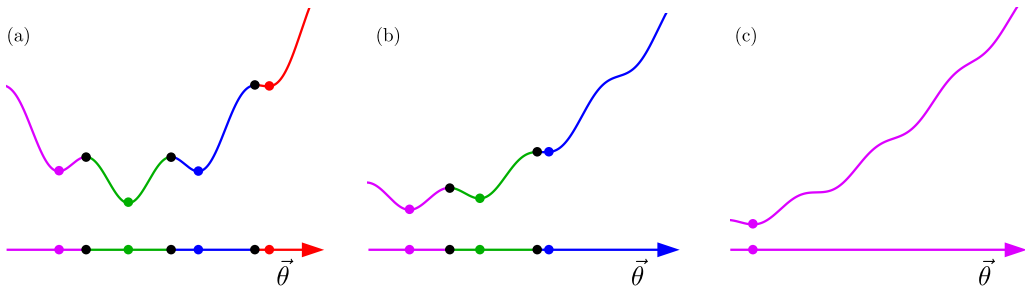


Figure 25: (Figure taken from [69]) Schematic illustration of the projection of the Lyapunov function \mathcal{U} of Eq. (6.21) in one dimension, with $P_i \in [-\beta, \beta]$. The value of β increases from left to right, leading to saddle-node bifurcations. Colored dots and lines are stable fixed points and their respective basins of attraction. Black dots are unstable fixed points. Each stable fixed point gets closer to an unstable fixed point [panels (a) and (b)], but the volume of the basins of attraction does not change much unless one fixed point loses stability [panel (c)]. Fixed points with large winding numbers [red region in panel (a)] lose stability before fixed points with lower winding numbers (blue and green regions).

6.4 Non-identical frequencies

We introduced our method in the simplest case of a cycle network with identical frequencies. To generalize our understanding of the problem, we now add non-identical frequencies to the same cycle network. Even if we cannot obtain the stable fixed points analytically, we can find them numerically and then apply the same numerical procedure as in the identical frequency case. Instead of Eq. (6.2), our single-cycle model is now defined by

$$\dot{\theta}_i = P_i - K \sin(\theta_i - \theta_{i-1}) - K \sin(\theta_i - \theta_{i+1}), \quad i = 1, \dots, n, \quad (6.20)$$

with P_i randomly and homogeneously taken in $[-\beta, \beta]$, satisfying $\sum_i P_i = 0$. For small values of β , the non-identical frequencies almost always lead to small variations of the fixed points [73], and thus the volume of the basins of attraction should not change much. To find the stable fixed points of Eq. (6.20), we start with the fixed points for $\beta = 0$ given in Eq. (6.5) and follow them with a 4th-order Runge-Kutta implementation of Eq. (6.20), while gradually increasing β to the desired value. This allows to identify and follow numerically the location of the stable fixed point $\vec{\theta}^{(q)}(\vec{P})$, which is not anymore given by Eq. (6.5), but is still characterized by its winding number q . We then perturb this stable fixed point in 1000 random directions with increasing magnitude as in Eq. (6.17) and apply the same procedure as in Section 6.2 to evaluate the volumes of the basins of attraction.

Results are shown in Figure 24 for $n = 83$ and $\beta = 0, 0.01, 0.02, 0.05, 0.1$. For values of q which are neither too small nor too large, the linear behavior of α_τ is preserved, especially for small β . As can be expected [67], as soon as we add some finite natural frequencies, the fixed points with large q lose stability. More surprising, at first glance, is the abrupt drop of α_τ for large q with little change at small q . We offer an explanation for this behavior.

The dynamics of Eq. (1.3) is given by the gradient of the Lyapunov function, Eq. (2.38),

$$\begin{aligned} \mathcal{U}(\vec{\theta}) &= - \sum_i P_i \theta_i + \sum_{i < j} K_{ij} [1 - \cos(\theta_i - \theta_j)], \\ \dot{\theta}_i &= - \frac{\partial \mathcal{U}}{\partial \theta_i}. \end{aligned} \quad (6.21)$$

Increasing β modifies \mathcal{U} [the first term on the right-hand side of Eq. (6.21)] and makes the fixed points move in angle space. Eventually, a stable fixed point $\vec{\theta}^{(q)}$ will meet an unstable fixed point and then lose stability through a saddle-node bifurcation. In Figure 25, we give a schematic illustration of \mathcal{U} on a cycle, projected on an appropriate direction in angle space, such that stable and unstable fixed points are aligned in one angle dimension. As long as a fixed point remains stable, the volume of its basin of attraction does not change much [compare the green segments in

β	$q_{\max}(\beta)$: Eq. (6.27)	$q_{\max}(\beta)$: numerical
0	20.75	{20, 20, 20, 20, 20}
0.01	17.14	{17, 17, 18, 18, 18}
0.02	15.62	{16, 16, 17, 17, 17}
0.05	12.56	{13, 14, 14, 15, 15}
0.1	8.97	{10, 11, 12, 12, 13}

Table 2: Maximal values of q with respect to β , estimated by Eq. (6.27) and obtained with 5 random frequency distributions following our simulations of the dynamics of Eq. (1.3).

Figures 25(a) and 25(b)]. The fixed point then abruptly vanishes when β becomes too large. Since α_τ is an average over many randomly chosen directions, its value abruptly drops when the stable fixed point vanishes.

Recalling Eq. (3.8), the angle difference on the edge between vertices k and $k+1$ is given by

$$\Delta_{k,k+1} = \arcsin(\varepsilon_q + P_{k,k+1}^*/K). \quad (6.22)$$

For the sake of simplicity and without loss of generality, we take $K = 1$. The frequencies P_k are taken randomly, homogeneously and independently in the interval $[-\beta, \beta]$. Their expectation and variance are

$$\mathbb{E}(P_k) = 0 \quad \text{and} \quad \text{var}(P_k) = \beta^2/3. \quad (6.23)$$

Expectation and variance of $P_{k,k+1}^*$, defined in Eq. (2.13), are then

$$\mathbb{E}(P_{k,k+1}^*) = 0 \quad \text{and} \quad \text{var}(P_{k,k+1}^*) = k \cdot \beta^2/3. \quad (6.24)$$

For n sufficiently large, we then expect typical excursions of magnitude $\sqrt{k}\beta/\sqrt{3}$ for $P_{k,k+1}^*$, away from its average $\mathbb{E} = 0$. We know from Section 3 that on cycles with finite natural frequencies, stable fixed points may have one angle difference slightly larger than $\pi/2$ before losing stability at $\pi/2 + \delta$. We observed that δ is always small, thus we will approximate the loss of stability to happen when $\Delta_{k,k+1} = \pi/2$, i.e. when the argument of the arcsine in Eq. (6.22) is equal to one. Finally, we approximate ε_q by its value when $\beta = 0$,

$$\varepsilon_q \approx \sin(2\pi q/n). \quad (6.25)$$

Putting everything together and taking k to be the average value of the indices, i.e. $k = n/2$, Eq. (6.22) becomes

$$\sin(2\pi q_{\max}/n) + \sqrt{n}\beta/\sqrt{6} = 1, \quad (6.26)$$

which gives a maximal possible value for q before losing stability, with respect to β ,

$$q_{\max}(\beta) = (2\pi)^{-1}n \arcsin(1 - \sqrt{n}\beta/\sqrt{6}). \quad (6.27)$$

Simulated and estimated values of q_{\max} are given in Table 2 for various values of β . Even if the simplifications assumed to obtain Eq. (6.27) underestimate q_{\max} , it is in fair agreement with values obtained numerically.

6.5 Meshed networks

We finally extend the perturbation method described above to more complicated, meshed networks. It is a two-stage method where we first numerically identify fixed points of Eq. (1.3) on complex graphs and second perturb the obtained stable fixed points in the same way as in Section 6.2.

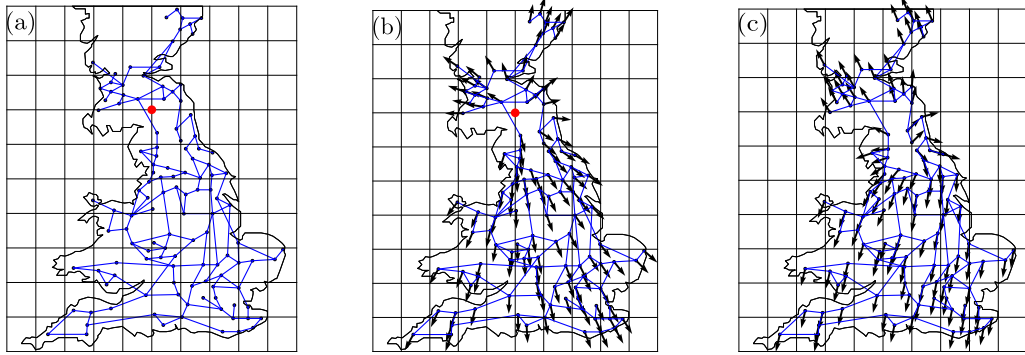


Figure 26: (Figure taken from [69]) (a): Geographic embedding of the UK high voltage network in the plane, with a square lattice. (b): Initial condition with $q = 1$, constructed with Eq. (6.29). (c): Stable fixed point towards which the initial state of panel (b) converges under the dynamics of Eq. (1.3) with $P_i = 0$, $\forall i$.

6.5.1 Identifying stable fixed points

Stable fixed points are much harder to find on complex graphs. Except for the $\vec{\theta}^{(0)} = (0, \dots, 0)^\top$ fixed point for equal frequencies, they are usually impossible to find analytically. To tackle this problem, we construct a numerical algorithm similar to but different from the one proposed in [63].

From Section 3, we know that two fixed points of Eq. (1.3) differ only by a collection of loop flows quantized by their winding numbers. Let us denote by

$$\vec{q}_{\mathcal{G}}(\vec{\theta}) = (q_1, q_2, \dots, q_c), \quad (6.28)$$

the winding vector of the state $\vec{\theta}$ on the interaction graph \mathcal{G} . Assuming $|\Delta_{ij}| < \pi/2$ for all connected vertices i and j , each stable fixed point $\vec{\theta}^*$ can be uniquely labelled by its winding vector $\vec{q}_{\mathcal{G}}(\vec{\theta}^*)$ [26, 63].

We search numerically for stable fixed points via an iterative process starting from initial states with $q \neq 0$, described by

$$\theta_i = q \arctan \left(\frac{y_i - y_0}{x_i - x_0} \right), \quad (6.29)$$

where (x_0, y_0) are the coordinates of a point in the embedding of the network in the plane, and the defined angles wind q times around the origin when travelling around the point (x_0, y_0) . To find stable fixed points, the algorithm reads:

1. Define a two-dimensional embedding of the network. Use this to superimpose a regular lattice of coordinates on the network. This is shown in Figure 26(a).
2. Set (x_0, y_0) to a node of the regular lattice.
 - a. Using Eq. (6.29), define a new initial state.
 - b. Follow numerically Eq. (1.3) on the considered meshed graph until a stable fixed point is reached.
 - c. Each stable fixed point can be unambiguously identified by its winding vector. Use this to determine if the fixed point just found is a new one. If yes, store it.
3. Go back to step 2.

As complex meshed network, we consider the UK high voltage network which is composed of 120 vertices and 165 edges (see Figure 27). To illustrate the algorithm just described, Figures 26(b)

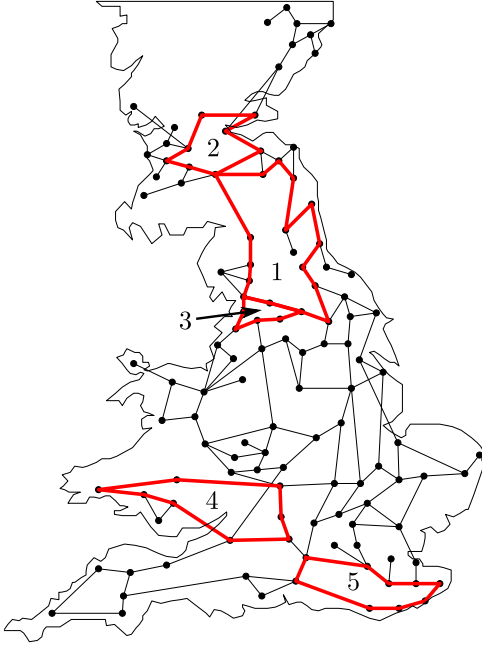


Figure 27: (Figure taken from [69]) High voltage UK AC transmission network used as meshed network. The five cycles we focus on are indicated in red. Note that cycle 4 is traversed but not interrupted by an edge.

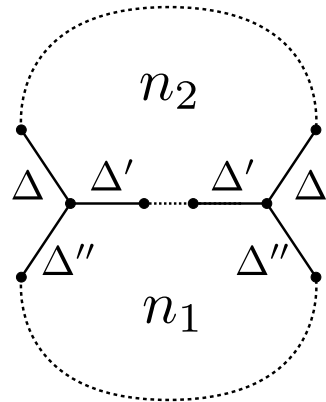


Figure 28: (Figure adapted from [69]) Two cycles sharing ℓ edges. The top cycle has n vertices and the bottom one m vertices. Angle differences of a fixed point of Eq. (1.3) with identical frequencies are given by Δ , Δ' and Δ'' .

and (c) show an initial condition and the stable state toward which it dynamically converges respectively. Stable fixed points with many non-zero winding numbers are obtained by setting $|q|$ to large values in Eq. (6.29), in our case $q \in \{-50, \dots, 50\}$. The dynamics will then split this initial large winding number into several smaller winding numbers, located on different cycles of the network. This method can be used on any network whether complex or regular, its vertices only need to be embedded in \mathbb{R}^2 . Time evolving Eq. (1.3) on the UK network with this initial condition returns only stable fixed points. In this way, we found more than 4000 different stable fixed points of Eq. (1.3) with $P_i = 0$.

6.5.2 Estimating the volume of basins of attraction

Having identified stable fixed points $\vec{\theta}^{(q)}$ of Eq. (1.3) on the UK network, we next follow the same procedure as in Section 6.2, and measure the volume of their basins of attraction. We focus on stable fixed points with non-zero winding number only on the five cycles in red in Figure 27. We introduce a shorthand notation with the winding numbers of these cycles only

$$\vec{q}_{\text{sh}} := (q_1, q_2, q_3, q_4, q_5). \quad (6.30)$$

Taking each cycle independently, the maximum winding numbers are $q_1^{\max} = 4$, $q_2^{\max} = 2$, $q_3^{\max} = 1$, $q_4^{\max} = 2$, $q_5^{\max} = 2$.

In Figure 29, we show α_τ of Eq. (6.19) for $\tau = 0.5$ and the interquartile values for various stable fixed points identified by their unique combination of winding numbers. For $P_i = 0$, Eq. (1.3) is symmetric under switching θ_i to $-\theta_i$, for all i . This implies that the volume of each basin of attraction is invariant under reversing the sign of all angles \vec{q}_G to $-\vec{q}_G$. This symmetry can be seen on Figure 29(a) which is symmetric under changing q_1 to $-q_1$, as there is only one cycle with a non-zero winding number. Alternatively, changing \vec{q}_G to $-\vec{q}_G$ interchanges panels (b) and (c) with q_1 and $-q_1$ swapped. For fixed points with more than one cycle carrying a non-zero winding number, there is no symmetry when reversing q_1 to $-q_1$ [see Figures 29(b)–(f)] and the asymmetry is even more significant if the cycles with non-zero winding numbers are close to each other [see

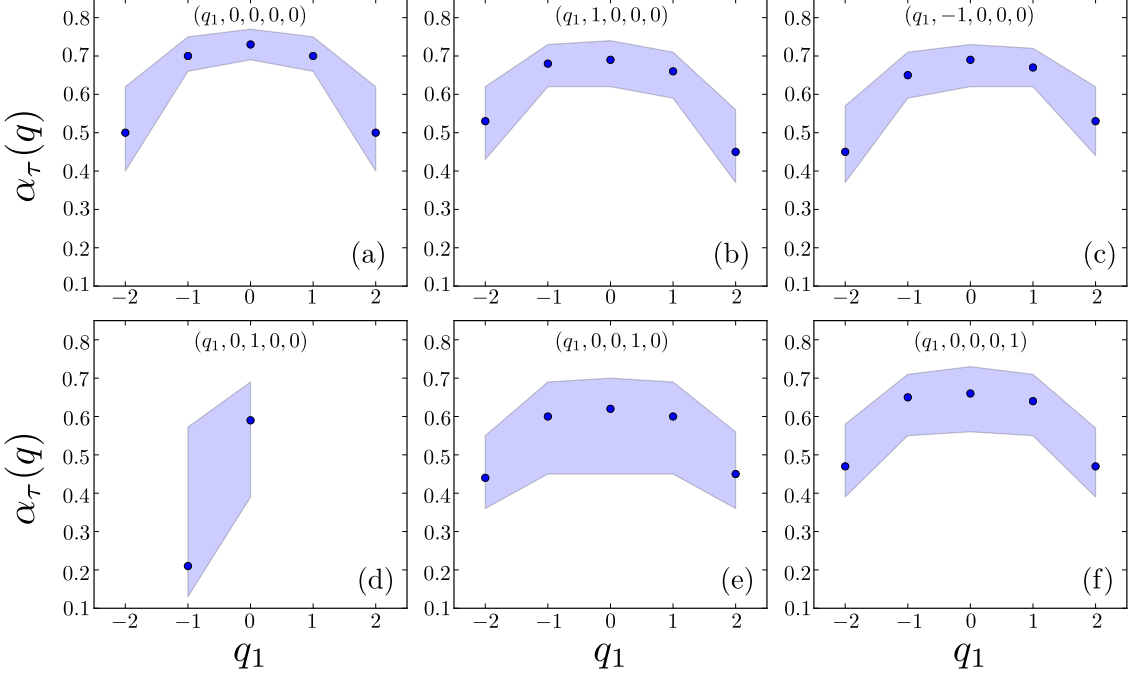


Figure 29: (Figure taken from [69]) Median (blue dots) and interquartiles (blue areas) of the values of $\alpha_{\vec{q},j}$ obtained from 1000 random perturbations $\vec{\epsilon}_j$ of fixed points of Eq. (1.3) with $P_i = 0$, $\forall i$ on the UK network of Figure 27 as a function of q_1 , the winding number on cycle 1.

Figures 29(b) and (d)], because there are few intermediate nodes which can screen the effect of one non-zero winding number on the other and so the cycles interact strongly.

In Figure 29(d), we did not find any fixed point with winding vector $\vec{q}_{sh} = (1, 0, 1, 0, 0)$ but we found one with $\vec{q}_{sh} = (-1, 0, 1, 0, 0)$. To understand this, we consider the simplified situation of two connected cycles of length n_1 and n_2 , sharing ℓ edges as depicted on Figure 28. We consider the case when $q^{(n_2)} = 1$ and $q^{(n_1)} = 0$. At a fixed point, Eq. (1.3) implies

$$\sin(\Delta) = \sin(\Delta') + \sin(\Delta''), \quad (6.31)$$

and Eq. (2.24) gives

$$(n_1 - \ell) \cdot \Delta'' - \ell \cdot \Delta' = 2\pi q^{(n_1)} = 0. \quad (6.32)$$

From Section 4, if $\ell > 1$, we have $|\Delta|, |\Delta'|, |\Delta''| \leq \pi/2$. Eqs. (6.31) and (6.32) imply that $\Delta > \Delta'$. Therefore, to have $q^{(n_2)} = 1$, we must have $\Delta > 2\pi/n_2$. Thus, if we add edge-sharing cycles with zero winding number to a main cycle with a non-zero winding number, some of the angle differences must increase. When Δ is large, this can bring $\Delta > \pi/2$ where stability is lost (see Section 4). Adding a cycle carrying a non-zero winding number makes the situation even more critical. If we isolate cycles 1 and 3, which correspond to Figure 28 with $n_1 = 7$, $n_2 = 16$ and $\ell = 2$, an easy calculation shows that there exist stable fixed points with $(q^{(16)}, q^{(7)}) = (1, 1)$ and $(q^{(16)}, q^{(7)}) = (1, -1)$. However, when we consider the complete network, only the solution with $(q^{(16)}, q^{(7)}) = (1, -1)$ remains stable. This comes from the fact that, when both winding numbers have the same sign, the angle differences on the shared edges benefit only to one of the cycles. The other cycle then has to make a winding number out of a reduced number of edges, implying larger angle differences. Finally, when we take the complete UK network, we put cycles next to the two initial ones and make the angle differences even larger, until stability is lost. When the winding numbers have opposite sign, both cycles benefit from the angle differences on the shared edges, which leads to smaller angle differences than in the previous case. This explains why the fixed point $\vec{q}_{sh} = (-1, 0, 1, 0, 0)$ is stable while $\vec{q}_{sh} = (1, 0, 1, 0, 0)$ is not.

To conclude this section, we note that a meshed network has an effect similar to the case considered in Section 6.4 with $P_i \neq 0$ in that, compared to the single-cycle network, (i) there are

fewer stable fixed points with large winding numbers and (ii) the volume of basins of attraction of fixed points with small winding numbers seem to be unaffected.

7 Bridging the gap between Kuramoto and electrical networks

In Section 1.1 we made several assumptions which allowed us to simplify the swing equations and to rewrite them as the Kuramoto model. We then obtained some results concerning the number of stable fixed points and the basins of attraction of the Kuramoto model. Our aim is now to determine if our results can be extended to the more detailed swing equations.

Among other assumptions, we considered that:

- the coupling constant is the same for all edges of the network;
- the angle variable have no inertia, meaning that their dynamics are first-order;
- the power transmissions are lossless.

We will now review these assumptions and see how removing each of them influence the results obtained in this manuscript.

7.1 Non-identical coupling

The approach developed in this manuscript can be straightforwardly adapted to different coupling strengths on different edges, substituting K_{ij} for $K a_{ij}$. The dynamics are then given by the general Eq. (1.3), which we recall here

$$\dot{\theta}_i = P_i - \sum_{j=1}^n K_{ij} \sin(\theta_i - \theta_j), \quad i = 1, \dots, n. \quad (7.1)$$

The balance equations at each vertex, Eq. (2.9), is then

$$P_i = \sum_{j=1}^n K_{ij} \sin(\theta_i - \theta_j), \quad i = 1, \dots, n. \quad (7.2)$$

Along a cycle, the loop flow parameter, denoted ε previously, is not preserved anymore. According to Theorem 2.3, the preserved quantity is the loop flow, but as the coupling is not the same on each edge, it cannot be split as the product of K and ε as we did in Sections 3 and 4. Then we denote the loop flow by $\Sigma \in \mathbb{R}$ and rewrite the flow on an edge as

$$P_{i,i+1} = P_{i,i+1}^* + \Sigma, \quad i = 1, \dots, n, \quad (7.3)$$

with the reference flow $P_{i,i+1}^*$ defined as

$$P_{i,i+1}^* := \sum_{j=1}^i P_j, \quad i = 1, \dots, n. \quad (7.4)$$

For all i , $|P_{i,i+1}| \leq K_{i,i+1}$, which gives the following lower and upper bounds on the loop flow Σ ,

$$\Sigma_{\min} := \max_i \{-K_{i,i+1} - P_{i,i+1}^*\}, \quad \Sigma_{\max} := \min_i \{K_{i,i+1} - P_{i,i+1}^*\}. \quad (7.5)$$

The expression for the angle differences, Eqs. (3.2) and (3.3), is modified as follows

$$\Delta_{i,i+1} = \arcsin \left(\frac{P_{i,i+1}}{K_{i,i+1}} \right) = \arcsin \left(\frac{P_{i,i+1}^* + \Sigma}{K_{i,i+1}} \right). \quad (7.6)$$

Summing the angle differences still gives an integer multiple of 2π , which quantizes the number of fixed points.

We cannot normalize the parameter that characterizes the loop flow, but it is not a problem for our results as long as we guarantee that the ratio $\Sigma/K_{i,i+1}$ is preserved for all i when taking the limits $K_{i,i+1} \rightarrow \infty$ simultaneously for all i . It means that in Section 3.2, instead of taking the

limit $K \rightarrow \infty$, we would define a parameter $\alpha \in \mathbb{R}$, and define $K_{i,i+1} := \alpha K_{i,i+1}^*$ and $\Sigma := \alpha \Sigma^*$. All results of Section 3.2 are then obtained by taking the limit $\alpha \rightarrow \infty$, and results of Section 3.3 are obtained by decreasing α . Considering identical coupling strengths was then a simplifying assumption, but does not limit the results of Sections 3 and 4. Namely, the number of stable fixed points of Eq. (7.1) is bounded from above as

$$\mathcal{N} \leq 2 \cdot \text{Int}[(n-1)/4] + 1, \quad (7.7)$$

for cycle networks, and

$$\mathcal{N} \leq \prod_{k=1}^c [2 \cdot \text{Int}(n_k/4) + 1], \quad (7.8)$$

for stable fixed points with all angle differences smaller than $\pi/2$ on planar networks with identical frequencies.

7.2 Second-order dynamics

In their usual formulation, the swing equations (1.2) take into account the inertia of the rotating machines in the network [3], which yields (neglecting conductance)

$$I_i \ddot{\theta}_i + D_i \dot{\theta}_i = P_i - \sum_{j=1}^n |V_i||V_j|B_{ij} \sin(\theta_i - \theta_j), \quad i = 1, \dots, n, \quad (7.9)$$

and the corresponding **second-order Kuramoto model** [30] can be written as

$$I_i \ddot{\theta}_i + D_i \dot{\theta}_i = P_i - \sum_{j=0}^n K_{ij} \sin(\theta_i - \theta_j), \quad i = 1, \dots, n, \quad (7.10)$$

where we take $I_i \in \mathbb{R}_{>0}$ and $D_i \in \mathbb{R}_{\geq 0}$. The second order term has no influence on the fixed points, Eqs. (1.3) and (7.10) have exactly the same fixed points. We recall here the argument of [5], showing that a fixed point is stable under the dynamics of Eq. (7.10) if and only if it is stable under the dynamics of Eq. (7.1).

Defining the variable $\omega_i := \dot{\theta}_i$, Eq. (7.9) is rewritten as the pair of equations

$$\begin{cases} \dot{\theta}_i = \omega_i \\ I_i \dot{\omega}_i = -D_i \omega_i + P_i - \sum_{j=1}^n K_{ij} \sin(\theta_i - \theta_j). \end{cases} \quad (7.11)$$

Assuming $I_i \neq 0$ and linearizing Eqs. (7.11) around a fixed point $(\vec{\theta}^*, \vec{\omega}^*)^\top$, a small perturbation $(\delta\vec{\theta}, \delta\vec{\omega})^\top$ evolves according to the following dynamics

$$\frac{d}{dt} \begin{pmatrix} \delta\vec{\theta} \\ \delta\vec{\omega} \end{pmatrix} = \underbrace{\begin{pmatrix} 0 & \mathbf{1} \\ I^{-1} \cdot \mathcal{J}(\vec{\theta}^*) & -I^{-1}D \end{pmatrix}}_{\bar{\mathcal{J}}} \cdot \begin{pmatrix} \delta\vec{\theta} \\ \delta\vec{\omega} \end{pmatrix}, \quad (7.12)$$

where \mathcal{J} is the Jacobian matrix defined in Eq. (2.36), and $I := \text{diag}(\vec{I})$ and $D := \text{diag}(\vec{D})$ are the diagonal matrix of inertias and dampings respectively. The fixed point $(\vec{\theta}^*, \vec{\omega}^*)^\top$ is linearly stable if and only if all eigenvalues of the matrix $\bar{\mathcal{J}}$ have non-positive real part. An eigenvalue $\nu \in \mathbb{C}$ of $\bar{\mathcal{J}}$ satisfies

$$\bar{\mathcal{J}} \cdot \begin{pmatrix} \vec{x} \\ \vec{y} \end{pmatrix} = \begin{pmatrix} \nu \vec{x} \\ \nu \vec{y} \end{pmatrix}, \quad (7.13)$$

which we write as the two matricial equations

$$I^{-1} \mathcal{J} \vec{x} - I^{-1} D \vec{y} = \nu \vec{x} \quad \left. \begin{array}{l} \vec{y} = \nu \vec{x} \end{array} \right\} \implies \nu^2 I \vec{x} + \nu D \vec{x} - \mathcal{J} \vec{x} = 0. \quad (7.14)$$

Projecting Eq. (7.14) on the eigenvector \vec{x} yields

$$a\nu^2 + b\nu - c = 0, \quad (7.15)$$

where $a := \vec{x}I\vec{x} > 0$, $b := \vec{x}D\vec{x} \geq 0$ and $c := \vec{x}\mathcal{J}\vec{x}$. An eigenvalue of $\tilde{\mathcal{J}}$ satisfies then

$$\nu_{\pm} = \frac{-b \pm \sqrt{b^2 + 4ac}}{2a}. \quad (7.16)$$

Clearly, $\text{Re}(\nu_-)$ is necessarily negative and only $\text{Re}(\nu_+)$ might be positive. If the fixed point is linearly stable for the first order model, i.e. \mathcal{J} is negative semidefinite, then c is negative and $\text{Re}(\nu_+)$ as well. The real part of ν_+ changes sign when c vanishes, which, by definition of \vec{x} requires at least one of the Lyapunov exponents to be non-negative. The fixed point is then stable for the second-order Kuramoto model, Eq. (7.10), if and only if it is stable for the first-order Kuramoto model, Eq. (1.3).

Hence, neglecting inertia has no influence on the results of Sections 3 and 4 because they deal with steady states and the dynamics are not involved further than in the stability analysis. However, results of Sections 5 and 6 cannot be extended to the second-order equations (7.9) because the trajectories of the two systems are different. A priori, the size and shape of the basins of attraction of Eqs. (1.3) and (7.10) are completely different, only the equilibria remain unchanged in the state space.

7.3 Dissipative lines

Dissipation in electrical networks is related to conductance, which is small in very high voltage networks, and it translates in Eq. (1.2) by a small ratio $G_{ij}/B_{ij} \leq 0.1$. In a first approximation, G_{ij} can then be neglected, as we did until now.

If we do not neglect G_{ij} , Eq. (1.3) has the form

$$\dot{\theta}_i = P_i - \sum_{j=1}^n [B_{ij} \sin(\theta_i - \theta_j) - G_{ij} \cos(\theta_i - \theta_j)], \quad i = 1, \dots, n, \quad (7.17)$$

where we included the voltage amplitude $|V_i|$, still assumed constants, in the parameters B_{ij} and G_{ij} and we recall from Eq. (1.2) that $G_{ii} = -\sum_j G_{ij}$. Defining

$$\phi_{ij} := \arctan(G_{ij}/B_{ij}), \quad \text{and} \quad K_{ij} := \sqrt{B_{ij}^2 + G_{ij}^2}, \quad (7.18)$$

we rewrite Eq. (7.17) as

$$\dot{\theta}_i = P_i - \sum_j K_{ij} \sin(\theta_i - \theta_j - \phi_{ij}), \quad i = 1, \dots, n, \quad (7.19)$$

which has been called the Kuramoto-Sakaguchi model [74]. Note that in this case, natural frequencies do not sum up to zero. Consider an equilibrium $\vec{\theta}^*$ of Eq. (7.17) and sum all equations over i ,

$$\sum_{i=1}^n P_i = \sum_{i,j} B_{ij} \sin(\theta_i^* - \theta_j^*) - G_{ij} \cos(\theta_i^* - \theta_j^*) = \sum_{i < j} G_{ij} [1 - 2 \cos(\theta_i^* - \theta_j^*)], \quad (7.20)$$

which is not zero in general.

The question of multiple fixed points then needs some more information to be solved. Consider for instance the cycle network of Figure 2 with zero natural frequencies, $P_i \equiv 0$. The state with identical angles $\theta_i \equiv \theta^*$ is obviously a fixed point of Eq. (7.17) for this network. Trying to add a loop flow, say clockwise, we see that we need all angle differences to be positive. But in this case, the cosine terms in Eq. (7.20) are strictly lower than 1, and the sum of natural frequencies has to be positive. There is then no solution with a loop flow and zero natural frequencies at the same time, if frequencies are fixed.

Seeing the system as an electrical network clarifies what we just observed. Adding a loop flow implies a larger flow on the edges and a larger flow implies more dissipated power. The generators then need to compensate for the extra power dissipated. To define our problem completely, we then need to specify which buses of the network will compensate for the losses along the edges. In particular, the number of fixed points of our system will depend on this choice.

Robustness of Loop Flows against Dissipation

Including dissipation changes the dynamics of the system considered, but we can expect that for a small ratio G_{ij}/B_{ij} , the dynamics will not change qualitatively. We reproduce here the simulations performed in Section 5, adding the dissipation term. Our simulations confirm our expectations, showing that adding a moderate dissipation term, only a small quantitative change occurs.

We consider identical parameters for all edges of the network, i.e. $B_{ij} \equiv B$ and $G_{ij} \equiv G$ for all edges $\langle ij \rangle$. Eq. (7.17) is then

$$\dot{\theta}_i = P_i - \sum_{j=1}^n a_{ij} [B \sin(\theta_i - \theta_j) + G (1 - \cos(\theta_i - \theta_j))] , \quad i = 1, \dots, n . \quad (7.21)$$

Process 1. In Figure 30 (green lines), we apply the same mechanism as in Figure 13 (reproduced with blue lines in Figure 30), with $G/B = 0.03$. Oscillator x is in charge of compensating for the dissipation, i.e. its natural frequency is $P_x + \Delta P$, where ΔP is dynamically tuned to balance the system such that a fixed point can be reached. The value of ΔP depends on the state of the system as we will see. The system starts at $P_y = 0$ with $q = 0$, and P_y is then increased until the loss of stability of all fixed points, and it is then decreased to zero. We observe that the behavior of the system with dissipation is similar to that without dissipation. The fixed point with winding number $q = 0$ loses stability at a value of P_y close to the lossless case, and upon reduction of P_y , the system remains at a $q = -1$ fixed point. Figure 30(c) shows that the value of ΔP is approximately doubled in the $q = -1$ fixed point compared to the $q = 0$ one, for small P_y . From the point of view of power systems, this means that x needs to inject more power in the system to maintain the synchronous state.

Process 2. In Figure 31, we reproduced the results presented in Figure 15, with finite dissipation, i.e. $G/B = 0.01$ (green lines) and $G/B = 0.03$ (red lines). The behavior after removing the edge (in red in the inset of Figure 31) is not qualitatively modified by the addition of dissipation. The only change being a shift of the loss of stability to smaller values of P . Again, the system remains at the $q = 1$ fixed point upon continuous reduction of P after removing the edge. The evolution of the system is not qualitatively changed by the moderate amount of dissipation introduced. As in the previous case, the value of ΔP necessary to compensate for the dissipation is much larger for the $q = 1$ fixed point than for the $q = 0$ one [Figure 31(c)].

Process 3. Figure 32 makes it clear that the mechanism of removing an edge and adding it back proceeds in the same way with finite dissipation. On the network represented in the inset of Figure 32(c) with $G/B = 0.03$, we start at the stable fixed point with winding number $q = 0$, we then remove the indicated edge, let the system dynamically stabilize and then add back the edge. The final state of this process depends on the ratio P/B . When P is small, removing the edge does not change the angle much, and after adding back the edge, the system converges back to the $q = 0$ stable fixed point [yellow area in Figure 32(a)]. However, at larger values of P , the transient brings the system to the $q = 1$ stable fixed point [green area in Figure 32(a)]. Figure 32(b) shows that the transition to $q = 1$ occurs precisely when the angle differences between the vertices at the two ends of the removed edge reaches π at the stable fixed point just before adding back the edge, in agreement with the $G = 0$ case presented in Section 5.

As previously noted, with finite dissipation, the values of natural frequencies at oscillators x and y in the inset of Figure 32(c) depends on the fixed point. In this case, we fix the natural frequency of y at $-P$ and adapt the natural frequency of x as $P + \Delta P$, to obtain an equilibrium of Eq. (7.17). It is then clear that ΔP depends on the winding number of the fixed point of our system. In Figures 32(d) and (e), we show what happens if the natural frequency of x is

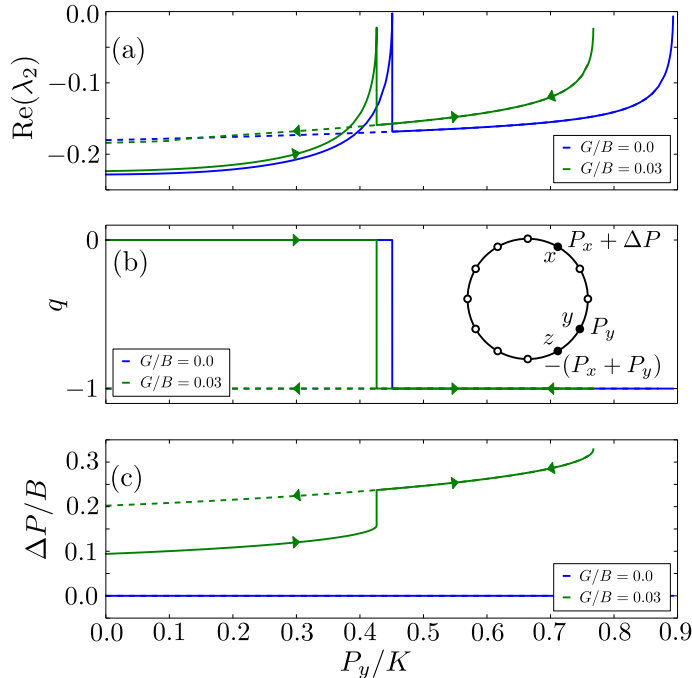


Figure 30: (Figure adapted from [67]) Dynamical generation of loop flows by increase of a natural frequency for a cycle with $n = 12$ vertices and edges with coupling K . Oscillator x has a positive natural frequency $P_x = K$ and oscillator y has a non-negative natural frequency P_y which is varied. Oscillator z compensates for both these positive natural frequencies with $P_z = -(P_x + P_y)$. In the dissipative case (green lines, $G/B = 0.03$), oscillators x compensate for the dissipated flows. The other oscillators have small random natural frequencies summing to zero to make the model more generic. Panel (a) shows the real part of the Lyapunov exponent λ_2 , which clearly indicates the values of P_y where stability is lost, i.e. $\lambda_2 \rightarrow 0$. As in the $G = 0$ case (blue lines, same as Figure 13), the fixed point with winding number $q = -1$ survives for larger P_y than the $q = 0$ stable fixed point. Panel (b) shows the winding number of the stable fixed point and corroborate the fact that the mechanism is the same with small dissipation as without dissipation. Panel (c) shows the increase of natural frequency at oscillators x needed to compensate for the dissipation. This amount can be computed by Eq. (7.20) and is larger for the $q = -1$ stable fixed point.

changed from its value at the $q = 1$ stable fixed point, to its value at the $q = 0$ stable fixed point [Figure 32(d)] and vice-versa [Figure 32(e)]. In both cases, the winding number is not changed, synchrony is preserved, but the imbalance of natural frequencies lead to a decrease (resp. increase) of all angles. Thus changing the natural frequencies to their values at another stable fixed point does not necessarily bring the system to it.

We finally export the knowledge obtained from investigating simple systems to a network model with the topology of the UK high voltage AC power grid [5, 75]. Figure 33 illustrates loop flow creation and robustness, and enhanced dissipation. The system is initially stabilized at a fixed point with zero winding number on all of its cycles. It is perturbed by removing an edge, at the position indicated in Figure 33(e). The state is then left to stabilize towards a new fixed point, after which it is again perturbed by adding back the removed edge. Finally, natural frequencies are modified to their initial value, trying to bring the system back to its initial state with $q = 0$ (without success). Similarly to the cycle model considered in Figure 32, removing the edge makes essentially one angle difference significantly change [see Figure 33(a)], and the same angle difference changes when the edge is added back. Figure 33(c) shows that removing the edge changes the winding number and thus creates a loop flow, which is not deleted when the natural frequencies are brought back to their initial values. The loop flow created doubles the amount of dissipation, as can be seen in Figure 33(d), even if it only affects a small part of the network, as can be seen in Figure 33(e).

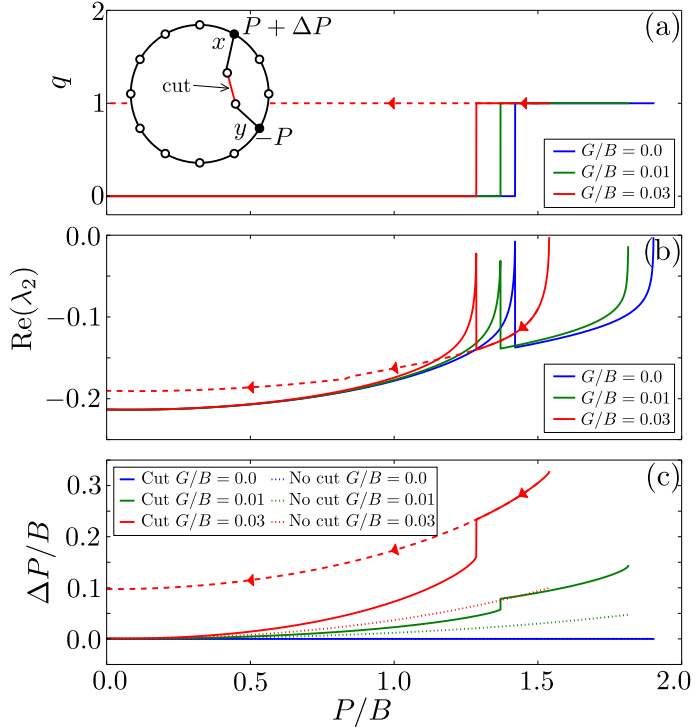


Figure 31: (Figure adapted from [67]) Loop flow creation by edge removing in a double cycle network with $n = 14$ vertices and coupling K . Oscillator x has positive natural frequency $P + \Delta P$, where ΔP compensates for the dissipation, oscillator y has negative natural frequency $-P$, and all other oscillators have small random natural frequencies, to make the model more generic. Different values of G are considered $G = 0$ (blue lines, same as Figure 15), $G/B = 0.01$ (green lines) and $G/B = 0.03$ (red lines). Panel (a) shows the winding number on the large cycle in the inset and panel (b) shows the real part of the Lyapunov exponent. The changes of both quantities are qualitatively the same for all values of G , which corroborates our claim that a moderate amount of dissipation does not change the behavior of such dynamical systems. Panel (c) shows the increase of natural frequency required to oscillator x to compensate for the dissipation. For $P = 0$ and $q = 0$, there is no flow in the network, and $\Delta P = 0$, but we see that for $q = 1$, the flows are non-zero and a finite value of ΔP is needed to compensate for the resulting dissipation.

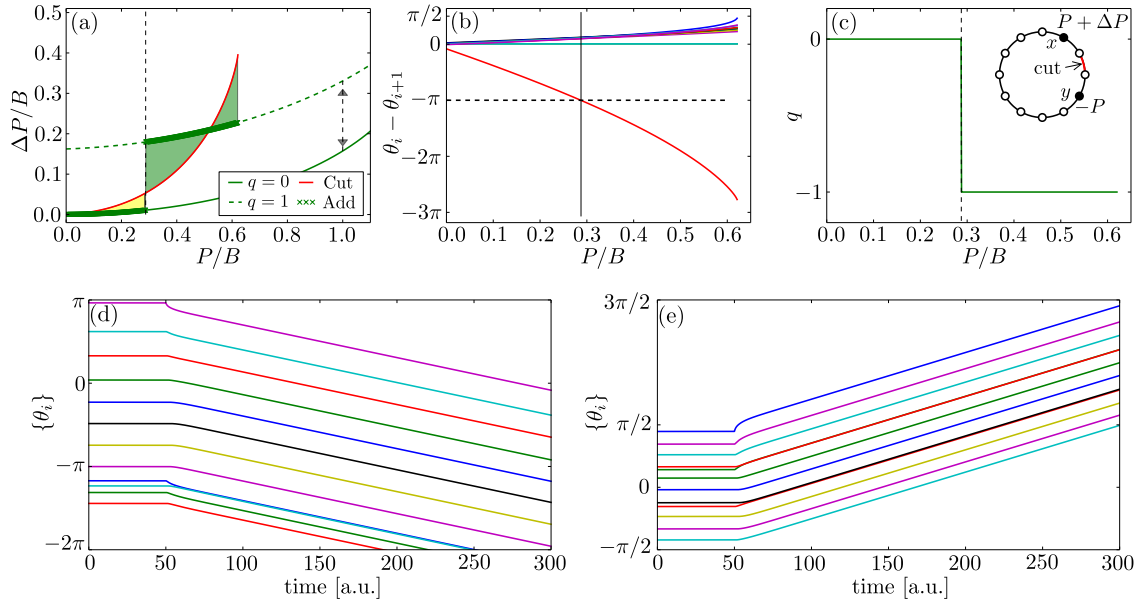


Figure 32: (Figure adapted from [67]) Loop flow creation under the mechanism of removing an edge and adding it back, with finite dissipation, $G/B = 0.03$, for the network shown in the inset of panel (c). For all values of P , we start at the $q = 0$ stable fixed point, then remove the edge indicated in the inset of panel (c), let the system dynamically converge. We then add back the removed edge and let again the system evolve to a stable fixed point. Panels (a) and (c) show that the final state remains at winding number $q = 0$ for sufficiently small P , and moves to $q = 1$ for larger P . Panel (a): Compensation of dissipation at oscillator x for the $q = 0$ stable fixed point (solid green line), the $q = 1$ stable fixed point (dashed green line) and after removing the indicated edge (red solid line). The red line stops at $P/K \approx 0.62$ above which there is no stable fixed point for the network with the edge removed. The green crosses indicate the value of ΔP after adding back the edge. Panel (b): angle differences before adding back the edge. The jump to $q = 1$ occurs when the angle difference between the two ends of the removed edge exceeds π , in complete agreement with the results of Section 5, on the projected Lyapunov function, even with dissipation. Panel (c): final winding number after edge addition. Panel (d): time evolution of the oscillators' angles, starting at the stable fixed point with winding number $q = 1$ and changing ΔP to its value for the stable fixed point with winding number $q = 0$ at time $t = 50$. The system does not converge to the $q = 0$ fixed point, but remains synchronous with winding number $q = 1$ and negative velocity for all angles. Panel (e): same as panel (d), but from $q = 0$ to $q = 1$.

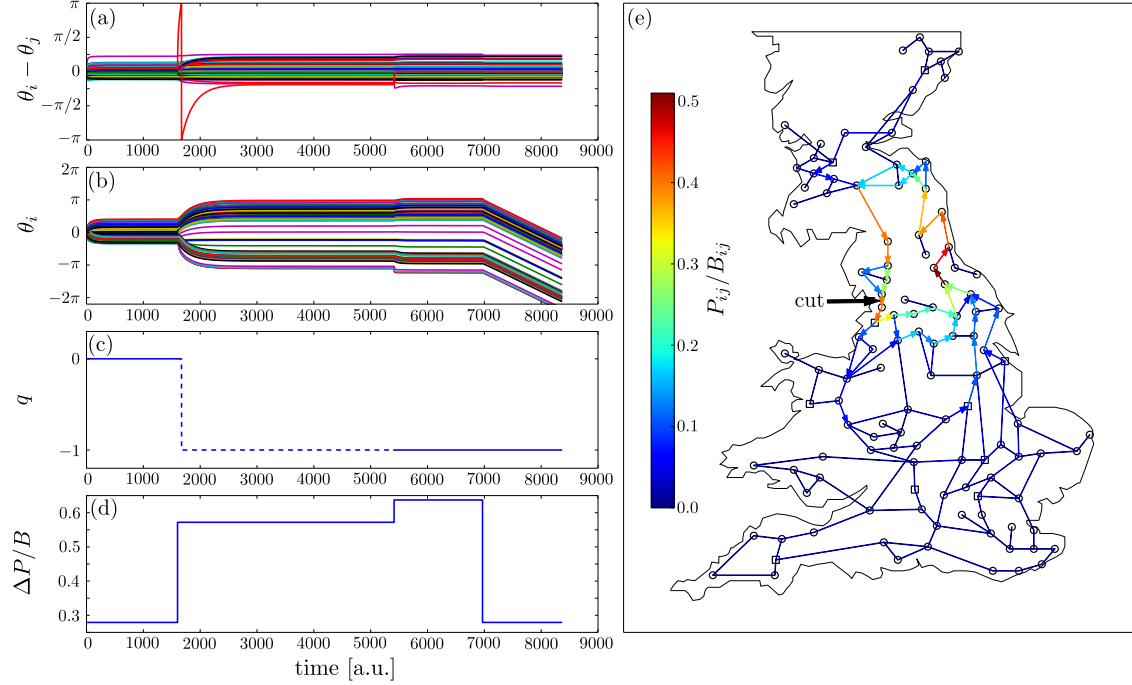


Figure 33: (Figure adapted from [67]) Creation of a loop flow in a complex network with the topology of the UK transmission grid, under the mechanism of removing an edge and adding it back. The network is sketch in panel (e). The edge parameter B_{ij} is proportional to the length of the edge $\langle ij \rangle$, and $G_{ij}/B_{ij} \equiv 0.1$. There are 10 oscillators (denoted by squares) with positive natural frequencies $P_1 = 0.5B + \Delta P/10$, and 110 oscillators (denoted by circles) with negative natural frequencies $P_2 = -B/22$, where B is the average value of the couplings B_{ij} , and ΔP is the value obtained in Eq. (7.20), required to compensate for the dissipation. Panels (a)–(d): angle differences, angles, winding number q on the large central cycle and dissipation as a function of time. Starting at a flat start (all angle are zero), we first let the system dynamically converge to a stationary synchronous state with zero winding number. The edge indicated in panel (e) is then removed at time $t = 1600$ and the system converges to a new synchronous state with increased dissipation. The edge is added back at time $t = 5410$ and left to stabilize, a loop flow has been created, with $q = -1$. At time $t = 6970$, the value of ΔP is forced to its initial value, trying to remove the loop flow. The imbalance of natural frequencies brings the system to a new synchronous state, with reduced overall frequency, all angles are decreasing. The dashed line in panel (c) indicates that q is not defined for $t \in [1600, 5410]$, when the cycle is open. Panel (e): color-coded difference in flows between the initial, $q = 0$ stationary state and the final, $q = -1$ state, in units of B_{ij} . Arrows indicate the direction of the flow difference only when the latter exceeds $0.05B_{ij}$.

8 Conclusion

Different fixed points of the Kuramoto model [Eq. (2.5)] with arbitrary interaction graph, differ by a collection of loop flows (defined in Section 2) on the fundamental cycles of the network (Theorem 2.3). A loop flow in a network can be detected by the computation of the winding number of a fixed point on the different cycles of the interaction graph. Loop flows and winding numbers give a framework to investigate the number of stable fixed points of the Kuramoto model for particular graph topologies.

As the number of fixed points of Eq. (2.5) is related to the number and length of the cycles of the interaction graph, we first focused on the simplest graph able to carry multiple fixed points: the cycle. In the particular case of cycle networks, we derived an upper bound on the number of stable fixed points of the Kuramoto model with cyclic interactions, Eq. (3.1),

$$\mathcal{N} \leq 2 \cdot \text{Int}[(n-1)/4] + 1, \quad (8.1)$$

which is algebraic in n , the length of the cycle. It significantly improves the exponential bounds obtained in [46, 76]. Our result generalizes the bounds obtained by Ochab and Góra [45], dealing in particular with angle differences larger than $\pi/2$, and extends the results of Rogge and Aeyels [44] to bidirectional couplings.

As parallel results, we obtained some sharp conditions for the fixed points on a cycle network with some angle differences in $(-\pi, -\pi/2) \cup (\pi/2, \pi]$ to be stable. We showed that at most one angle difference can be larger than $\pi/2$ in a stable fixed point. Moreover, any stable fixed point with an angle difference larger than $\pi/2$ can be directly connected to a fixed point with all angle differences in $[-\pi/2, \pi/2]$ for the same network at larger coupling K .

Considering more general graphs, we were able to generalize the bound Eq. (8.1) to the Kuramoto model with identical frequencies and planar interaction graph, Eq. (4.1),

$$\mathcal{N} \leq \prod_{k=1}^c [2 \cdot \text{Int}(n_k/4) + 1]. \quad (8.2)$$

This bound applies to the stable fixed points with all angle differences in $[-\pi/2, \pi/2]$. If such a network has stable fixed points with some angle differences larger than $\pi/2$, they are not encompassed in the bound Eq. (8.2). This bound is algebraic in the number of vertices on each cycle of the network, which is as well a significant improvement on earlier bounds that were exponential in the number of vertices, for all fixed point solutions (stable and unstable) [46, 47].

We showed the bound (8.2) to be valid for planar networks. Our approach in Section 4 is valid for any network topology until Theorem 4.2, which only applies to planar networks. All later results cannot be applied directly to general network topologies. Furthermore, our derivation of Eq. (8.2), is valid under the assumption that all fixed point solutions have angle differences $|\Delta_e| \leq \pi/2$ on all edges e of the network. We found that networks with either no or strictly more than one edge common to any two cycles carry stable fixed point solutions with only $|\Delta_e| \leq \pi/2$, therefore Eq. (8.2) holds generically for the number of stable fixed points of Eq. (2.5) on such interaction graphs.

For graphs with edges single-shared by two cycles, some stable fixed point might have some angle differences larger than $\pi/2$ as illustrated in Section 4.2. The winding number on one such cycle is bounded from above by

$$|2\pi q_k| \leq (n_k - n'_k)\pi/2 + n'_k\pi \quad (8.3)$$

with n'_k counting the number of edges on the k^{th} cycle single-shared with another cycle (as in the right panel of Figure 9) and for which an angle difference larger than $\pi/2$ does not necessarily lead to instability. We therefore conjecture the following upper bound for the number of stable fixed points on generic planar networks,

$$\mathcal{N} \leq \prod_{k=1}^c [2 \cdot \text{Int}((n_k + n'_k)/4) + 1]. \quad (8.4)$$

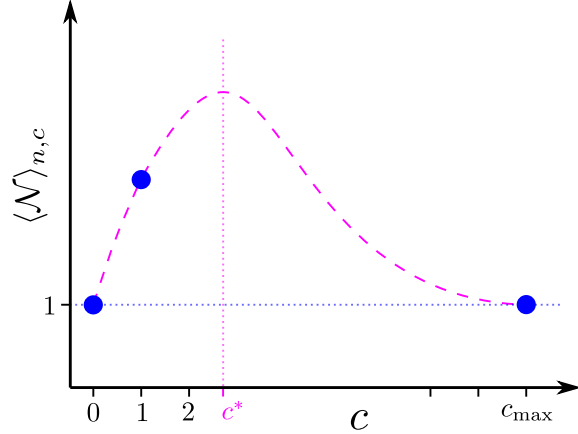


Figure 34: Average number of stable fixed points of Eq. (1.3) with respect to the number of cycles in the network c for a given number of oscillators n . Average is taken over realizations of graphs with n vertices and c cycles. The blue dots are known and the dashed purple line is conjectured.

In trying to rigorously confirm this bound we could not prove the one-to-one correspondence, obtained in Proposition 4.1, between fixed point solutions and loop flow vectors when $|\Delta_e| > \pi/2$ for some edges. Eq. (8.4) is therefore a conjecture which we could not disprove numerically, but have yet to prove rigorously.

Equal frequencies correspond to the $K \rightarrow \infty$ limit of the Kuramoto model, Eq. (2.5), and it is an open question whether our upper bound, Eq. (8.2), remains valid upon reducing K , when the spectrum of natural frequencies P_i influences the fixed points. In Section 3, we managed to show that any stable fixed point solution at a given value of K remains stable upon increasing K for a single-cycle network, meaning conversely that new stable fixed point solutions do not appear as K is reduced. While we expect the same to hold for any network, we have been unable so far to rigorously extend the argument of Section 3 beyond single-cycle networks. We expect Eq. (8.2) to be an upper bound for any K , but have not been able to rigorously prove it.

The structure of Eq. (8.2) identifies two opposite tendencies determining \mathcal{N} . On one hand more cycles means more terms in the product, which would suggest a larger number of stable fixed points. Furthermore, having more cycles increases the possibility to have two cycles sharing a unique edge, which allows larger angle differences and possibly more stable fixed points. On the other hand, more cycles for a fixed number of vertices implies shorter cycles, and according to Eq. (8.2) again, this suggests less stable fixed points. The number of stable fixed points is then a trade-off between these two tendencies. This trade-off can be illustrated by considering the average number $\langle \mathcal{N} \rangle$ of stable fixed points of Eq. (4.1), taken over all realizations of connected graphs with n vertices and c cycles. For $c = 0$, all graph realizations are trees, which have a unique stable fixed point solution. For $c = 1$, we already know that the average number of stable fixed points will increase and be bounded by $2 \cdot \text{Int}[(n-1)/4] + 1$ (see Section 3). But, as c increases further, the average number of stable fixed points will start to decrease at some point, to finally reach a unique stable fixed point for sufficiently connected networks [35, 36, 37]. We then conjecture that $\langle \mathcal{N} \rangle$ increases for $c < c^*$ and decreases for $c > c^*$ with some critical value $c^* \in [0, (n-1)(n-2)/2]$ (see Figure 34).

A non-monotonic behavior of the average $\langle \mathcal{N} \rangle$ with respect to c has been reported numerically in [46], in apparent contradiction with the above argument. According to [46, Figure 7], any network with $n = 8$ vertices and $c = 4$ cycles should have a unique solution, no matter its topology, because the average and variance reported for the number of fixed point are 1 and 0 respectively. But considering the network of Figure 35, where $n = 8$ and $c = 4$, we are able to build more than one stable fixed points, which we show in Figure 35 (a), (b) and (c). The numerical method used in [46] probably missed such a case in the sampling of networks considered.

Section 5 describes some processes leading to a change of stable fixed point of Eq. (2.5). Our main conclusion is that such changes of fixed point require a drastic change in the network parameters, which are in our cases, either a modification of the interaction graph by removing or

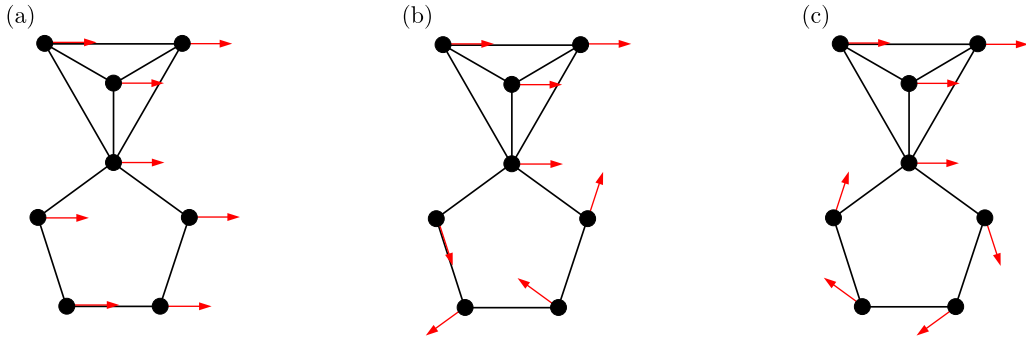


Figure 35: Example of a network with $n = 8$ vertices and $c = 4$ cycles, where multiple stable fixed points exist for identical frequencies. Three fixed points are shown, the red arrows represent the angle of each oscillator. Each of them has a different winding number of the bottom cycle: (a) $q = 0$, (b) $q = -1$ and (c) $q = 1$. All angle differences are lower than $\pi/2$ and thus by Corollary 2.7, the three fixed points are stable.

adding an edge, or a change of natural frequencies sufficient to destabilize the initial fixed point. We furthermore showed that bringing continuously the system to its initial parameters does not bring it back to its initial fixed point.

We explain this behavior by the fact that different fixed points are characterized by winding numbers, which are discrete quantities. A continuous change of the parameters of the system, whose dynamics is continuous, thus cannot lead to a change of winding number. “Jumping” from a fixed point to another requires a discontinuous modification of the network, which can be the destabilization of a fixed point, or a modification of the interaction graph topology, by removing or adding an edge. Tyloo et al. [27] investigate escapes from the basin of attraction of a fixed point under noisy natural frequencies. In this case, the amplitude of the noise needs to be sufficiently large to push the system from a basin of attraction to another.

In Section 6, we have developed a numerical method to investigate the volume of basins of attraction of fixed points in dynamical systems. Our method first locates the stable fixed points of the dynamical system, taking advantage of our knowledge thereof, obtained in Sections 3 and 4. Second, it perturbs them in random directions with increasing magnitude. The proportion of perturbed states that converge back to the initial fixed point allows to evaluate the radius of the basin of attraction and then its volume.

Based on this idea and following the work of Wiley et al. [52], we investigated the volumes of the basins of attraction of the various stable fixed points of the Kuramoto model on a cycle with identical frequencies, Eq. (6.2). Contrasting with the Gaussian distribution suggested in [52], we obtained analytical evidences that the volume of the basin of attraction is proportional to $(1 - 4q/n)^n$. We confirmed these findings with numerical simulations. We then extended the application of our method to the Kuramoto model on a cycle with non-identical frequencies and to the Kuramoto model on meshed networks. This generalization render the investigations of the basins of attraction much less tractable, which imposes to rely on numerics. Moderate non-identical frequencies on cyclic networks does not change the linear dependence between the volume of the basins of attraction and the corresponding winding numbers, at least for winding number not too small and not too large. On our example of complex network, our investigations allows to understand how winding numbers on different cycles of the network influence each other.

We believe that our method significantly speeds up investigations about the basins of attraction of dynamical systems. Compared to other existing methods to investigate basins of attraction, our method has three main advantages:

- It does not require a Lyapunov function of the dynamical system considered [77, 78], which is complicated to find in general;
- It is not limited to quadratic or polynomial systems [79];
- The investigation is guided by our knowledge of the system and avoids to randomly pick initial conditions in the state space [52, 60].

These advantages come with the drawback that we limit our investigations to the volume of the basins of attraction and have no indications about their shape. In particular, our method is probably not adapted to the investigation of fractal basins of attraction [80].

References

- [1] *Statistique suisse de l'électricité 2016*. Tech. rep., Swiss Federal Office of Energy (2017).
- [2] *Perspectives nergtiques pour 2035*. Tech. Rep. 1, Swiss Federal Office of Energy (2007).
- [3] J. Machowski, J. W. Bialek, and J. R. Bumby. *Power system dynamics* (Wiley, Chichester, U.K), 2nd ed. (2008).
- [4] A. R. Bergen and V. Vittal. *Power Systems Analysis* (Prentice Hall) (2000).
- [5] T. Coletta and P. Jacquod. *Phys. Rev. E* **93**(3) (2016).
- [6] C. Huygens. *Oeuvres complètes de Christiaan Huygens* (Société hollandaise des sciences, La Haye) (1983).
- [7] M. L. Cartwright. *J. Lond. Math. Soc.* **1**(3), 367 (1960).
- [8] Y. Kuramoto. *Chemical Oscillations, Waves and Turbulence*, vol. 19 of *Springer Series in Synergetics* (Springer Berlin Heidelberg) (1984).
- [9] A. T. Winfree. *J. Theoret. Biol.* **16**(1), 15 (1967).
- [10] Y. Kuramoto. In H. Araki (ed.), *Lecture Notes in Physics, vol. 39. International Symposium on Mathematical Problems in Theoretical Physics*, pp. 420–422 (Springer, Berlin) (1975).
- [11] Y. Kuramoto. *Prog. Theor. Phys. Suppl.* **79**, 223 (1984).
- [12] G. B. Ermentrout. *J. Math. Biol.* **22**(1), 55 (1985).
- [13] J. L. van Hemmen and W. F. Wreszinski. *J. Stat. Phys.* **72**(1-2), 145 (1993).
- [14] S.-Y. Ha and M. Slemrod. *J. Differ. Equ.* **251**(10), 2685 (2011).
- [15] J. Buck. *Q. Rev. Biol.* **63**(3), 265 (1988).
- [16] G. B. Ermentrout. *J. Math. Biol.* **29**(6), 571 (1991).
- [17] C. C. Chen, V. Litvak, T. Gilbertson, A. Kühn, C. S. Lu, S. T. Lee, C. H. Tsai, S. Tisch, P. Limousin, M. Hariz, and P. Brown. *Exp. Neurol.* **205**(1), 214 (2007).
- [18] K. Lehnertz, S. Bialonski, M.-T. Horstmann, D. Krug, A. Rothkegel, M. Staniek, and T. Wagner. *J. Neurosci. Methods* **183**(1), 42 (2009).
- [19] Z. Lu, K. Klein-Cerdeña, S. Lee, T. M. Antonsen, M. Girvan, and E. Ott. *Chaos* **26**(9), 094811 (2016).
- [20] K. Wiesenfeld, P. Colet, and S. H. Strogatz. *Phys. Rev. Lett.* **76**(3), 404 (1996).
- [21] K. Wiesenfeld, P. Colet, and S. H. Strogatz. *Phys. Rev. E* **57**(2), 1563 (1998).
- [22] O. Simeone, U. Spagnolini, Y. Bar-Ness, and S. H. Strogatz. *IEEE Signal Process. Mag.* **25**(5), 81 (2008).
- [23] R. Baldoni, A. Corsaro, L. Querzoni, S. Scipioni, and S. Tucci Piergiovanni. *IEEE Trans. Parallel Distrib. Syst.* **21**(5), 607 (2010).
- [24] Y. Wang, F. Núñez, and F. J. Doyle. *IEEE Trans. Control Syst. Technol.* **21**(4), 1455 (2013).
- [25] J. W. Simpson-Porco, F. Dörfler, and F. Bullo. *IFAC Proc. Vol.* **45**(26), 264 (2012).
- [26] F. Dörfler, M. Chertkov, and F. Bullo. *Proc. Natl. Acad. Sci.* **110**(6), 2005 (2013).
- [27] M. Tyloo, R. Delabays, and P. Jacquod. *Under preparation* (2018).
- [28] E. Mallada and A. Tang. *J. Phys. A* **46**(50), 505101 (2013).

- [29] S. H. Strogatz. *Physica D* **143**(1), 1 (2000).
- [30] J. A. Acebrón, L. L. Bonilla, C. J. Pérez Vicente, F. Ritort, and R. Spigler. *Rev. Mod. Phys.* **77**(1), 137 (2005).
- [31] F. Dörfler and F. Bullo. *Automatica* **50**(6), 1539 (2014).
- [32] A. Jadbabaie, N. Motee, and M. Barahona. *Proc. of the 2004 IEEE ACC* pp. 4296–4301 (2004).
- [33] F. Dörfler and F. Bullo. *Proc. of the 51st IEEE CDC* (2012).
- [34] S. Jafarpour and F. Bullo. *arXiv:1711.03711* (2017).
- [35] D. Aeyels and J. A. Rogge. *Prog. Theor. Phys.* **112**(6), 921 (2004).
- [36] R. E. Mirollo and S. H. Strogatz. *Physica D* **205**(1), 249 (2005).
- [37] R. Taylor. *J. Phys. A* **45**(5), 055102 (2012).
- [38] A. J. Korsak. *IEEE Trans. Power App. Syst.* **PAS-91**(3), 1093 (1972).
- [39] C. J. Tavora and O. J. M. Smith. *IEEE Trans. Power App. Syst.* **PAS-91**(3), 1138 (1972).
- [40] P. F. C. Tilles, F. F. Ferreira, and H. A. Cerdeira. *Phys. Rev. E* **83**(6) (2011).
- [41] A. Kłos and J. Wojcicka. *Int. J. Elect. Power Energy Syst.* **13**(5), 268 (1991).
- [42] J. Baillieul and C. I. Byrnes. *IEEE Trans. Circuits Syst.* **29**(11), 724 (1982).
- [43] J. W. Milnor. *Morse Theory* (Princeton University Press) (1963).
- [44] J. A. Rogge and D. Aeyels. *J. Phys. A* **37**(46), 11135 (2004).
- [45] J. Ochab and P. F. Góra. *Acta Phys. Pol. B [Proc. Suppl.]* **3**(2), 453 (2010).
- [46] D. Mehta, N. S. Daleo, F. Dörfler, and J. D. Hauenstein. *Chaos* **25**(5), 053103 (2015).
- [47] T. Chen, D. Mehta, and M. Niemerg. *arXiv:1603.05905* (2016).
- [48] R. Delabays, T. Coletta, and P. Jacquod. *J. Math. Phys.* **57**(3), 032701 (2016).
- [49] R. Delabays, T. Coletta, and P. Jacquod. *J. Math. Phys.* **58**(3), 032703 (2017).
- [50] N. Janssens and A. Kamagate. *Int. J. Elect. Power Energy Syst.* **25**(8), 591 (2003).
- [51] T. K. Roy and A. Lahiri. *Chaos Solitons Fractals* **45**(6), 888 (2012).
- [52] D. A. Wiley, S. H. Strogatz, and M. Girvan. *Chaos* **16**(1), 015103 (2006).
- [53] A. Hatcher. *Algebraic Topology* (Cambridge University Press) (2002).
- [54] N. Biggs. *Algebraic graph theory* (Cambridge University Press), second ed. (1993).
- [55] J. W. Milnor. *Topology from the Differentiable Viewpoint* (Princeton University Press) (1997).
- [56] A. M. Lyapunov. *The general problem of the stability of motion*. Ph.D. thesis, University of Kharkov (1892).
- [57] A. M. Lyapunov. *Int. J. Control* **55**(3), 531 (1992).
- [58] M. Pai. *Power System Stability: Analysis by the Direct Method of Lyapunov* (North-Holland Publishing Company) (1981).
- [59] H.-D. Chiang and J. S. Thorp. *IEEE Trans. Autom. Control* **34**(12), 1229 (1989).
- [60] P. J. Menck, J. Heitzig, N. Marwan, and J. Kurths. *Nat. Phys.* **9**, 89 (2013).

-
- [61] P. Schultz, P. J. Menck, J. Heitzig, and J. Kurths. *New J. Phys.* **19**(2), 023005 (2017).
 - [62] R. A. Horn and C. R. Johnson. *Matrix Analysis* (Cambridge University Press, New York) (1986).
 - [63] D. Manik, M. Timme, and D. Witthaut. *Chaos* **27**(8) (2017).
 - [64] L. G. Khazin and E. E. Shnol. *Stability of Critical Equilibrium States* (Manchester University Press) (1991).
 - [65] W. Cheney. *Analysis for Applied Mathematics* (Springer, New York) (2001).
 - [66] W. Gander, M. J. Gander, and F. Kwok. *Scientific Computing - An Introduction using Maple and MATLAB* (Springer International Publishing) (2014).
 - [67] T. Coletta, R. Delabays, I. Adagideli, and P. Jacquod. *New J. Phys.* **18**(10), 103042 (2016).
 - [68] F. Dörfler and F. Bullo. *Proc. of the 2011 IEEE ACC* (2011).
 - [69] R. Delabays, M. Tyloo, and P. Jacquod. *Chaos* **27**(10), 103109 (2017).
 - [70] R. K. Pathria and P. D. Beale. *Statistical mechanics* (Elsevier), 3rd ed. ed. (2011).
 - [71] S.-Y. Ha and M.-J. Kang. *SIAM J. Appl. Math.* **72**(5), 1549 (2012).
 - [72] L. De Ville. *Nonlinearity* **25**(5), 1473 (2012).
 - [73] R. Gilmore. *Catastrophe Theory for Scientists and Engineers* (Wiley New York) (1981).
 - [74] H. Sakaguchi and Y. Kuramoto. *Prog. Theor. Phys.* **76**(3), 576 (1986).
 - [75] D. Witthaut and M. Timme. *New Journal of Physics* **14**(8), 083036 (2012).
 - [76] H. D. Nguyen and K. S. Turitsyn. In *IEEE PES General Meeting - Conference Exposition* (2014).
 - [77] R. Genesio, M. Tartaglia, and A. Vicino. *IEEE Trans. Autom. Control* **30**(8), 747 (1985).
 - [78] E. Najafi, R. Babuka, and G. A. D. Lopes. *Nonlinear Dyn.* **86**(2), 823 (2016).
 - [79] F. Amato, C. Cosentino, and A. Merola. *Automatica* **43**(12), 2119 (2007).
 - [80] C. Grebogi, E. Ott, and J. A. Yorke. *Science* **238**(4827), 632 (1987).